ANL/EBR-066

PROSPECTUS FOR OPERATING EBR-II WITH HIGH-WORTH CONTROL RODS

by

R. A. Cushman, B. R. Sehgal, and V. W. Lowery*

EBR-II Project
Argonne National Laboratory
Argonne, Illinois-Idaho Falls, Idaho

September 1972

*U.S. Atomic Energy Commission, Division of Reactor Development and Technology

Work performed under the auspices of the U.S. Atomic Energy Commission

TABLE OF CONTENTS

LIST OF FIGURES

LIST OF FIGURES

(continued)

LIST OF FIGURES

(continued)

LIST OF TABLES

PROSPECTUS FOR OPERATING EBR-II WITH HIGH-WORTH CONTROL RODS

by

R. A. Cushman, B. R. Sehgal, and V. W. Lowery

ABSTRACT

An analysis of operation of EBR-II with a system of high-worth control rods (HWCR's) has been completed. Use of a HWCR system instead of the present control rods will result in a reduction in the required number of control rods (from 10 to 8 or less) while providing a greater amount of controllable reactivity insertion. Operation of the control-rod system as part of the plant protective system is not affected, and the result of the uncontrolled insertion of an HWCR is not, in principle, different from that of a standard control rod. No significant safety problem is introduced by the use of a system of HWCR's. Operation with HWCR's is recommended.

I. INTRODUCTION

A need for more experimental space in EBR-II has been the main reason for development of a high-worth control rod.

EBR-II was designed to operate with 12 standard control rods, alternating with driver-fuel subassemblies in the 24 core positions in row 5.[1,2] Figure 1 shows the locations of the control rods in the core. Each control rod is raised or lowered from above by a drive mechanism that penetrates both the primary-tank cover and the reactor-vessel cover, and the 12 nozzles for the control-rod drives are the only penetrations that are directly above the core during operation of EBR-II. These 12 positions, therefore, are the only ones available for use for special experimental equipment, such as an instrumented subassembly, that requires access during reactor operation. Utilization of such instrumented equipment is common; the complete complement

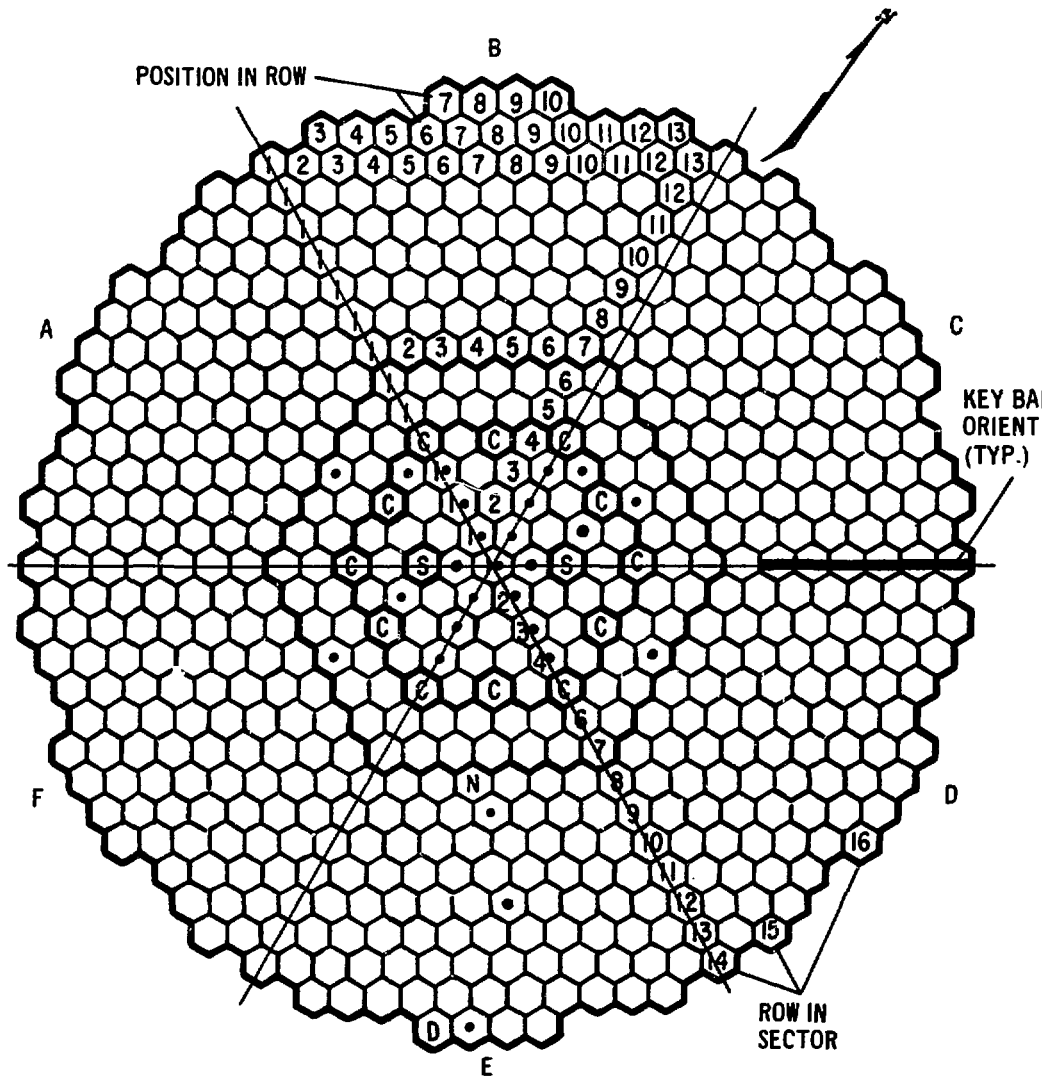

LEGEND

1.	SECTORS	A to F
2.	CONTROL RODS (12)	C
3.	SAFETY RODS (2)	S
4.	THERMOCOUPLES (26)	•
5.	FIXED DUMMY	D
6.	NEUTRON SOURCE	N
7.	GRID POSITIONS	
	CORE	61
	INNER BLANKET	66
	OUTER BLANKET	510
	TOTAL	637

Fig. 1. Design Arrangement of Control Rods and Other Subassemblies in the Reactor

of 12 control rods has been in EBR-II for only 1409 of the 51,518 MWd of operation from run 1 (Aug 1, 1964) through run 53E (Jan 14, 1972).[3]

In addition to several instrumented subassemblies, other devices such as drop rods, oscillator rods, and the incore instrument test facility have been located in control-rod positions. The EBR-II Operating Limits, together with run-length considerations, impose a requirement for 10 control rods of the present design. In order to free more of the control-rod locations for other uses, it was necessary to design a different type of control rod that provided a greater variation in reactivity between the full-in and the full-out position. Such a control rod has been developed and tested, and this document presents the case for operating EBR-II with such high-worth control rods (HWCR's).

Two types of high-worth control rods were considered (a) an all-poison rod would replace the fuel portion of the existing rod with a poison material, such as B_4C with a higher-than-normal ^{10}B content, and add reactivity to the core by removing the poison; (b) a fuel-absorber rod, on the other hand, would add a poison section above the present fuel region and would add reactivity by the combination of adding fuel and removing poison. The latter approach was selected as the basis of the HWCR. It had the advantage of keeping the core more uniform (since the fueled portions of the control rods are normally at least 80% inserted) and thus causing less perturbation of the flux in the subassemblies adjacent to the control-rod locations.

The design of an HWCR of fuel-absorber type was virtually completed in October 1968.[4] Two HWCR's were then built, using natural B_4C as the poison material, and were used sequentially in EBR-II. The first rod operated during runs 46B through 50D and the second during runs 50E through 53E. During this time, it was possible to run with only nine control rods (runs 48A-51C), since the one HWCR provided greater reactivity control than the standard control rod it replaced. The first HWCR is now undergoing destructive analysis; and the results of both the in-pile testing and the subsequent nondestructive and destructive analyses in a hot cell indicate that operation with a system of HWCR's will be permissible as well as desirable. The subsequent sections of this report (a) briefly describe the design of the HWCR, (b) give details of the steady-state neutronic

and thermal-hydraulic characteristics of the seven-row core expected when the system of HWCR's is adopted, (c) discuss the worths, measured and calculated, of standard and high-worth control rods in cores with a depleted-uranium blanket and with a stainless steel reflector, (d) present the safety analysis, from both reactivity and nonreactivity considerations, and (e) present recommendations for utilization of HWCR's in EBR-II.

The following ground rules were set up for considering operation of EBR-II with HWCR's:

(1) The driver fuel considered in the study was Mark-IA fuel with a burnup limitation of 1.8 at. %.

(2) The core used as the basis of the neutronic and thermal-hydraulic calculations was one projected for operation in February 1973. The projection was made in February 1971 and was expected to be typical of subsequent cores.

(3) The core was reflected with stainless steel subassemblies in rows 7-10, since the installation of the stainless steel reflector in EBR-II was scheduled to occur before the HWCR's were available for all control-rod positions. (The stainless steel reflector was actually installed in May 1972.)

(4) The reactivity requirements for a system of HWCR's were as shown in Table I. The value of the burnup reactivity given in Table I is higher than would be necessary from the standpoint of optimum fuel utilization, but is used for later operational flexibility.

II. BRIEF DESCRIPTION OF HIGH-WORTH CONTROL ROD

Details of the EBR-II control-rod design are given in the EBR-II System Design Descriptions[5] and only a brief description is presented here.

The layout of the EBR-II core and blanket is based on a hexagonal array, with a center-to-center spacing of 2.320 in. The control-rod subassemblies maintain this spacing through the use of a guide thimble, a hexagonal tube with the same 2.290-in. distance across its flats that a core or blanket subassembly has. This guide thimble is semipermanently installed in a control rod position (the last of the original 12 guide thimbles was replaced in December 1971); and control-rod subassemblies, oscillator-rod subassemblies,

TABLE I. Reactivity Ground Rules for a High-worth Control-rod System

Shutdown Margin (2.35% Δk/k)[a]	1010 Ih
Power-Reactivity Decrement to 62.5 MWt	110 Ih
Reactivity-adjustment Increment	100 Ih
Cushion on Operating Limits	100 Ih
Burnup (2000 MWd at 0.15 Ih/MWd)	300 Ih
Total Minimum Worth of Control-rod System	1620 Ih

[a] 1% Δk/k = 430 Ih

or instrumented subassemblies operate within the envelope provided by the thimble. The design of the original Mark-I control-rod subassembly is shown in Fig. 2.

The present EBR-II control rod is similar to that shown in Fig. 2 except for details of the bushings at the lower portion of the control rod. The changes in the bushings have been made to provide an increased holddown effect, and this increased holddown effect will also be a feature of the HWCR. The differences between the present control rod and the HWCR are internal.

The basic difference is that the HWCR provides a region for poison material (B_4C) above the fuel region (see Fig. 3). The fueled portions of both control rods are identical, containing 61 Mark-IA fuel elements arranged in a hexagonal array with a 0.223-in. pitch. The space above the fuel in a present control rod contains a sodium deflector, sodium, and the upper shield. In the HWCR, this space contains seven 36-in.-long capsules (Fig. 4), arranged on 0.665-in. centers. Each capsule contains 14 in. of natural B_4C at its lower end. Above the B_4C pellets is an Inconel spring 1-3/8 in. long, and above the spring is a stainless steel shield plug 8 in. long. The shield plug is welded in place and forms a seat for the spring. The spring prevents the B_4C pellets from shifting during control-rod motion and allows for axial expansion of the B_4C column. The stainless steel shield plug contains three axial grooves, which permit the helium released in the (n,α) reaction with ^{10}B during operation of the HWCR to move up to the plenum region at the top of the capsule. The capsule nominally contains one atmosphere of helium when fabricated.

The 3-ft-long closely spaced bundle of B_4C capsules increases the pressure drop in the subassembly above the fuel region, and a corresponding decrease is required in the portion below the fuel. This decrease has been accomplished by redesigning the lower reflector shield. An additional change in the flow characteristics has been required because of the installation of the stainless steel reflector in rows 7-10. The increased neutron flux in the lower axial reflector in row 5 caused by the stainless steel radial reflector causes a significant amount of power to be produced in a control rod in the down position. Preliminary analysis indicated that

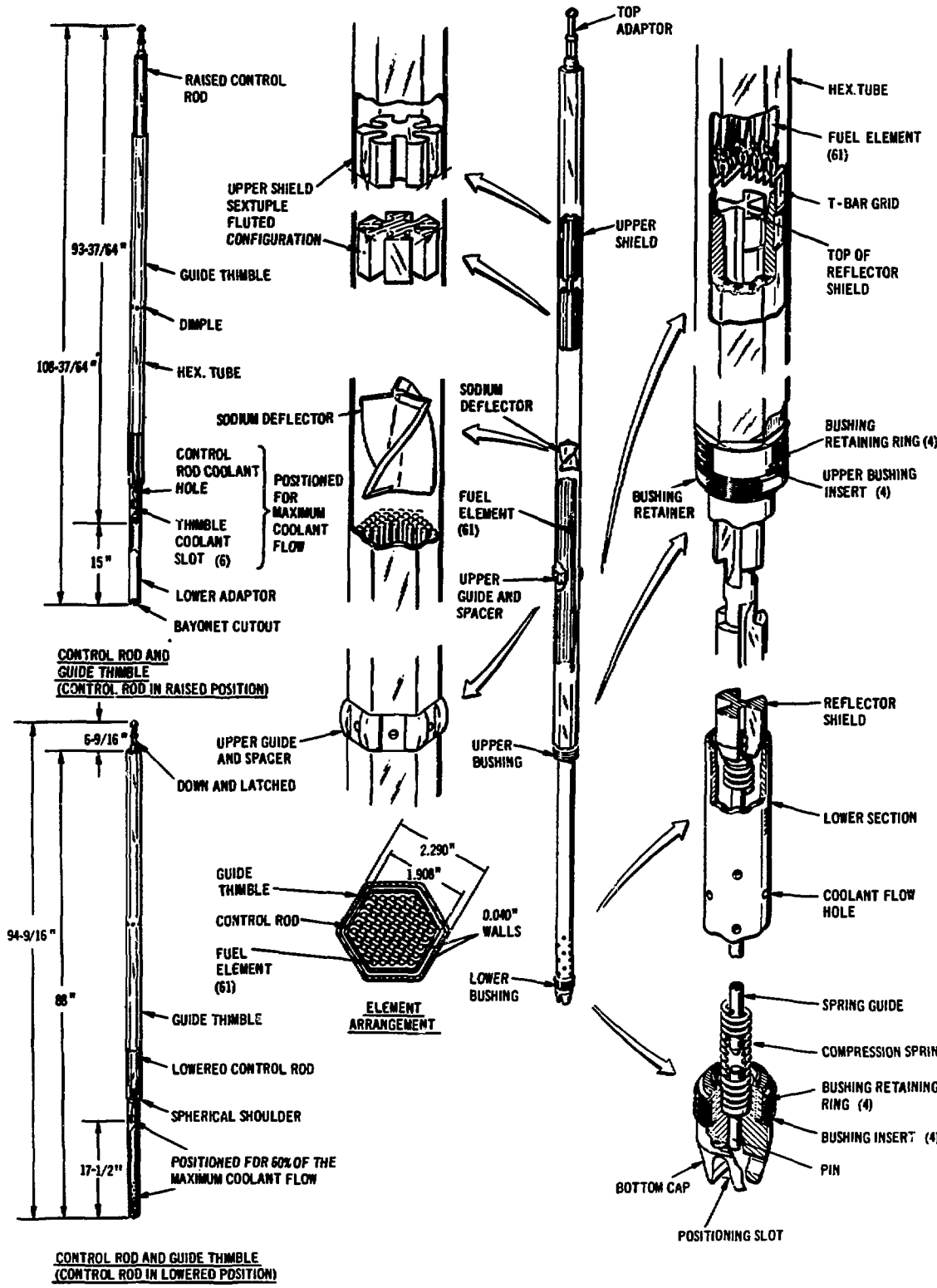

Fig. 2. Mark-I Control-rod Subassembly

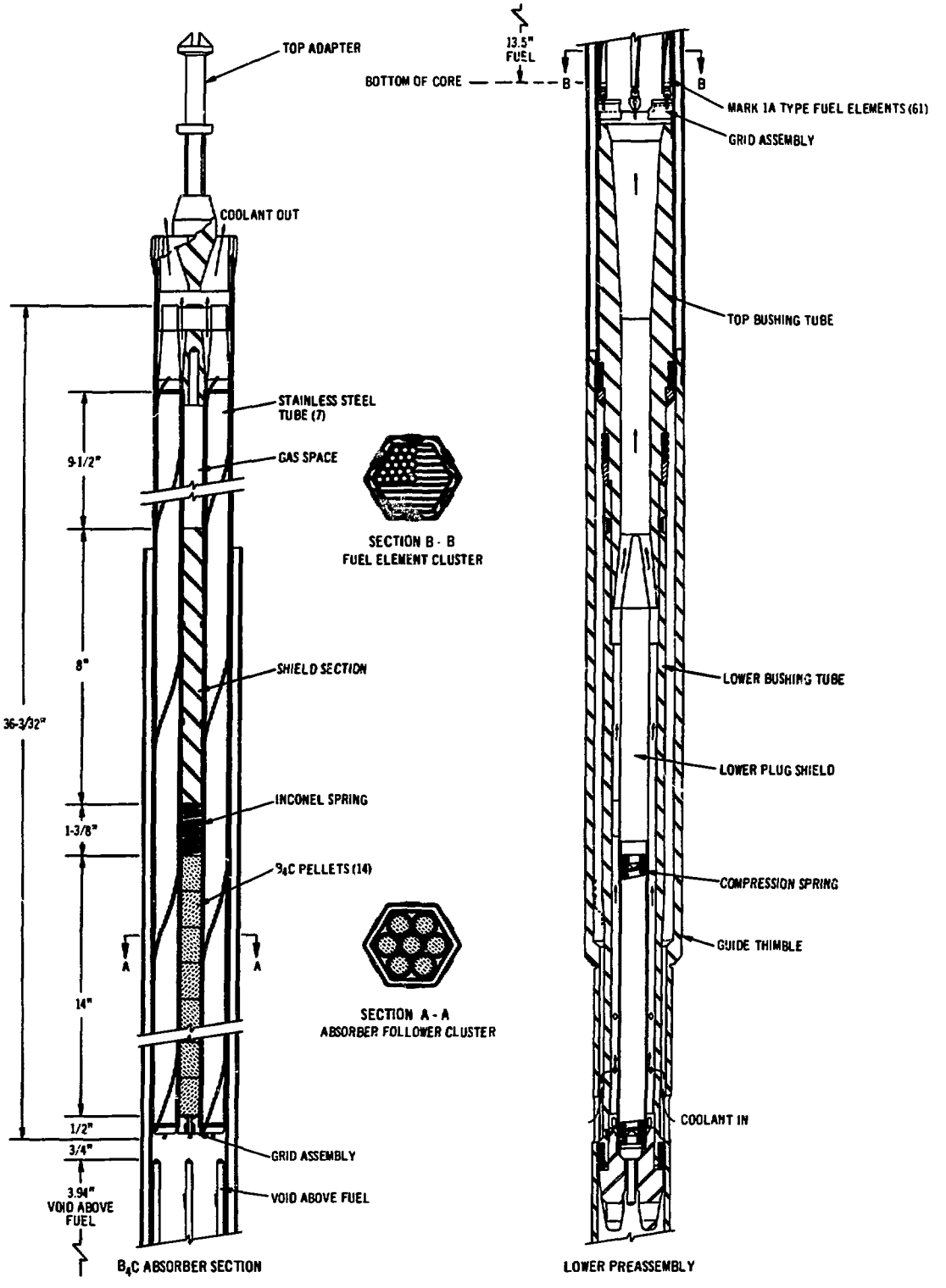

Fig. 3. High-worth Control-rod Subassembly

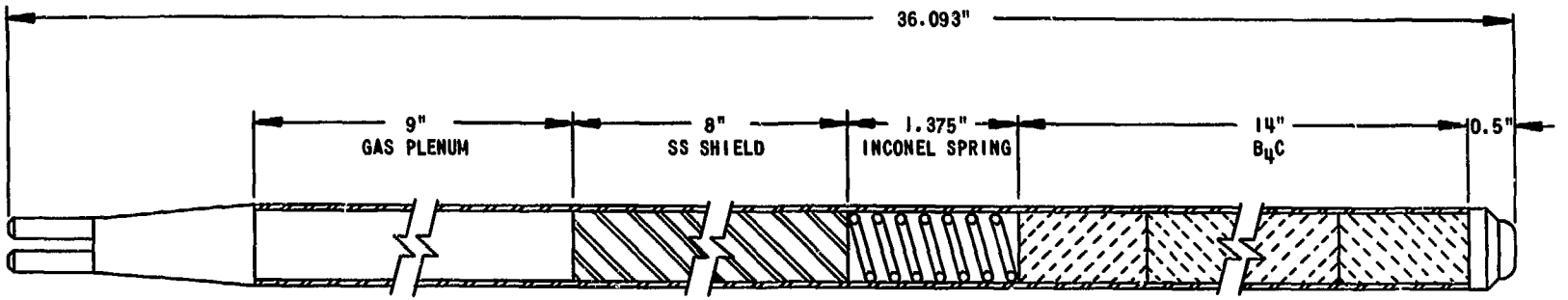

LENGTH		36.093"
TUBING	OD	0.625"
	ID	0.555"
	WALL THICKNESS	0.035"
	MATERIAL	304LSS
PELLET	DIAMETER	0.549"
	LENGTH	1.000"
	MATERIAL	B_4C
WIRE WRAP	DIAMETER	0.030"
	HELICAL PITCH	6"

Fig. 4. B_4C Capsule Used in HWCR's

72% as much fission power might be produced in a control rod in the fully withdrawn position (no fuel in the core region) as in the fully inserted position.* A change was therefore made in the tapered region of the lower adapter which controls flow as a function of rod position, and there is now greater sodium flow through the control rod at small insertions. Figure 5 shows the results of tests of flow variation[6] as a function of control-rod insertion for the HWCR and present control rods.

Outwardly, the present and the high-worth control rods are similar, and they are completely interchangeable as far as their non-neutronic aspects are concerned. No change in the fuel-handling or control-rod-drive system is required; the HWCR was designed to be compatible w[illegible] existing EBR-II system.

III. STATIC CALCULATIONS FOR PROJECTED CORES

This section discusses the steady-state neutronics and thermal-hydraulics calculations carried out on two cores projected for operation in about February 1973. The two cores, which are really variations of a single core caused by the difference in the composition of rows 7-10, were established to provide a reference configuration for subsequent determination of the worth of the HWCR's and for kinetics studies based on use of the HWCR's. Although the calculations were carried out as part of the HWCR effort, they were insensitive to the type of control rod used, because they assumed that the fueled portion, which is identical for both present and high-worth control rods, was fully inserted into the core.

The two cores are shown in Figs. 6 and 7. The loading shown in Fig. 6 was projected, in early 1971, as one representative of that expected in early 1973. The number of experimental subassemblies available for irradiation at that time will have increased beyond the current value. There are

---

*Note that throughout this report, rod "insertion" means insertion of reactivity by insertion of the fuel section into the core (and for an HWCR, simultaneous removal of the B_4C section). When the rod is in the "withdrawn" or "down" position, the fuel section is below the core, so that the rod must be raised for insertion.

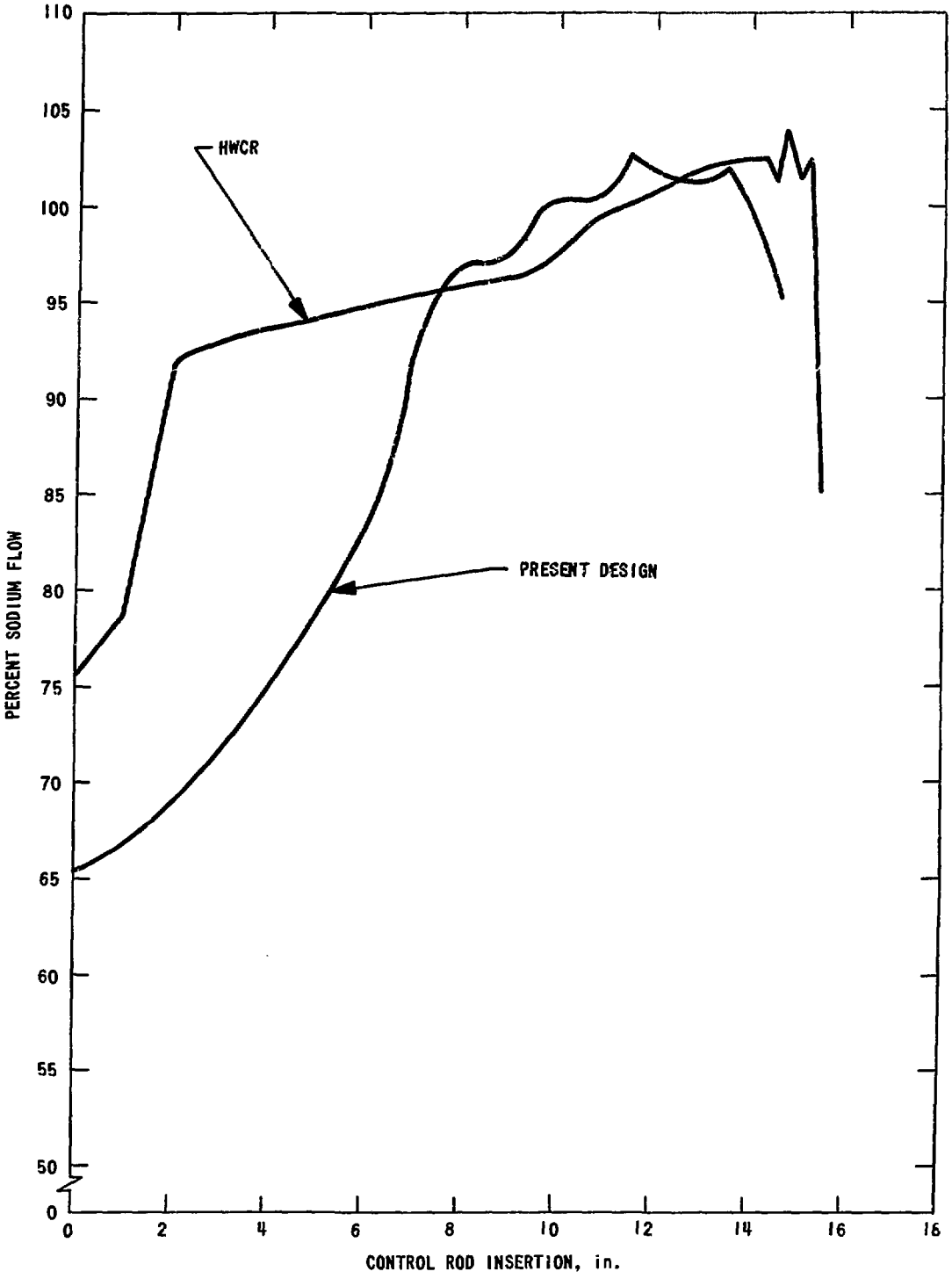

Fig. 5. Control-rod Flow as a Function of Control-rod Insertion, for Sodium at 800°F and a Constant ΔP of 15 psi

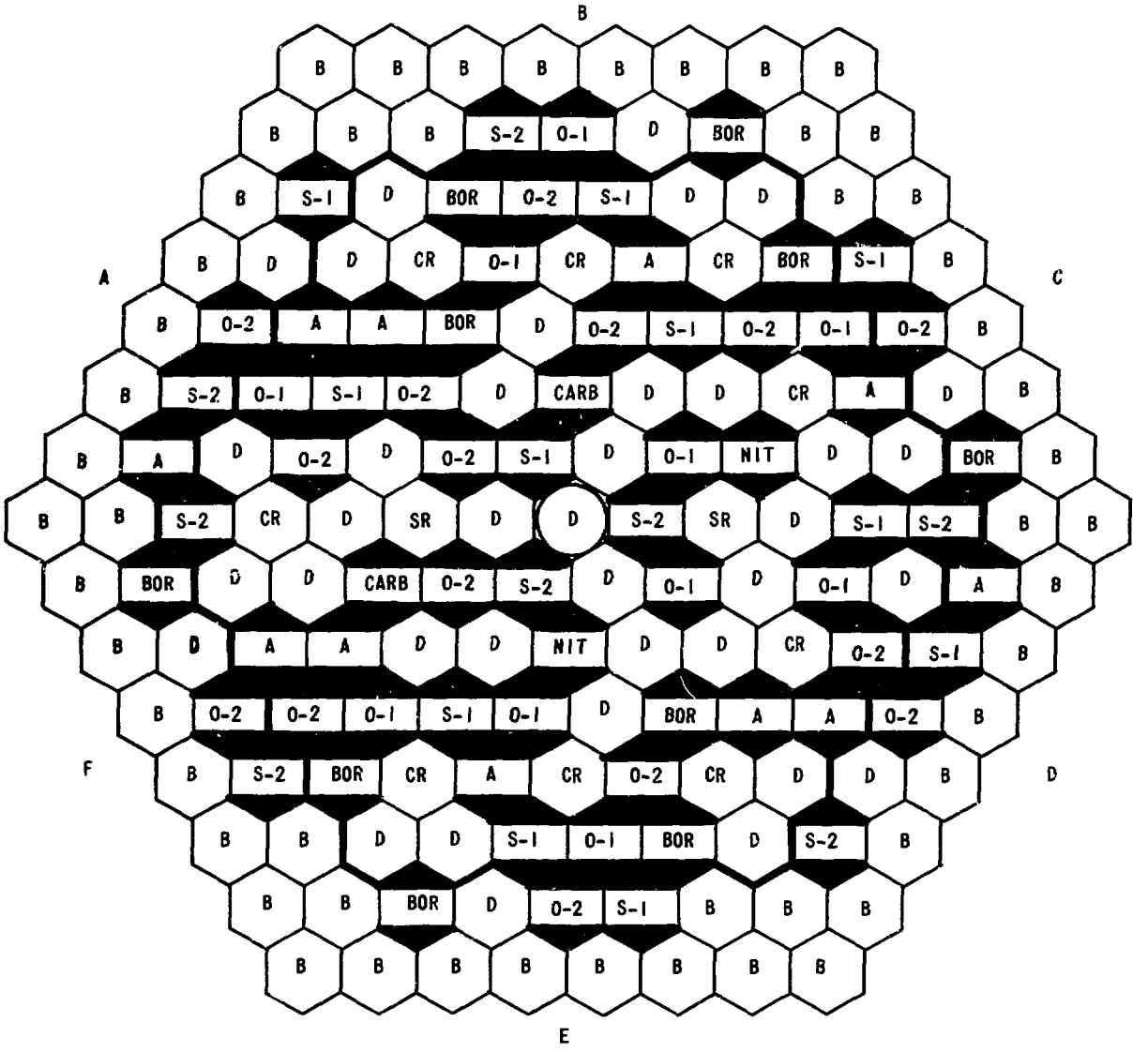

SEE TABLE II FOR KEY TO SUBASSEMBLY TYPES

Fig. 6. Projected Loading Pattern for EBR-II with Depleted-uranium Blanket

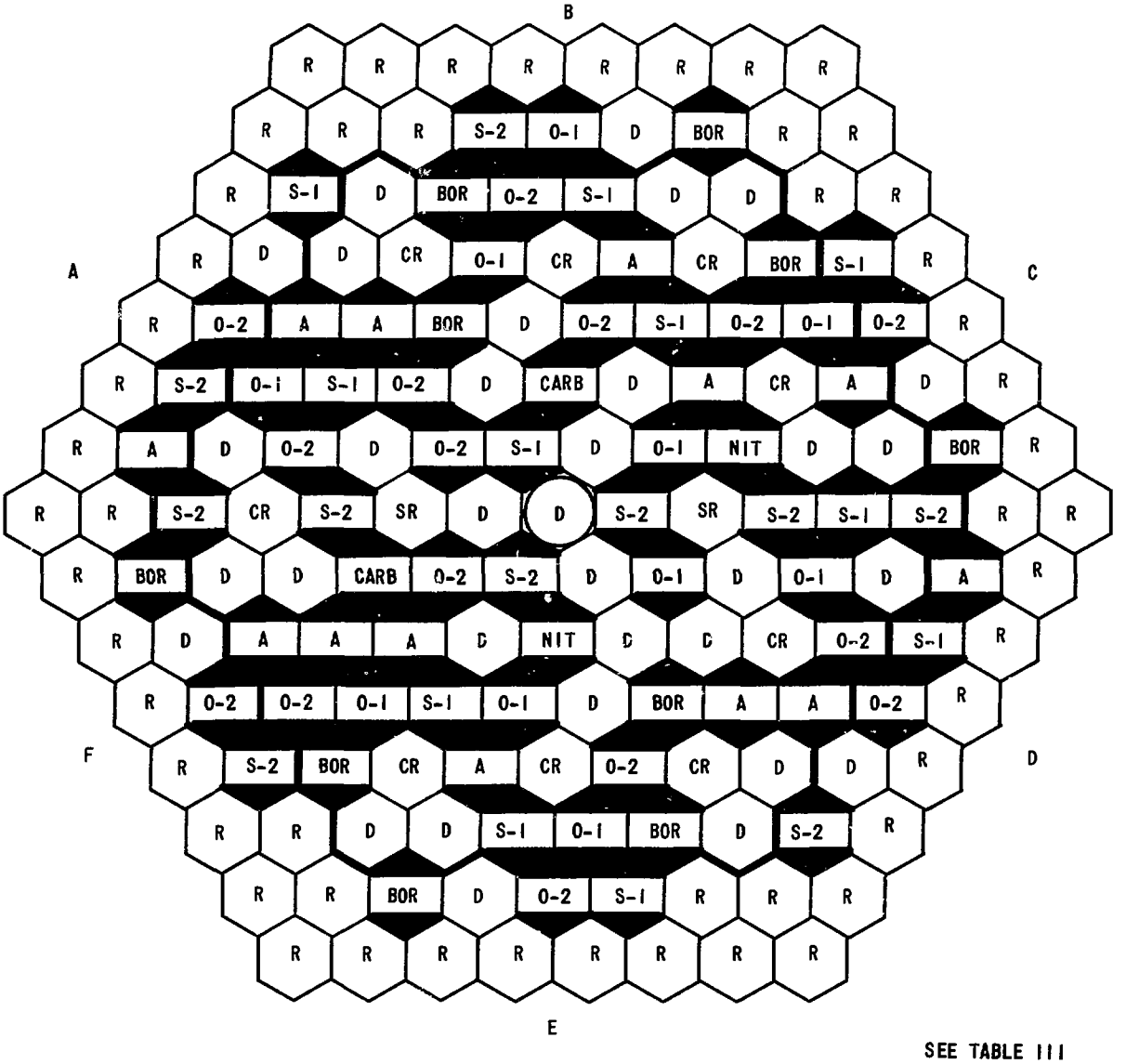

SEE TABLE III FOR KEY TO SUBASSEMBLY TYPES

Fig. 7. Projected Loading Pattern for EBR-II with Stainless Steel Reflector

69 experimental subassemblies in the loading of Fig. 6 and 73 in Fig. 7. The difference in the loading is due to replacement of four driver subassemblies in row 4 with experimental subassemblies to make up for the increased reactivity effect of the stainless steel reflector. The cores are representative rather than typical: all oxide-fuel-element experiments are represented by only two types, O-1 and O-2; and all structural experiments are represented by two types, S-1 and S-2 (where O-1, O-2, and S-1 are actual experimental subassemblies that have been irradiated in EBR-II); likewise, encapsulated oxide, carbide, and nitride fuels are represented by only one type each. The loadings of Fig. 6 and 7 are tabulated by rows in Tables II and III, respectively, together with the nomenclature for each type of subassembly. A more detailed description of the core composition is given in Ref. 7, including a breakdown of the volume fractions of the materials in each type of subassembly.

A. Neutronics of Reference Core

Static reactor-physics calculations were carried out for these two projected EBR-II cores reflected, respectively, by (a) depleted uranium in rows 7 through 16, and (b) stainless steel in rows 7 through 10 and depleted uranium in rows 11 through 16. Results were obtained for criticality, power generated in each subassembly, and the reactivity worths of the HWCR's at several positions along their axial travel. Calculations were made using the transport-theory code DOT with S_4 approximation in XY and RZ geometry, and using the diffusion theory code CITATION in RZ geometry.

The calculations were performed with the 29-group cross-section set derived from the ENDF/B version-I, category-1 data using the code MC^2. The cross sections for the core region were calculated in MC^2 at critical buckling and for the other regions at zero buckling. The detector cross sections were averaged over the spectra of the different regions.

The axial bucklings used for the DOT XY calculations for the core with stainless steel reflector were: 0.0023 cm^{-2} for the core subassemblies and 0.00085 cm^{-2} for the stainless steel and depleted-uranium subassemblies. The buckling used for the core reflected by depleted uranium in rows 7 to 16 was 0.0023 cm^{-2} for both core and depleted-uranium subassemblies.

TABLE II. Loading of Fig. 6 Projected Core with Depleted-uranium Blanket

Row No.	Number per Row of Various Types of Subassemblies											
	D	0-1	0-2	S-1	S-2	A	CARB	BOR	NIT	CR	SR	B
1	1											
2	3			1	2							
3	4	2	2				1		1		2	
4	9	1	2	2			1	2	1			
5	2	3	3	2		5				9		
6	12	3	3	2	2	4		4				
7	6	1	5	4	4	2		4				10
Core Total	37	10	15	11	8	11	2	10	2	9	2	10

D ≡ Driver (Mark-IA) ≈52% ^{235}U enriched

0-1 ≡ Oxide-fuel-element experimental subassembly X062

0-2 ≡ Oxide-fuel-element experimental subassembly X093

S-1 ≡ Structural experimental subassembly X099

S-2 ≡ Structural experimental subassembly X099 with half as much steel

A ≡ 19-pin encapsulated-oxide-fuel experimental subassembly X064

CARB ≡ Carbide-fuel experimental subassembly: X079 with 1.33 times the fuel, and sodium reduced by 50 g

NIT ≡ Nitride-fuel experimental subassembly: same as CARB above except uranium carbide replaced by uranium nitride

CR ≡ High-worth Mark-IA-fueled control rod

SR ≡ Mark-IA-fueled safety rod

BOR ≡ Natural-boron-filled (≈400 g) 7-pin subassembly

B ≡ Depleted-uranium-blanket subassembly

TABLE III. Loading of Fig. 7 Projected Core with Stainless Steel Reflector in Rows 7-10

	Number per Row of Various Types of Subassemblies											
Row No.	D	O-1	O-2	S-1	S-2	A	CARB	BOR	NIT	CR	SR	R
1	1											
2	3			1	2							
3	4	2	2				1		1		2	
4	5	1	2	2	2	2	1	2	1			
5	2	3	3	2		5				9		
6	12	3	3	2	2	4		4				
7	6	1	5	4	4	2		4				10
Core Total	33	10	15	11	10	13	2	10	2	9	2	10

D ≡ Driver (Mark-IA) ≈52% ^{235}U enriched

O-1 ≡ Oxide-fuel-element experimental subassembly X062

O-2 ≡ Oxide-fuel-element experimental subassembly X093

S-1 ≡ Structural experimental subassembly X099

S-2 ≡ Structural experimental subassembly X099 with half as much steel

A ≡ 19-pin encapsulated-oxide-fuel experimental subassembly X064

CARB ≡ Carbide-fuel experimental subassembly: X079 with 1.33 times the fuel, and sodium reduced by 50 g

NIT ≡ Nitride-fuel experimental subassembly: same as CARB above except uranium carbide replaced by uranium nitride

CR ≡ High-worth Mark-IA-fueled control rod

SR ≡ Mark-IA-fueled safety rod

BOR ≡ Natural boron-filled (≈400 g) 7-pin subassembly

R ≡ Stainless steel reflector subassembly

Table IV lists the calculations performed. More emphasis was placed on the stainless-steel-reflected core, because the stainless steel reflector was scheduled to be installed before the HWCR system was operative. However, a considerably greater body of calculations and knowledge had been built up for depleted-uranium-blanketed cores, and such correlations provided a basis for the analysis. It was found from the DOT RZ calculation (No. 1 in Table IV) that the axial distribution of power production in the stainless-steel-reflected core, unlike the depleted-uranium-blanketed core, becomes more flat in the outer rows of the core. The row axial distributions in terms of local/average power ratio are shown in Table V.

Calculations 3 and 5 of Table IV were used to obtain the subassembly-by-subassembly variation in power in the XY plane. For these calculations, the control rods were in the fully inserted position. The calculated k_{eff} for the two cases were 1.01132 and 1.01087 for the stainless-steel-reflected and depleted-uranium-blanketed cores, respectively. The relative subassembly power, as provided by the POWER subroutine of these DOT XY problems (see Section III.B below), was used to obtain temperature distributions for the subsequent kinetics calculations described in Section V.

The results of calculations 6-13 in Table IV are discussed in Section IV, Control-rod Worths. More details of all the neutronics calculations are given in Ref. 7.

B. Thermal Hydraulics of Reference Cores

The DOT XY calculations discussed above yield detailed subassembly-by-subassembly power-distribution results, so that one can observe the effects of the heterogeneity of the core. This feature is extremely valuable when one wishes to carry out calculations for an actual core loading. If, however, one wishes to generalize from a particular loading, the amount of detail available is not required. Therefore, in the reference loadings analyzed for this report, the results of the DOT XY calculations were processed to give an average relative radial fission-rate distribution for driver subassemblies in each type of core position (e.g., 3N2, 6N3, as indicated in Fig. 1). In each case, the radial fission-rate distribution was normalized to 1.000 at the core center.

TABLE IV. List of Neutronics Calculations

Calculation No.	Core Configuration	Code	Position[a] of Nine HWCR's	Geometry	Reflector
1	Fig. 7	DOT	Up	RZ	SS
2	Fig. 7	DOT	Down	RZ	SS
3	Fig. 7	DOT	Up	XY	SS
4	Fig. 7	DOT	Down	XY	SS
5	Fig. 6	DOT	Up	XY	Dep. U
6	Fig. 7	CITATION	Up	RZ	SS
7	Fig. 7	CITATION	8 cm below up	RZ	SS
8	Fig. 7	CITATION	8 cm above down	RZ	SS
9	Fig. 7	CITATION	Down	RZ	SS
10	Fig. 6	CITATION	Up	RZ	SS
11	Fig. 6	CITATION	8 cm below up	RZ	Dep. U
12	Fig. 6	CITATION	8 cm above down	RZ	Dep. U
13	Fig. 6	CITATION	Down	RZ	Dep. U

[a] The positions in terms of rod insertion in inches (used in Section V) are as follows:

Up = 14 in. of rod insertion
8 cm below up = 10.85 in. of rod insertion
8 cm above down = 3.15 in. of rod insertion
Down = 0 in. of rod insertion

TABLE V. Axial Power Distribution (Local/Average) for Rows 1-7 in the Stainless-steel-reflected Core

Distance from Core Bottom, cm	Power-density Ratios, Local/Average						
	Row 1	Row 2	Row 3	Row 4	Row 5	Row 6	Row 7
1.150	0.910	0.923	0.911	0.930	0.949	0.968	1.011
3.449	0.938	0.943	0.937	0.944	0.953	0.957	0.972
5.748	0.987	0.987	0.985	0.986	0.988	0.986	0.990
8.048	1.031	1.028	1.029	1.025	1.022	1.017	1.011
10.347	1.065	1.062	1.064	1.058	1.052	1.045	1.033
12.646	1.089	1.086	1.088	1.081	1.073	1.065	1.049
14.946	1.102	1.098	1.100	1.093	1.084	1.076	1.057
17.245	1.102	1.099	1.101	1.094	1.084	1.076	1.056
19.544	1.091	1.088	1.090	1.083	1.074	1.066	1.048
21.844	1.067	1.064	1.067	1.061	1.053	1.047	1.031
24.143	1.032	1.029	1.032	1.028	1.022	1.018	1.006
26.442	0.987	0.984	0.987	0.985	0.983	0.980	0.975
28.742	0.930	0.929	0.931	0.933	0.936	0.938	0.942
31.041	0.866	0.868	0.868	0.874	0.884	0.894	0.910
33.34	0.805	0.812	0.807	0.823	0.842	0.868	0.910

For the stainless-steel-reflected core, the effect of axial power flattening in the outer rows of the core was taken into account by increasing the fission rate in the driver subassemblies of rows 6 and 7 by 2.5% and 5%, respectively. Curves of the relative radial fission-rate distribution for the reference cores are shown in Fig. 8. The stainless steel reflector causes a flattening of the radial distribution, compared to the depleted-uranium reflector.

The relative radial fission-rate distribution, although basic to solution of the problem, does not give the relative radial power distribution as the material in rows 7-10 is changed. Two additional factors enter into the power distribution. One is that, for a given reactor power, the proportion generated in the core region must increase as the blanket in rows 7-10 is replaced by stainless steel. The power produced in rows 7-10 of the blanket decreases as stainless steel subassemblies are installed; this decrease amounts to about 8% of the total. Therefore, the core power fraction increases from 88-90% of the total to 96-98%. The other factor is that, because of the increased reactivity effect of the stainless steel reflector as the material in rows 7-10 is changed, fuel must be removed from the core. Normally, for this purpose, experimental subassemblies replace driver subassemblies. The effect of removing fuel is to increase the power density in the fuel remaining.

The POWDIST program takes all of these factors into account. The relative radial fission-rate distribution, the number of effective subassemblies in each type of core position, and the fraction of the power produced in the core region are all provided as input. (It is possible to consider either six or seven rows as comprising the core region.) An effective subassembly is defined as one that is just equivalent to a driver subassembly. This value can be obtained either from the POWER output subroutine of the DOT XY problem, or from the subassembly-composition input to the DOT XY problem. Normally, the POWER output subroutine has been used because it is the simplest. Both methods were used for the reference cores, however, because all of the fueled experimental subassemblies were of only five types. The agreement between the two methods was very good (within 0.5% for the NIT and A types), giving confidence that the POWER approach was satisfactory.

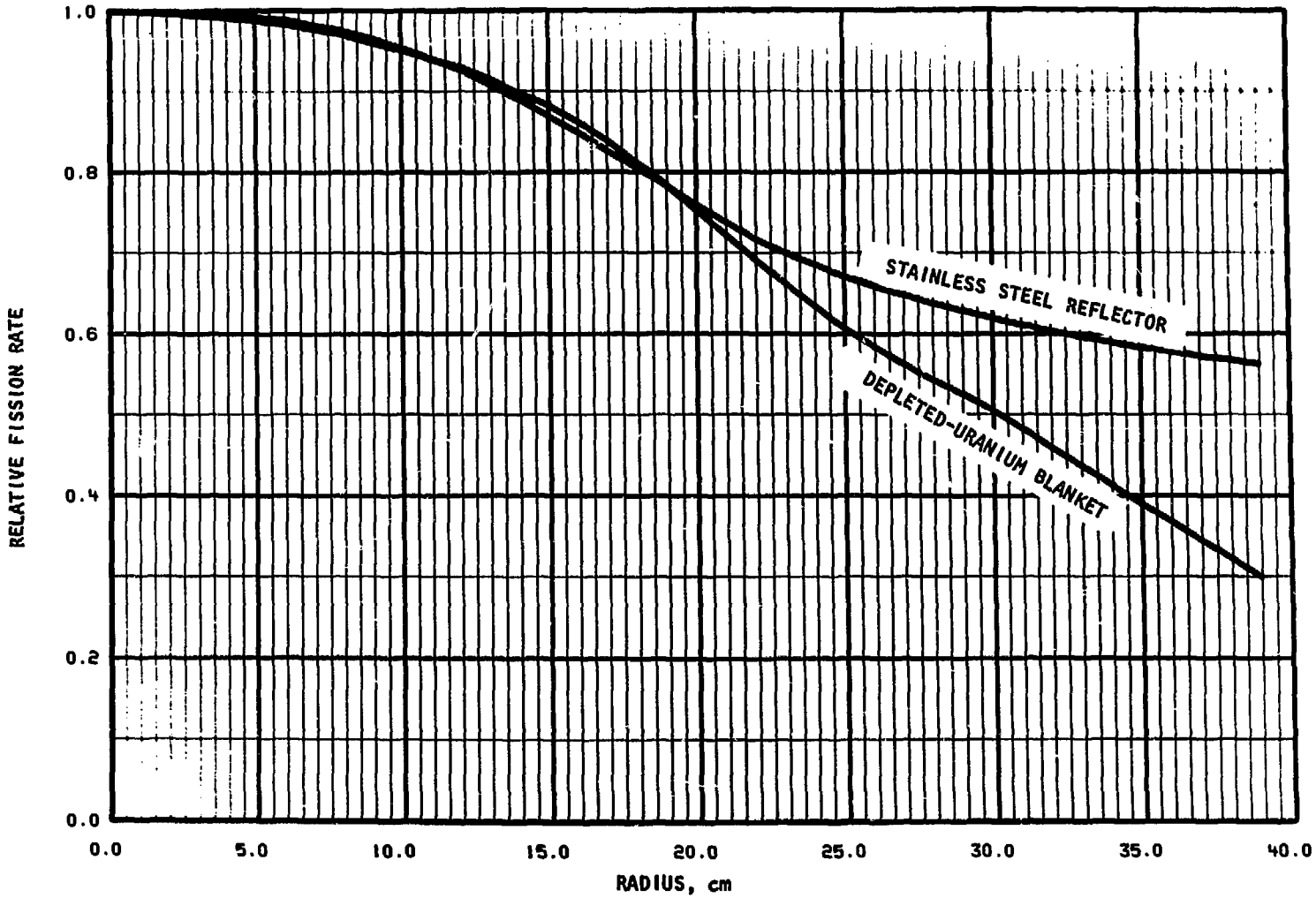

Fig. 8. Relative Fission-rate Distribution with Stainless Steel Relector and Depleted-uranium Blanket

The results of the POWDIST calculations are presented in Table VI, which gives the power per subassembly in each type of core position for the blanketed and the reflected cores and the ratio of the power from a reflected subassembly to that for a blanketed one. The table also gives the number of effective subassemblies used in the POWDIST calculations and the percentage of total power produced in the seven-row region under consideration. For the reference cores, seven rows were used for POWDIST, and all fueled experiments were within the seven rows. Although the values for the percentage of power may be in error, the range of error is no more than about 1%. Some assurance that the overall procedure is valid is given by the fact that the output of the DOT XY problems, if used directly for the 1A1 position, gives a stainless steel/depleted-uranium power ratio of 1.038, compared to the 1N1 value of 1.040 given in Table VI.

The POWDIST code also produces detailed subassembly-power distribution data for use directly in HECTIC calculations. The HECTIC calculations produce detailed temperature distributions within subassembly coolant channels and fuel elements. These calculations were performed for the hottest subassembly sector in each row, and the flowrates for the various rows in each of the cores were obtained using the EBRFLOW[8] code.

Pertinent results of the HECTIC calculations are presented in Table VII, together with the subassembly flowrates used. The values in Table VII are for the hottest channel in each row, but are based on an average radial power distribution, with no effect of flux tilting included. The DOT XY results showed an approximately $\pm 4\%$ variation from the average power for any core position in row 6 or row 7. Figures 9 and 10 show the coolant temperature, cladding inside temperature, fuel-surface temperature, and fuel-centerline temperature along the length of the hottest channel in the core for the depleted-uranium-blanketed and stainless-steel-reflected cores, respectively.

The data in Table VII lead to the conclusion that driver subassemblies are not seriously affected by the change from a depleted-uranium blanket to a stainless steel reflector. A problem may arise in experimental subassemblies where an increase in coolant flowrate does not adequately compensate for an increased linear heat rate.

TABLE VI. Results of POWDIST Calculations

Core Position	Power per Effective Subassembly, kW		Power Ratio, SS Refl. / Dep. U
	Dep. U	SS Refl.	
1N1	1096	1139	1.040
2N1	1079	1126	1.044
3N1	1022	1058	1.036
3N2	1041	1084	1.041
4N1	897	925	1.031
4N2,3	953	977	1.026
5N1	711	792	1.113
5N2,4	784	839	1.070
5N3	811	858	1.057
6N1	564	714	1.266
6N2,5	620	740	1.194
6N3,4	653	758	1.161
7N1	420	665	1.584
7N2,6	485	684	1.410
7N3,5	524	698	1.330
7N4	538	703	1.308
Number of Effective Subassemblies	73.67	70.50	
% of Power in Rows 1-7	92	97	

TABLE VII. Results of HECTIC Calculations for Hot Channel in an Average Driver Subassembly, by Rows, for Core Loadings with Depleted-uranium Blankets or Stainless Steel Reflectors in Rows 7-10

Row	Subassembly Flow, gpm[a]	Maximum Coolant Outlet Temp., °F[a]	Maximum Cladding Inside Temp., °F[a]	Maximum Fuel Center Temp., °F[a]
1	154.5/160.5	928/928	1000/990	1156/1144
2	154.5/160.5	927/928	999/996	1154/1144
3	133.9/139.0	954/956	1023/1018	1170/1161
4	99.0/102.7	1023/1020	1091/1082	1230/1208
5	83.6/86.8	1024/1026	1083/1081	1201/1191
6	72.3/75.1	1011/1036	1061/1090	1160/1198
7	72.3/75.1	956/1008	996/1061	1076/1170

[a] All tabulated values are in the form: depleted-uranium value/stainless-steel-reflector value. Uncertainty factors have been omitted.

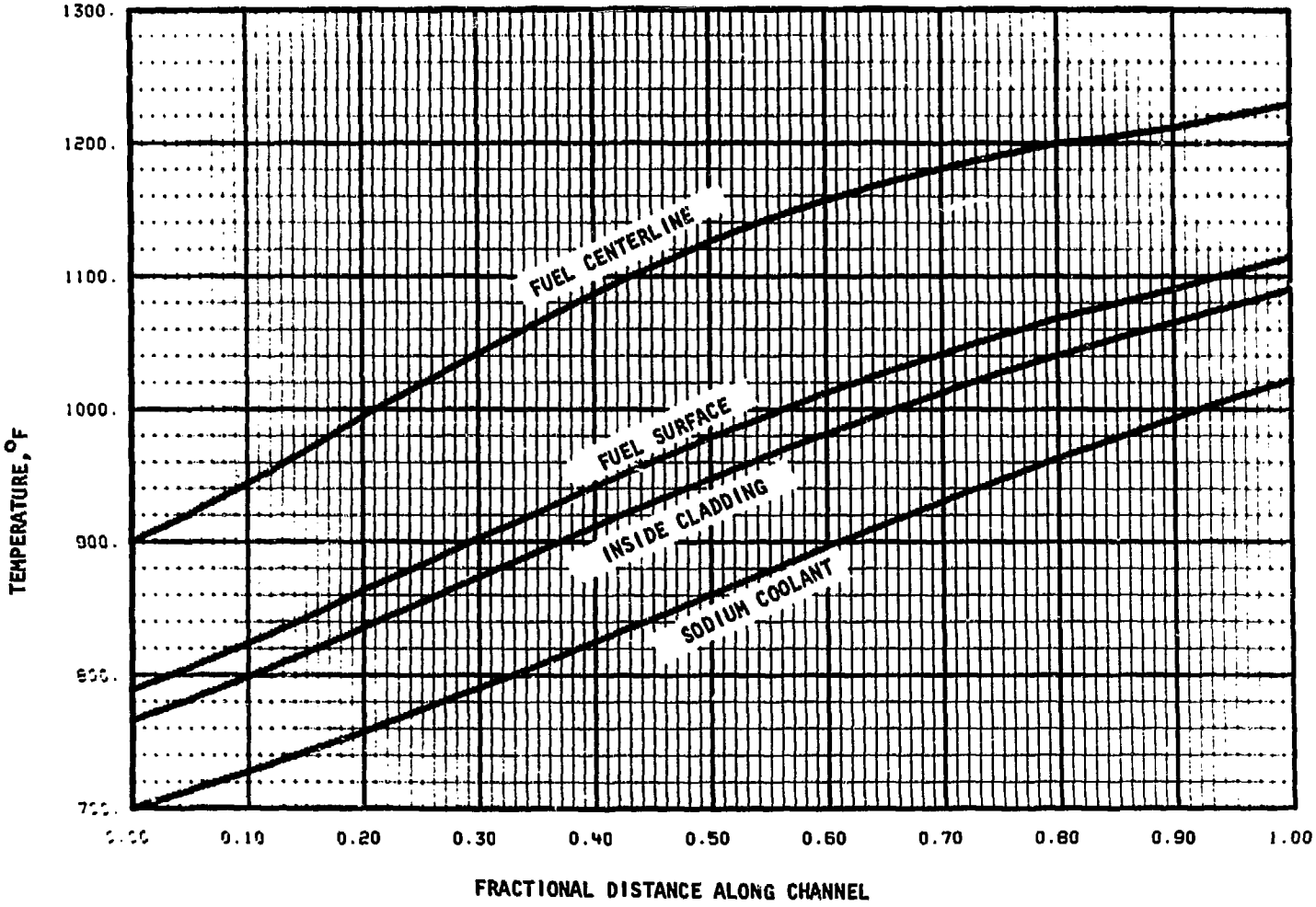

Fig. 9. Temperature Distribution in Hot Channel of Row 4 of Core with Depleted-uranium Blanket

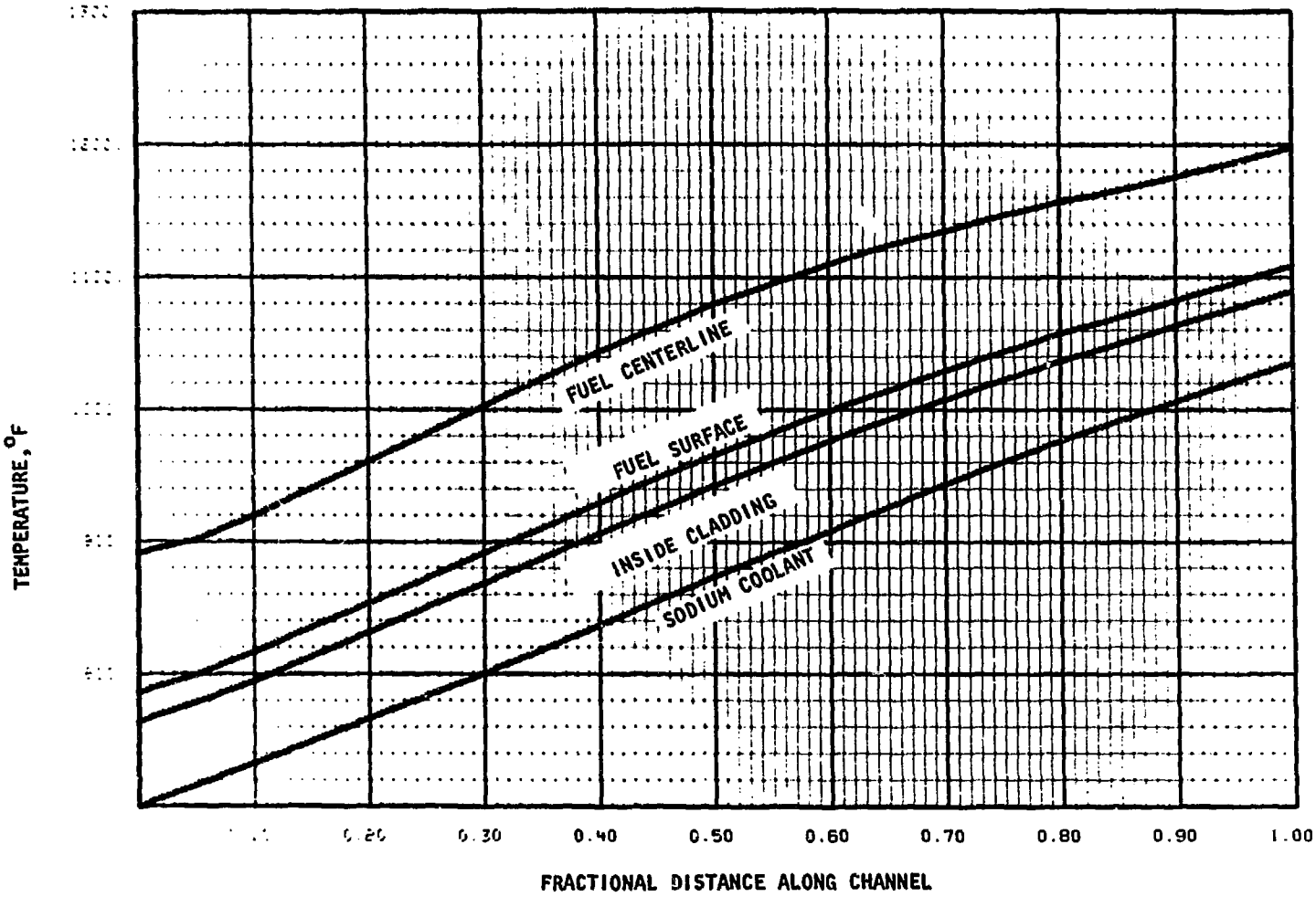

Fig. 10. Temperature Distribution in Hot Channel of Row 6 of Core with Stainless Steel Reflector

IV. CONTROL-ROD WORTHS

As discussed in Section III.A and shown in Table IV, a series of problems using the CITATION code was carried out to calculate the worth of the HWCR's as a function of position in both of the reference cores. There were nine control rods in each of the reference cores, although reactor operation with eight or less is expected, and the validity of the analyses is not affected by the choice of nine rods. The CITATION calculations were performed for RZ geometry, and the nine HWCR's were cylindrically homogenized throughout row 5. The different axial regions (i.e., gas plenum, upper reflector or shield, boron carbide, upper gap, pin tops, lower gap, and lower reflector) were treated individually, and four axial positions of the control rod were used: up, down and 8 cm away from both extremes. The four axial positions used, together with the axial heights of the seven regions of the HWCR, are shown in Fig. 11, and the composition of each of the seven regions is given in Table VIII. Each HWCR contains 887 g of natural B_4C, of which 135 g is ^{10}B.

The results of the eight CITATION calculations are summarized in Table IX, which gives the values of k_{eff} obtained in calculations 6 through 13 (Table IV), together with the average values of $\Delta k/k$ for a HWCR in the three positions different from the full-up position. These results show that the average worth of a HWCR for the depleted-uranium-reflected core is ≈6% less than that for the stainless-steel-reflected core.

Since the results in Table IX were obtained with CITATION code in 2D diffusion theory in RZ geometry, corrections for transport and for boron self-shielding effects may have to be applied. Results for k_{eff} from two DOT RZ transport-theory calculations (calculations Nos. 1 and 2) for the stainless-steel-reflected core in which the nine HWCR's are, respectively, in the "up" and "down" position in row 5, are shown in Table X. The transport-theory result for the average worth of one HWCR is ≈3% lower than the diffusion-theory result. Thus, the transport correction appears to be only ≈3%.

The subassembly-wide boron self-shielding was estimated from the boron activation obtained in the DOT XY calculation (calculation No. 4) in which the nine HWCR's were in the down position. The ratio of the boron

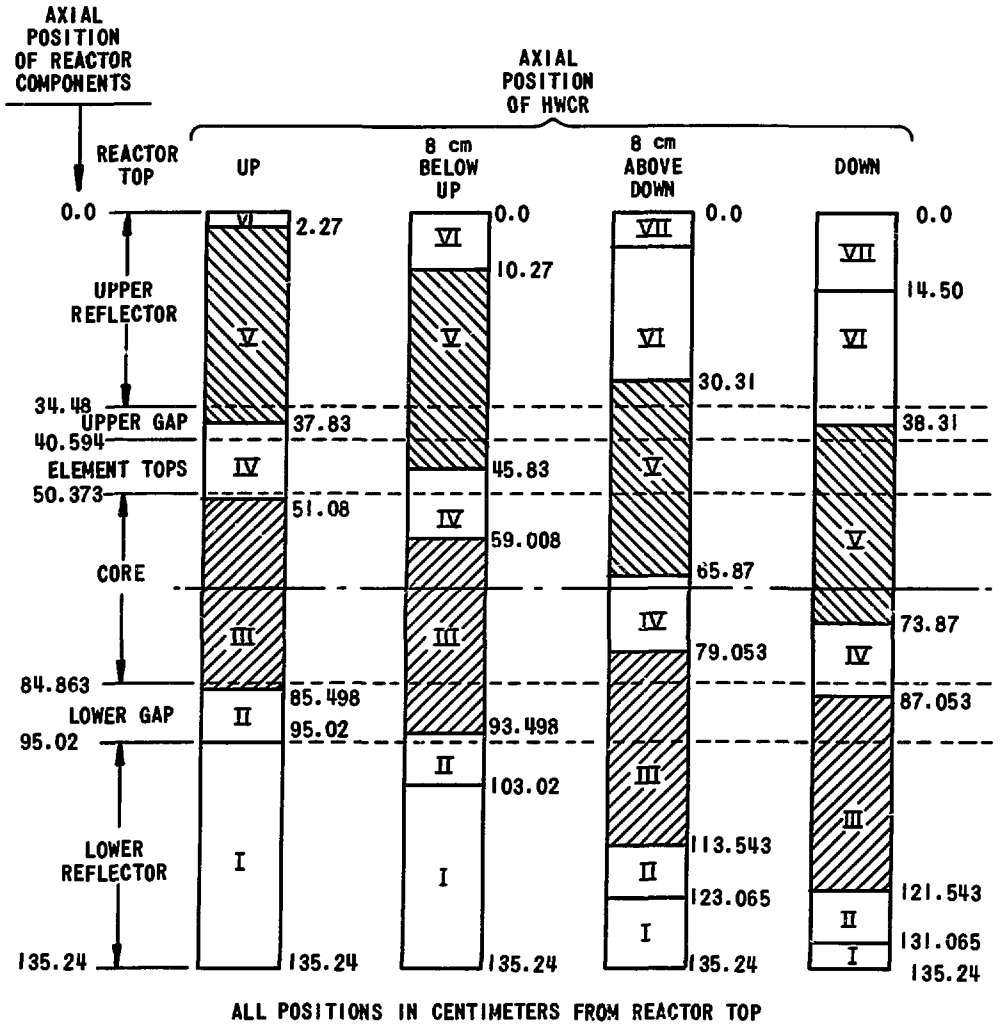

Fig. 11. Axial Positions Used in HWCR Calculations

TABLE VIII. Regional Compositions of the HWCR

Isotope	Homogenized Densities, atoms/barn-cm[a]						
	Region 1 (SS and Na)	Region II (SS and Na)	Region III (Fuel)	Region IV (SS and Na)	Region V (B_4C)	Region VI (SS and Na)	Region VII (SS and Na)
^{235}U			4.6546E-3				
^{239}Pu			1.9200E-6				
^{238}U			4.2493E-3				
Mo			6.1756E-4				
Nb			3.0140E-5				
Zr			5.0550E-4				
Fe	3.5525E-2	3.3039E-2	1.1664E-2	1.6760E-2	1.3608E-2	1.4625E-2	1.3608E-2
Ni	4.4978E-3	4.1830E-3	1.5970E-3	2.1034E-3	1.7079E-3	3.9487E-3	1.7079E-3
Cr	1.0152E-3	9.4410E-3	3.2696E-3	4.6250E-3	3.7554E-3	4.4342E-3	3.7554E-3
Na	9.2164E-3	1.0152E-2	1.3443E-2	1.3843E-2	9.6261E-3	9.2596E-3	9.2593E-3
C					9.2330E-3		
^{10}B					7.5100E-3		

[a] Values are given in exponential form; i.e., 3.5525E-2 = 0.035525

TABLE IX. Results of Rod-worth Calculations,

Using CITATION Code in RZ Geometry

Calculation No.	Reflector	Position of 9 HWCRs	k_{eff}	% Δk/k for 9 HWCRs	Average % Δk/k for 1 HWCR	Corrected Average % Δk/k for 1 HWCR
6	SS	Up	1.105404	--	--	--
7	SS	8 cm below up	1.005730	-0.953	-0.106	-0.097
8	SS	8 cm above down	0.964638	-5.000	-0.556	-0.510
9	SS	Down	0.948928	-6.547	-0.727	-0.667
10	Dep. U	Up	1.015588	--	--	--
11	Dep. U	8 cm below up	1.006429	-0.902	-0.100	-0.092
12	Dep. U	8 cm above down	0.967788	-4.707	-0.523	-0.480
13	Dep. U	Down	0.953214	-6.142	-0.682	-0.626

TABLE X. Results of Rod-worth Calculations,

Using DOT Code in RZ Geometry

Calculation No.	Reflector	Position of 9 HWCRs	k_{eff}	% Δk/k for 9 HWCRs	Average % Δk/k for 1 HWCR	Ratio to Diffusion-theory Value
1	SS	Up	1.03004	--	--	--
2	SS	Down	0.964657	6.348	0.705	0.970

activation averaged over the nine HWCR subassemblies to that averaged over all the subassemblies in row 5 was found to be 0.946. Thus the average subassembly-wide boron-self-shielding correction was taken as ≈5.4%.

Using the above corrections, the corrected average worths for one HWCR are shown in the last column of Table IX. The average worth of an HWCR in the stainless-steel-reflected core is -0.667% Δk/k, and in a depleted-uranium-blanketed core it is -0.626% Δk/k. Even though the core loading used in the calculations is projected, rather than actual, and is considerably more ordered and symmetrical than an actual core loading, there is a definite asymmetry in the worths of the various control rods. For the stainless-steel-reflected core loading with all the HWCR's in the down position, a rough measure of the worth asymmetry can be obtained from the asymmetry of the ϕ^2 values given in Table XI (where ϕ is defined in note a). The table gives the values of ϕ^2, the ratio of ϕ^2 to the average ϕ^2, and the deduced worth from an assumed proportionality of the worth to ϕ^2. The maximum deviations of the deduced worths from the average are ≈±21%.

As mentioned in Section I, a prototype high-worth control rod has been in EBR-II since run 46B (October 1970). The question naturally arises, how do the calculated values for the HWCR compare with those actually measured?

An analysis has been made of 19 reactor loadings, comprising runs 46B through 51C, to determine the worth of a HWCR in actual cores with a depleted-uranium blanket. During the first two loadings, the HWCR was in core position 5A3, on the flat of sector A (see Fig. 1). It was then moved to corner position 5C1, where it remained for the rest of its exposure. The measured worths of the rod on the flat were 264 and 277 Ih, and when adjusted for asymmetry effects, the average worth of the HWCR on the flat was 266 Ih. The measured worths of the HWCR in the corner position varied between 192 and 238, and averaged 217 Ih. When the measured corner worths were adjusted for asymmetry (by taking the ratio of the average worths of all control rods on the flats to the average of the two control rods on the flats adjacent to the HWCR and multiplying the worth of the HWCR by this ratio), the two former extreme values became 225 and 227 Ih, respectively, and the average for the 17 core loadings with the HWCR in 5C1 became 231 Ih. The worth of an HWCR on the flat was 1.15 times the worth at the corner.

TABLE XI. Asymmetry of Worths of HWCR's

in Stainless-steel-reflected Core

Position	ϕ^{2} [a]	$\frac{\phi^2}{\phi^2 \text{ avg}}$	Deduced Worth, % Δk/k	Deduced Worth, Ih [b]
5A1	2.4182E-4	1.056	0.704	302.8
5B1	2.0276E-4	0.885	0.592	253.9
5B3	2.4035E-4	1.049	0.700	301.0
5C1	1.8291E-4	0.799	0.533	229.0
5C3	2.6606E-4	1.162	0.755	333.2
5D3	2.7820E-4	1.215	0.810	348.4
5E1	2.0074E-4	0.877	0.585	251.4
5E3	2.4978E-4	1.091	0.727	312.8
5F1	1.9858E-4	0.867	0.578	248.7

ϕ^2 avg = 2.2902E-4 Avg worth = 0.667% Δk/k

[a] $\phi = \sum_{g=1}^{29} \phi(g)$ = total neutron flux/k_{eff}. Values are given in exponential form; i.e., 2.4182E-4 = 0.00024182

[b] 1% Δk/k = 430 Ih.

The average worths of standard control rods obtained for runs 47 through 52A were 158 Ih (flat) and 137 Ih (corner, and the flat-to-corner ratio was again 1.15. The worth of the HWCR was thus measured to be 1.69 times that of a standard rod in an operating core with a depleted-uranium blanket.

As Table XI shows, there were five corner rods (5N1) and four flat rods (5N3) in the calculated stainless-steel-reflected core. Their average worths were 257 Ih for corner rods and 324 Ih for flat rods, with a flat-to-corner ratio of 1.26. To determine if this change in ratio was to be expected with a stainless steel reflector, the average worths of control rods (flat and corner) were determined for an earlier period in which a stainless steel reflector had been used in rows 7 and 8 (runs 25-29A). The worths were also determined for the immediately following period in which the depleted-uranium blanket had been restored (runs 30A-33A). The results were, for runs 25-29A, that the standard rod was worth 148 Ih on the flat and 133 Ih on the corner, with a ratio of 1.11. Corresponding values for runs 30A-33A were 160, 143, and 1.12.

The flat-to-corner ratio of 1.26 obtained from Table XI may be too high. Consequently, the total worth of the nine rods in Table XI (viz., 2582 Ih) was retained, but the ratio of the flat-to-corner worths was arbitrarily set at 1.15 to agree with experience.* This resulted in new average worths, in a stainless steel-reflected core, of 309 Ih for a flat HWCR and 269 Ih for a corner HWCR. The calculated HWCR worths for a depleted-uranium-blanketed core are 6% less than the above, or 291 and 253 Ih, respectively.

The worths of various control rods in the different loadings, as discussed above, are presented in summary form in Table XII.

The calculated worths of HWCR's in a depleted-uranium-reflected core, after the adjustment of the flat-to-corner ratio, are 9% higher than the measured values of a single HWCR. The measured value of an HWCR is 1.69 times the measured value of a standard control rod.

---

*It is not obvious how reliable correlations and predictions for a four-row reflector with measurements in a two-row reflector can be; nevertheless, the indicated trend was applied.

TABLE XII. Summary of Calculated and Measured Control-rod Worths

Type of Rod	Material in Rows 7-10	Control-rod Worth, Ih		Flat/ Corner Ratio	How Obtained
		Flat	Corner		
Standard	Dep. U	158	137	1.15	Measured runs 47-52
HWCR (only one)	Dep. U	266	231	1.15	Measured runs 46B-52A
HWCR	Dep. U	305	242	1.26	Calculated
HWCR	Dep. U	291	253	1.15	Calculated, then adjusted
HWCR	SS	324	257	1.26	Calculated
HWCR	SS	309	269	1.15	Calculated, then adjusted
Standard	SS (2 rows)	148	133	1.11	Measured, runs 25-29A
Standard	Dep. U	160	143	1.12	Measured, runs 30A-33A

The shape of the worth curve as a function of insertion for the HWCR was measured in both flat and corner positions and found to be identical. The shape of the worth curve for the standard control rod is similar; and both are plotted in Fig. 12, where the worth is given as a percentage of total worth. Also shown in Fig. 12 are the four points calculated for the bank of nine HWCR's.

Although the shapes are similar for the two types of rods, there is significant difference between them. This difference is illustrated in Fig. 13, where the slopes of the curves of Fig. 12 have been plotted, so that the percentage of total rod worth added per inch of insertion is shown. The flatter portion of the curve appears at a lower insertion for the HWCR than for the standard control rod, an undesirable feature, because the boron portion of the rod is still well within the core region at this point. The control rod that is used as the regulating rod during operation is generally moved up and down through the flatter portion of its curve so that the operator can expect that a given motion produces a relatively constant amount of reactivity change. Although calculations have shown that a fully withdrawn HWCR produces less than a 5% variation in flux in adjacent subassemblies, it is undesirable to operate with the B_4C portion of the control rod in the core (i.e., at less than ≈8.5 in. of fuel insertion). Measurements have shown that operation of the single HWCR in the range of 7-14 in. insertion does not significantly affect the axial flux distribution as determined by worth of adjacent standard control rods or power production in surrounding subassemblies.[9]

The present mode of operation with standard control rods in EBR-II is to start a run with the "bank" position of the control rods (all but one) at 10-1/2 to 11 in. The regulating rod, which is one of the control rods (a different rod each run, so as to equalize use of all control rods over an extended period), moves from 6 to 9 in. as the run progresses and reactivity is burned out of the core. When the regulating rods reaches 9 in., the rods are rebanked further into the core, and the regulating rod is returned to the 6-in. position. This procedure is continued until the end of the run, when the rod bank is at 14 in. A similar approach is expected to be used with the system of HWCR's.

The control-rod worths tabulated in Table XII have been used to produce Table XIII, which presents the system worths for various combinations of control rods. The present mode of operation, with a depleted-uranium blanket, requires about 1400 Ih available in all the control rods,

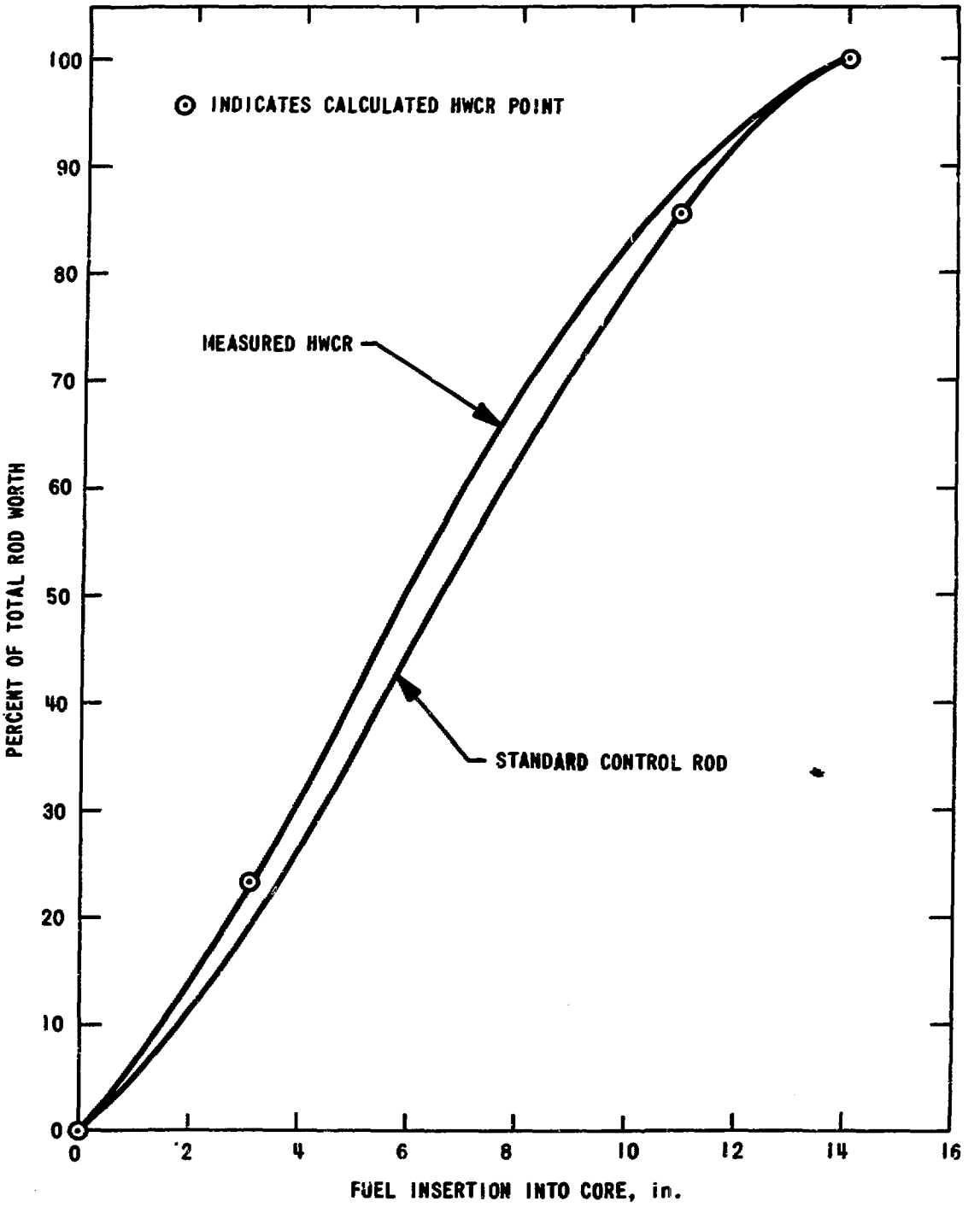

Fig. 12. Relative Control-rod Worths as a Function of Fuel Insertion

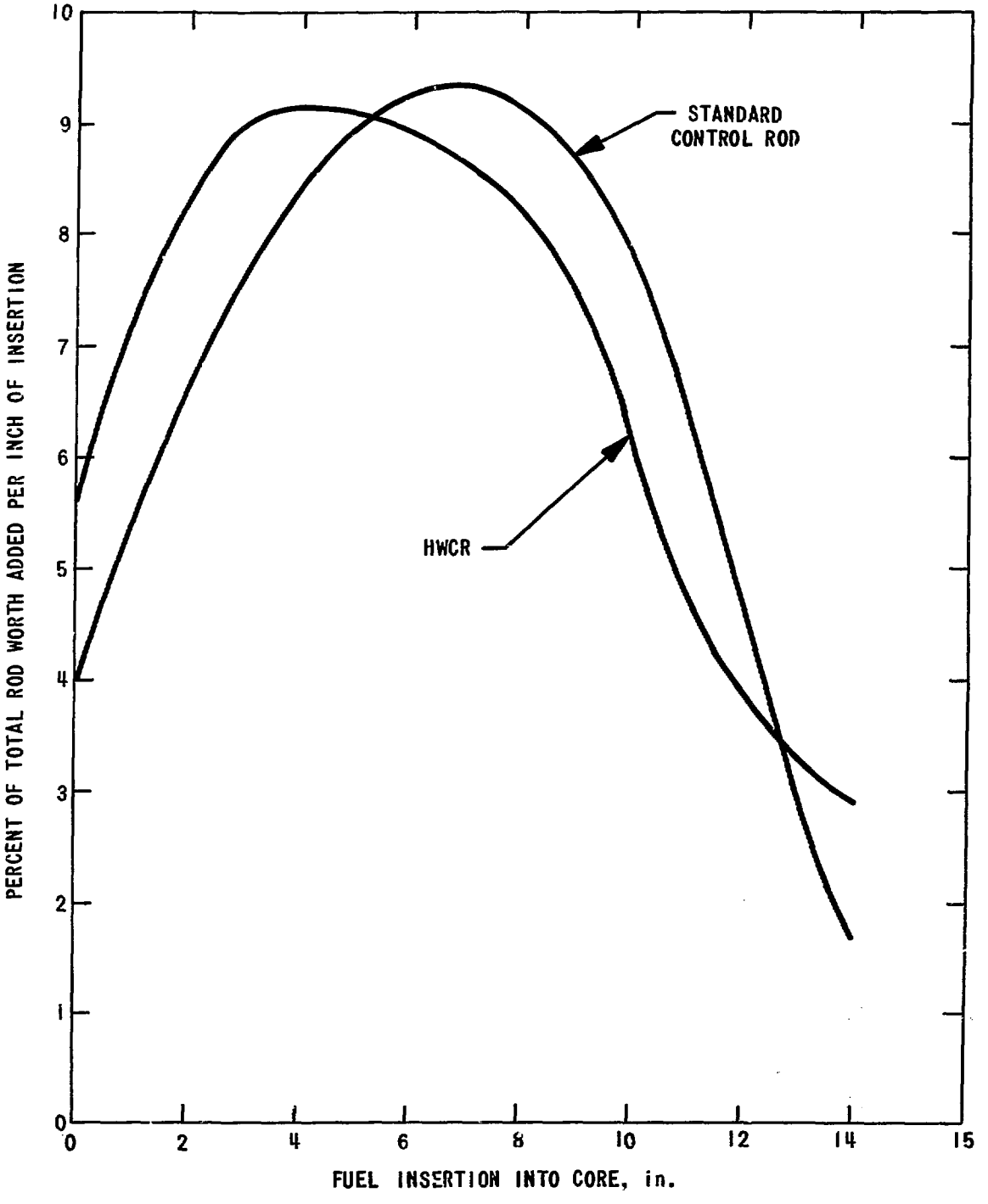

Fig. 13. Incremental Worth of Control Rods as a Function of Fuel Insertion

TABLE XIII. Total Worth of Control-rod Systems, Ih

Number and Type of Rods	Dep.-U Blanket			SS Reflector			
	Present Std. CR	Calc. HWCR Ratio= 1.26	Adjus. HWCR Ratio= 1.15	Calc. HWCR Ratio= 1.26	Adjus. HWCR Ratio= 1.15	0.913 Times Adjus. HWCR[a]	Prev. Col., But One Corner Rod a Std. CR
6 corner	822	1452	1518	1542	1614	1474	1374
6 corner, 1 flat	980	1757	1809	1866	1923	1756	1656
6 corner, 2 flat	1138	2062	2100	2190	2232	2038	1938
6 corner, 3 flat	1296	2367	2391	2514	2541	2320	2220
6 corner, 4 flat	1454	2672	2682	2838	2850	2602	2502
5 corner, 2 flat	1001	1820	1847	1933	1963	1792	1692
5 corner, 3 flat	1159	2125	2138	2257	2272	2074	1974
5 corner, 4 flat	1317	2430	2429	2581	2581	2356	2256
4 corner, 3 flat	1022	1883	1885	2000	2003	1829	1729
4 corner, 4 flat	1180	2188	2176	2324	2312	2111	2011

[a] Makes calculated values agree with measured worths of HWCR

and this requires at least ten standard control rods. Table I indicated that 1620 lh would be required with HWCR's. Table XIII shows that several combinations that require only seven control rods will be adequate, even if one of the seven is a standard control rod. This approach, which is shown in the last column of Table XIII, allows the regulating rod to be a standard control rod, with the advantages for regulation such a rod provides. Run lengths in excess of 3000 MWd will be possible with the use of eight control rods.

V. SAFETY ANALYSIS FOR HIGH-WORTH CONTROL ROD

The question of the safety of operating EBR-II with HWCR's has two basic aspects: the reactivity effects and the nonreactivity effects. The reactivity effects can also be considered from two aspects: Can a control-rod system utilizing HWCR's meet the operating limits and can it trip the reactor rapidly enough in the event it is called on to act by the plant protective system; and does the use of HWCR's result in too severe a reactivity insertion, under certain conditions, as compared to the standard control rods? The nonreactivity effects primarily involve the integrity of the B_4C capsule during its residence in the reactor. The two basic aspects of the safety evaluation of the HWCR are covered in turn in this section.

A. A Study of the Dynamic Response of Cores Containing High-worth Control Rods

1. Calculational Methods

Six hypothetical reactivity accidents and several loss-of-coolant flow sequences were considered in the EBR-II safety documents[1,2] to assess the safety characteristics of the EBR-II reactor and to estimate the consequences of the accidents. These were:

Case 1. The reactor is at the delayed-critical condition (zero power), with the safety rods out of the core. The safety rods are assumed to be driven into the active core in an uncontrolled manner at their normal speed of approximately 2 in./min.

Case 2. The reactor is at the delayed-critical, zero-power condition with the central driver-fuel subassembly removed. The central subassembly is then assumed to be loaded into the core at a regular speed of 6 in./min.

Case 3. The reactor is at the delayed-crtical, zero-power condition with a single control rod removed. The control rod is then assumed to be driven into the core in an uncontrolled sequence at 5 in./min.

Case 4. This case is similar to Case 3 except that the power transient begins at full operating power (62.5 MWt).

Case 5. In this hypothetical accident, the reactor is assumed to be at the delayed-critical, zero-power condition with a central driver-fuel subassembly being loaded into the core. A failure is then assumed to occur in the grapple mechanism, thereby dropping the driver-fuel subassembly into the core.

Case 6. The reactor is at the delayed-critical, zero-power condition with a central driver-fuel subassembly removed. This subassembly is then introduced at the highest speed of the gripper mechanism (72 in./min).

Case 7. This hypothetical accident is the only sequence involving loss of coolant flow. The accident sequence is initiated by a reactor trip, followed by loss of primary pumping power.

Of the seven hypothetical unprotected accidents postulated in the original safety documents, only Cases 3 and 4 will be affected by the change from the original standard control rods to the new high-worth control rods. Cases 1, 2, 6, and 7 are independent of the type of control-rod system as long as the amount of negative reactivity provided by the tripping of the control-rod bank is maintained as at present. This is due to the short time (<300 msec), relative to the duration of the accident, required for the rods to travel from the full-in to the full-out position under scram conditions. This high rate of reactivity removal nullifies any measurable effect on the accident from the slight difference between the worth curves (Fig. 12) of standard and high-worth control rods. In Case 5, melting is initiated in about 100 msec. The plant-protective system cannot act rapidly enough to prevent initiation of fuel melting. Therefore, only the accidents of Cases 3 and 4 have been reexamined to ascertain the effect of replacing standard control rods with high-worth control rods.

The analyses of Cases 3 and 4 were carried out with the EROS code. This code models the average thermal-hydraulic features of EBR-II by a series of average channels. Each channel represents a driver-fuel element and its associated sodium coolant.[10] In this analysis, there are eight such channels, one to represent the average metallic driver-fuel element in each of the seven rows of the core and one to represent the average control-rod fuel element in row 5. Each of these eight feedback channels is constructed of six radial regions: three to represent the fuel; and one each to represent the sodium bond, the cladding, and the coolant.

In the course of a reactivity transient, the power, and consequently the temperature, changes in each of these average channels. EROS calculates these changes in temperature and multiplies each of them by the portion of the total core feedback which is associated with that average channel. The eight feedback reactivities are then summed to obtain the total core feedback. The feedback and inserted reactivity are then summed to obtain the system reactivity, which is used in the point kinetics equation to recalculate power. This cycle is repeated at each time step until the accident is terminated. The result of an EROS calculation for a reactivity transient is a feedback-corrected power history for the reactor core. This power history can be used to calculate the temperature transient in any fuel element in the reactor.

The primary components of the EBR-II feedback network are: core driver-fuel axial expansion, core sodium-density effects, axial-reflector sodium-density effects, expansion of the stainless steel or uranium in the radial blanket, subassembly bowing, and control-rod expansion effects.[11] All of these components are negative except for the subassembly bowing, which is a small component for a depleted-uranium blanket and has been calculated to be a small component for the new stainless steel reflector.[12] A comparison of the major feedback components that have been calculated for various EBR-II core configurations is presented in Table XIV. The coefficients for this study were taken from data presented in Ref. 13 for a stainless-steel-reflected core (last column of the table). Of the major feedback components, only the core sodium density and driver-fuel axial expansion were considered in this report. For added conservatism, only

TABLE XIV. Components of the Temperature Coefficient of Reactivity ($\Delta k/k/^{o}F \times 10^{5}$)

Feedback Component	Original Prediction[a]	Run 26, SS Refl.[b]	Run 26 Dep. U[c]	Calc. for Dep. U[d]	Calc. for SS Refl.[e]
Core sodium density	-0.447	-0.462	-0.458	-0.478	-0.449
Density of sodium in radial blanket	-0.113	-0.069	-0.046	-0.082	-0.123
Density of sodium in axial blanket	-0.304	-0.444	-0.452	-0.239	-0.232
Axial expansion of fuel	-0.258	-0.196	-0.177	-0.266	-0.228
Density of uranium and SS in axial blanket	Uranium -0.016 SS -0.049	SS -0.079	SS -0.080	SS -0.098	SS -0.099
Density of uranium and SS in radial blanket	Uranium -0.052 SS -0.021	SS -0.084	Uranium -0.039 SS -0.052	Total -0.075	SS -0.151

[a] Ref. 2.

[b] Values from Ref. 11; run 26 with stainless steel reflector.

[c] Values estimated for a run-26 depleted-uranium blanket, using data from Ref. 11.

[d] Calculated values for depleted-uranium blanket from Ref. 13.

[e] Calculated values for stainless steel reflector from Ref. 13.

that portion of the core-sodium-density coefficient associated with the sodium in the driver fuel was assumed to provide reactivity feedback in a transient. This assumption effectively reduces the value of the core-sodium-density coefficient used in this report to 44% of that given in Table XIV. The feedback resulting from the expansion of the control-rod shafts was also used in this report when the accident was initiated with the reactor at full power.

Table XV presents the feedback coefficients used in this report, including the coefficients for HWCR shaft expansion. The coefficients were distributed as appropriate over the eight feedback channels to make the calculations.

In these analyses, the worth of the HWCR inserted during the postulated accident was assumed to be either 0.81% Δk/k (1.227$), or 0.50% Δk/k (0.7576$). The larger value corresponds to the greatest worth calculated for an HWCR in the projected stainless steel core (see Table XI) and 0.50% Δk/k corresponds to an HWCR of below-average worth or the worth of a peak standard control rod. Table XVI compares the control-rod insertion rates used in the past for standard control rods with the insertion rate of the greatest-worth rod of the HWCR type in a stainless-steel-reflected core.

As discussed above in this section, the Case-3 and -4 types of accident were selected for analysis with EROS. Case 3 corresponds to a control-rod-insertion-at-startup accident, and Case 4 corresponds to a control-rod-insertion-at-power accident. Five Case-3-type accidents and three Case-4-type accidents were analyzed, and the results of these are discussed below. It must be emphasized that in the analysis of these eight accidents, the plant protective system was assumed to be inoperative.

2. Case 3--HWCR Insertion at Startup

a. First Subcase at Startup

(1) Assumptions: The stainless-steel-reflected reactor is assumed to be just critical with 50 kW of power and full flow. The highest-worth control rod, which has a total worth of 1.227$, is assumed to be driven into the reactor at 5 in./min from full-out position. Feedback is assumed to consist of core-driver-fuel axial expansion and core-driver-fuel sodium expansion. There is no feedback assumed from control-rod expansion.

TABLE XV. Feedbacks Used in EROS Analyses of Cores Containing HWCR's

	Feedbacks for Cores with SS Refl., $/°F	Feedbacks for Cores with Dep. U, $/°F
1. Core-driver-fuel axial expansion	-0.00035	-0.00038
2. Core-driver-fuel sodium expansion	-0.00030	-0.00056
3. Control-rod-shaft expansion	0.096$/cm	-0.11$/cm
4. Blanket-sodium expansion	---	-0.00012
5. Blanket-uranium expansion	---	-0.00011

TABLE XVI. Reactivity-insertion Rates for One Control Rod

	Ref. 1	From ZPR-III Mockup	EBR-II Dry Critical	Ref. 2	Based on Run-37 Calibrations	Max. Calc. HWCR Values
Total reactivity worth, % Δk/k	<0.6	0.37	0.35	0.4	0.35	0.81
Drive speed, in./min	5.0	--	5.0	5.0	5.0	5.0
Effective stroke, in.	14.0	--	14.0	14.0	14.0	14.0
Reactivity insertion rates, Δk/k per sec						
Average	0.003	0.0022	0.0021	0.0021	0.0021	0.0048
Maximum	<0.006	0.0040	0.0030	<0.0041	0.0036	0.0067

(2) Results: The centerline temperature in the hottest metallic fuel pin is at 700.4°F at the initiation of the accident. Centerline temperatures in the hottest driver do not exceed 710°F until 53 sec into the transient. Melting in the hottest driver (1834°F) occurs at 79 sec. The fuel-cladding eutectic temperature (1319°F) is exceeded at 76 sec. The shortest reactor period is 4.16 sec and occurs 64.7 sec into the transient. The maximum excess reactivity of the system (inserted reactivity plus feedback) occurs at 66 sec and is 53¢.

Figure 14 is the temperature history in the hottest driver element. The curves are, from top to bottom, the fuel-centerline temperature, the fuel-surface temperature, the cladding temperature, and the sodium-coolant temperature. Figures 15, 16, and 17 are plots of the inserted reactivity, feedback, and system reactivity as functions of time.

b. Second Subcase at Startup

(1) Assumptions: Reactor conditions are the same as in the first subcase except that the inserted rod is worth 0.5% Δk/k (0.7676$) instead of 0.81% Δk/k (1.227$).

(2) Results: The initial temperature in the hottest driver is 700.4°F. The centerline temperature in the hottest driver does not excees 710°F until 72 sec into the transient. Melting in the hottest driver occurs at 112 sec. The fuel-cladding eutectic temperature is exceeded at 108 sec; the shortest reactor period occurs 88 sec into the transient and is 6.39 sec; and the maximum excess reactivity occurs 90 sec into the transient and is 45.14¢. Figure 18 is the temperature history in the hottest driver element.

c. Third Subcase at Startup

(1) Assumptions: Same as for the first subcase except that the coolant flowrate has been reduced to 1% of the full flowrate. The worth of the inserted rod is 1.227$.

(2) Results: The initial centerline and coolant temperatures in the hottest channel are 726.6°F and 726.4°F, respectively. Melting temperatures are reached in the peak driver element 82 sec into the transient. The fuel-cladding eutectic temperature is exceeded at 72 sec. The shortest reactor period is 5.6 sec and occurs 59.9 sec into the transient. The maximum excess reactivity occurs at 59.9 sec and is 47.3¢.

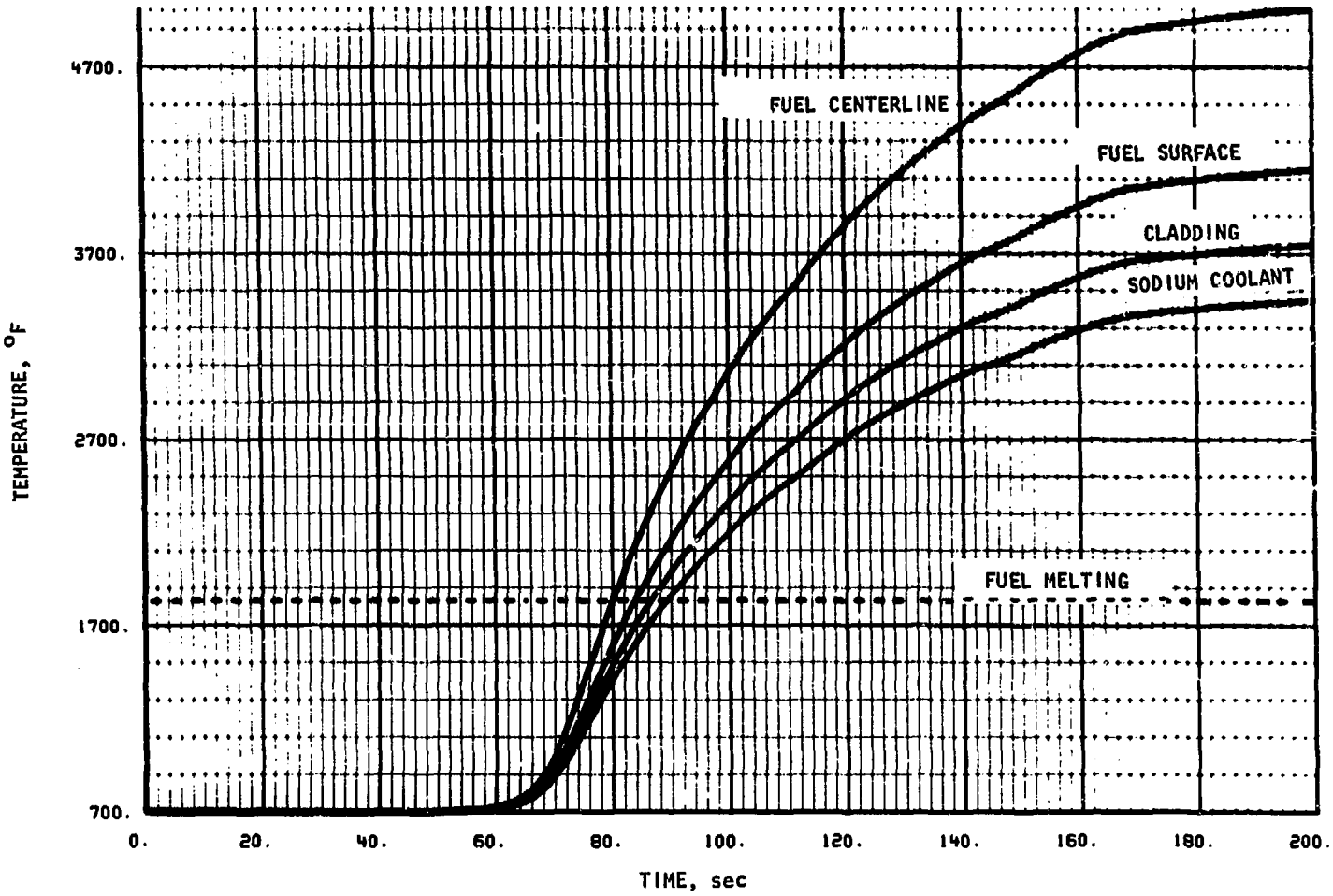

Fig. 14. Peak Driver-fuel-element Temperatures After One Control Rod Worth 1.227$ is Driven into a Stainless-steel-reflected Core; Initial Power of 50 kW and Full Flow

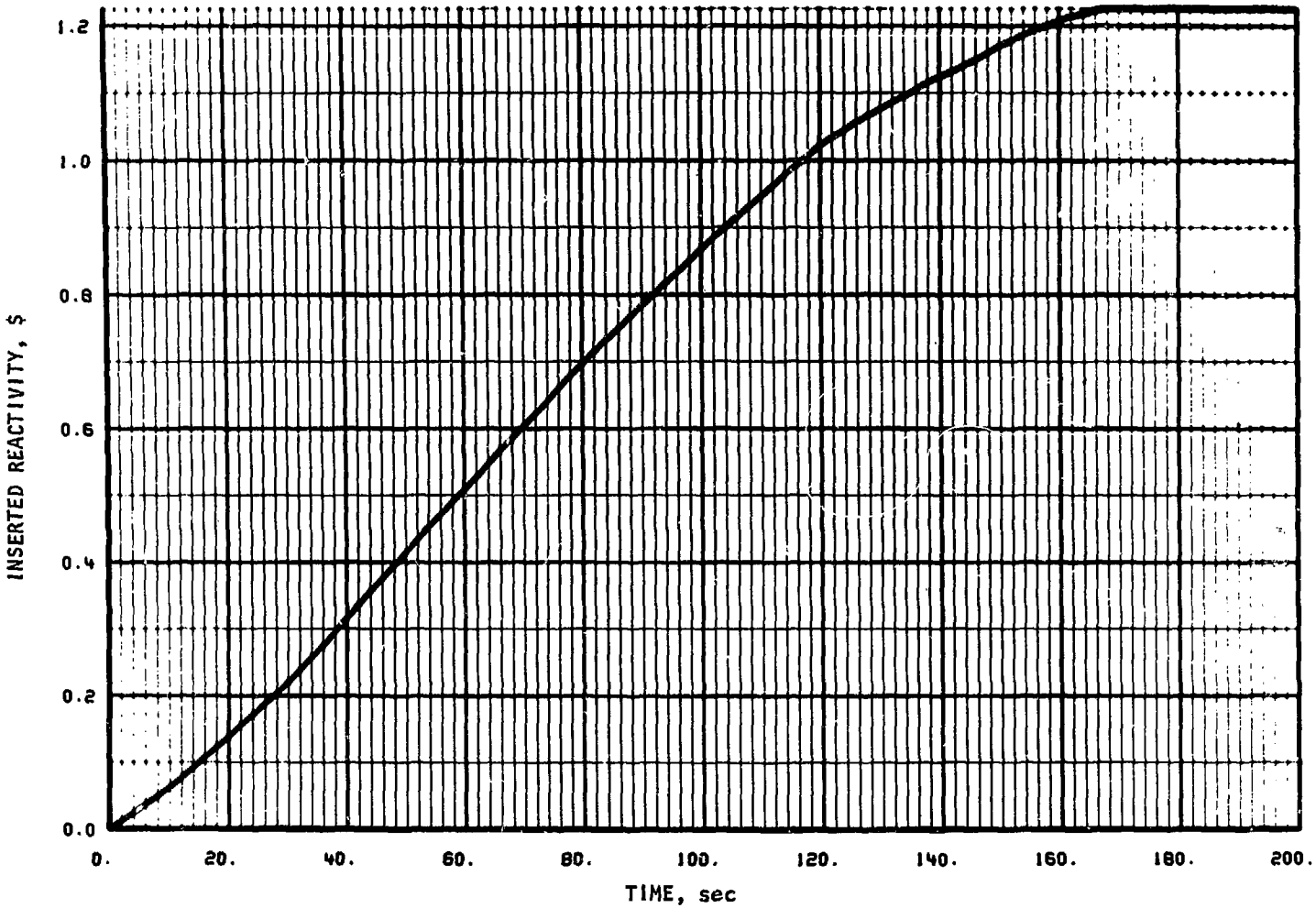

Fig. 15. Inserted Reactivity vs Time After One Control Rod Worth 1.227$ is Driven into a Stainless-steel-reflected Core; Initial Power of 50 kW and Full Flow

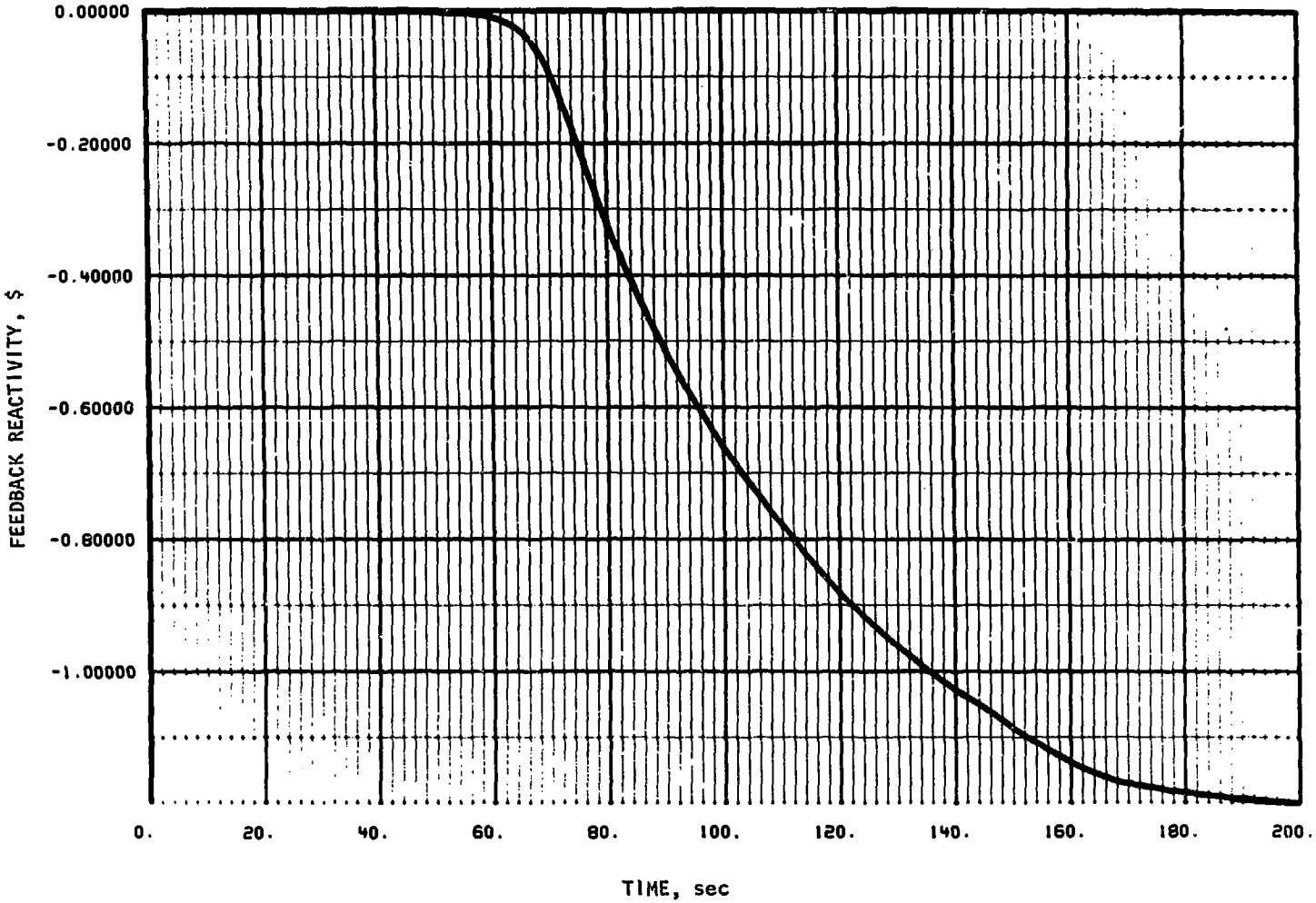

Fig. 16. Feedback Reactivity vs Time After One Control Rod Worth 1.227$ is Driven into a Stainless-steel-reflected Core; Initial Power of 50 kW and Full Flow

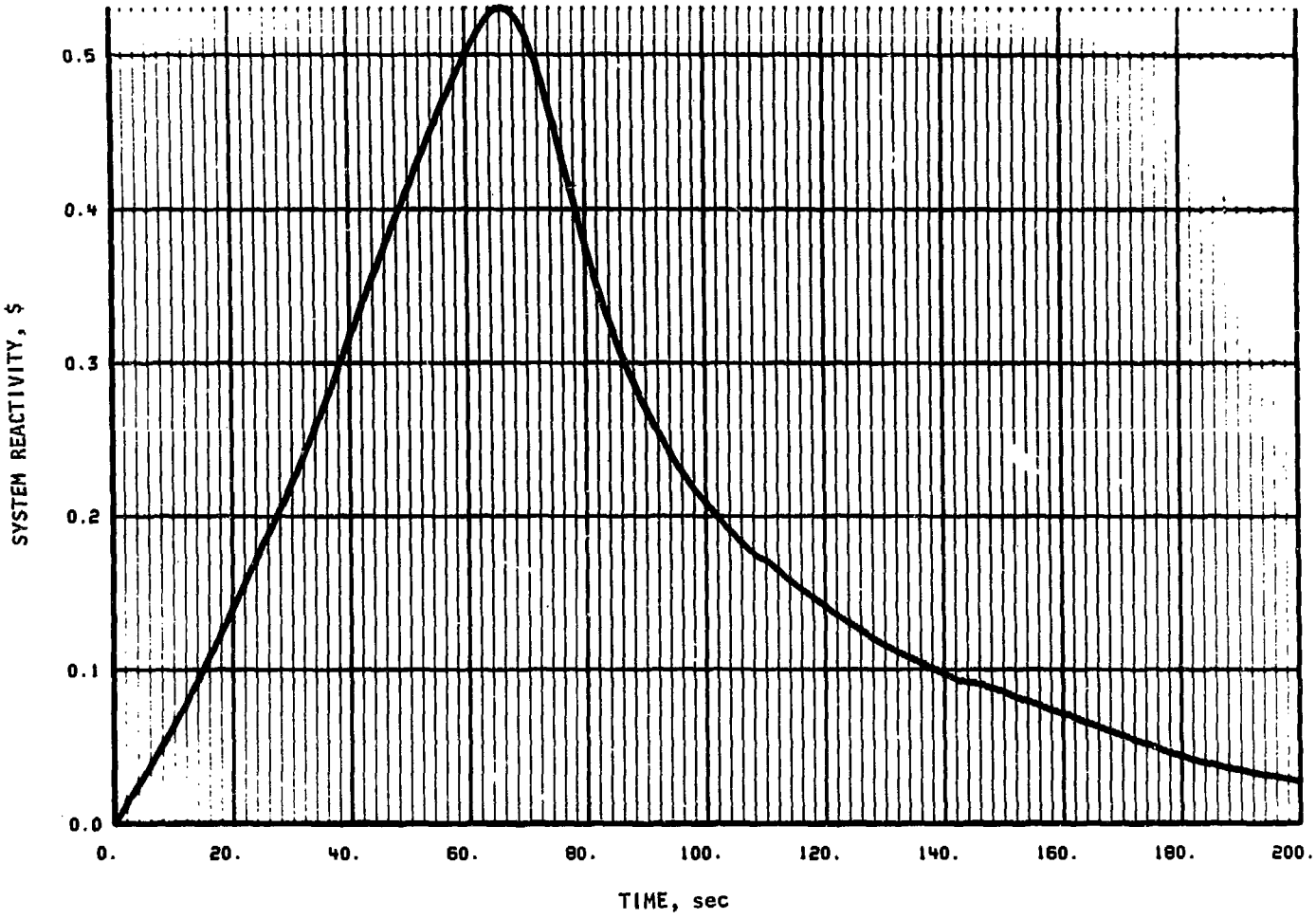

Fig. 17. System Reactivity vs Time After One Control Rod Worth 1.227$ is Driven into a Stainless-steel-reflected Core; Initial Power of 50 kW and Full Flow

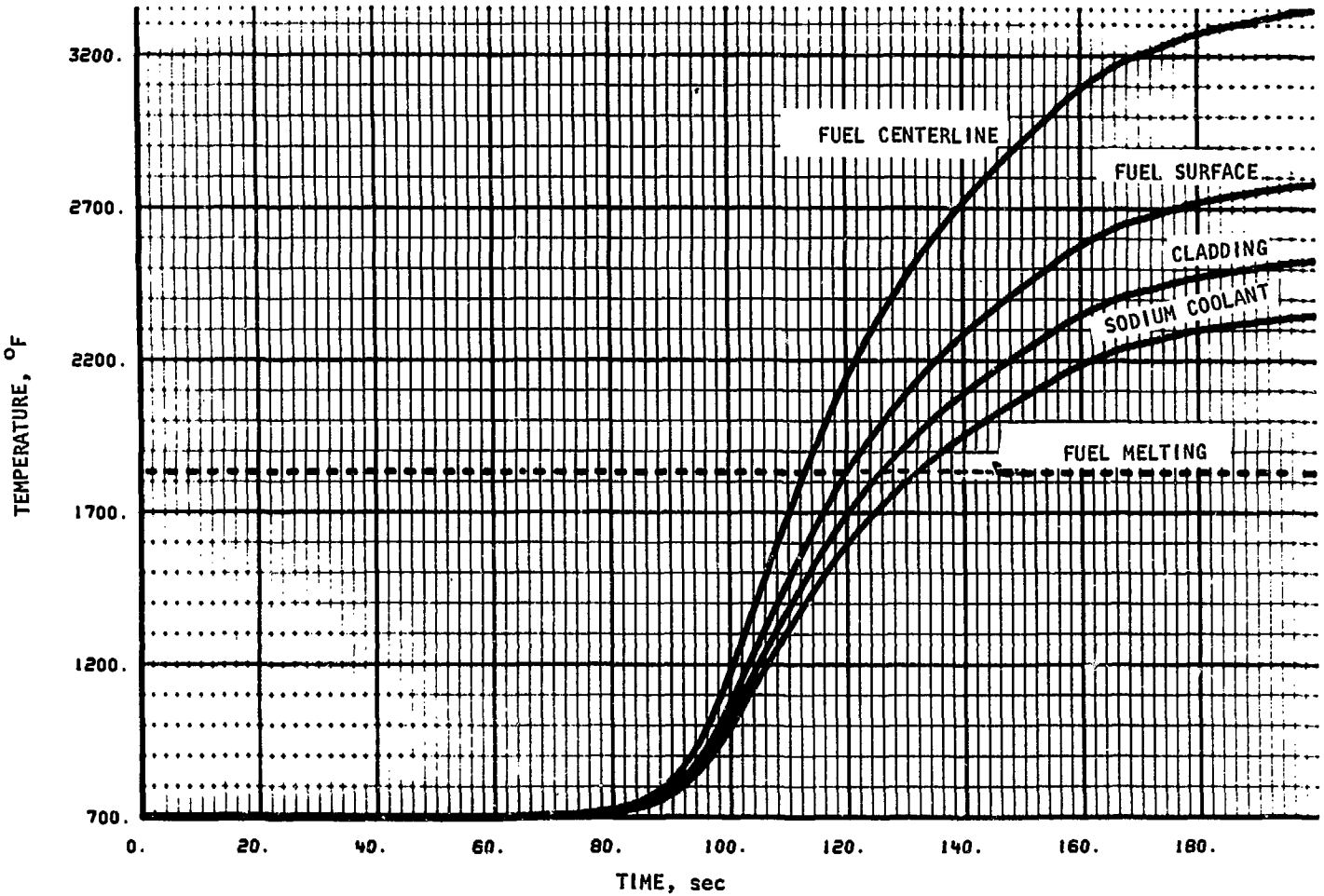

Fig. 18. Peak Driver-fuel-element Temperature After One Control Rod Worth 0.757$ is Driven into a Stainless-steel-reflected Core; Initial Power of 50 kW and Full Flow

Figure 19 is the temperature history in the hottest driver element. (As in previous figures for temperature, four curves have been drawn; but here the curves nearly coincide.)

d. Fourth Subcase at Startup

(1) Assumptions: The reactor configuration is the same as in the first subcase but with a power of 8 W and zero flow. The feedback is same as for all other stainless-steel-reflected cores. The worth of the inserted rod is 1.227$.

(2) Results: The initial center-line temperature in the peak metallic pin is less than 702°F. The temperature does not exceed 710°F until 75 sec into the transient. Melting occurs at 89 sec, and the eutectic temperature is reached at 86 sec. The minimum reactor period occurs at 80 sec into transient and is 1.73 sec. Maximum reactivity occurs at 80.5 sec and is 68.7¢. Figure 20 is the temperature history in the hottest driver element (four nearly coinciding curves are shown). Figures 21 and 22 are plots of feedback and system reactivity.

e. Fifth Subcase at Startup

(1) Assumptions: The core is blanketed with depleted uranium. The feedback consists of core-driver-fuel axial expansion, core-driver-fuel sodium expansion, blanket-uranium expansion, and blanket-sodium expansion. The power is assumed at 8 W and there is zero flow. The worth of the inserted rod is 1.227$.

(2) Results: Initial temperature in the hottest driver is 701.6°F. The peak center-line temperature in the fuel does not exceed 710°F until 89 sec into the transient and is 0.96 sec. The maximum excess reactivity occurs at 89.6 sec and is 77.6¢. Figure 23 is the temperature history in the hottest driver element (four nearly coinciding curves are shown).

3. Case 4--HWCR Insertion at Power

a. First Subcase at Power

(1) Assumptions: The stainless-steel-reflected reactor is assumed to be at 62.5 MWt with full flow. All HWCR's except one are assumed

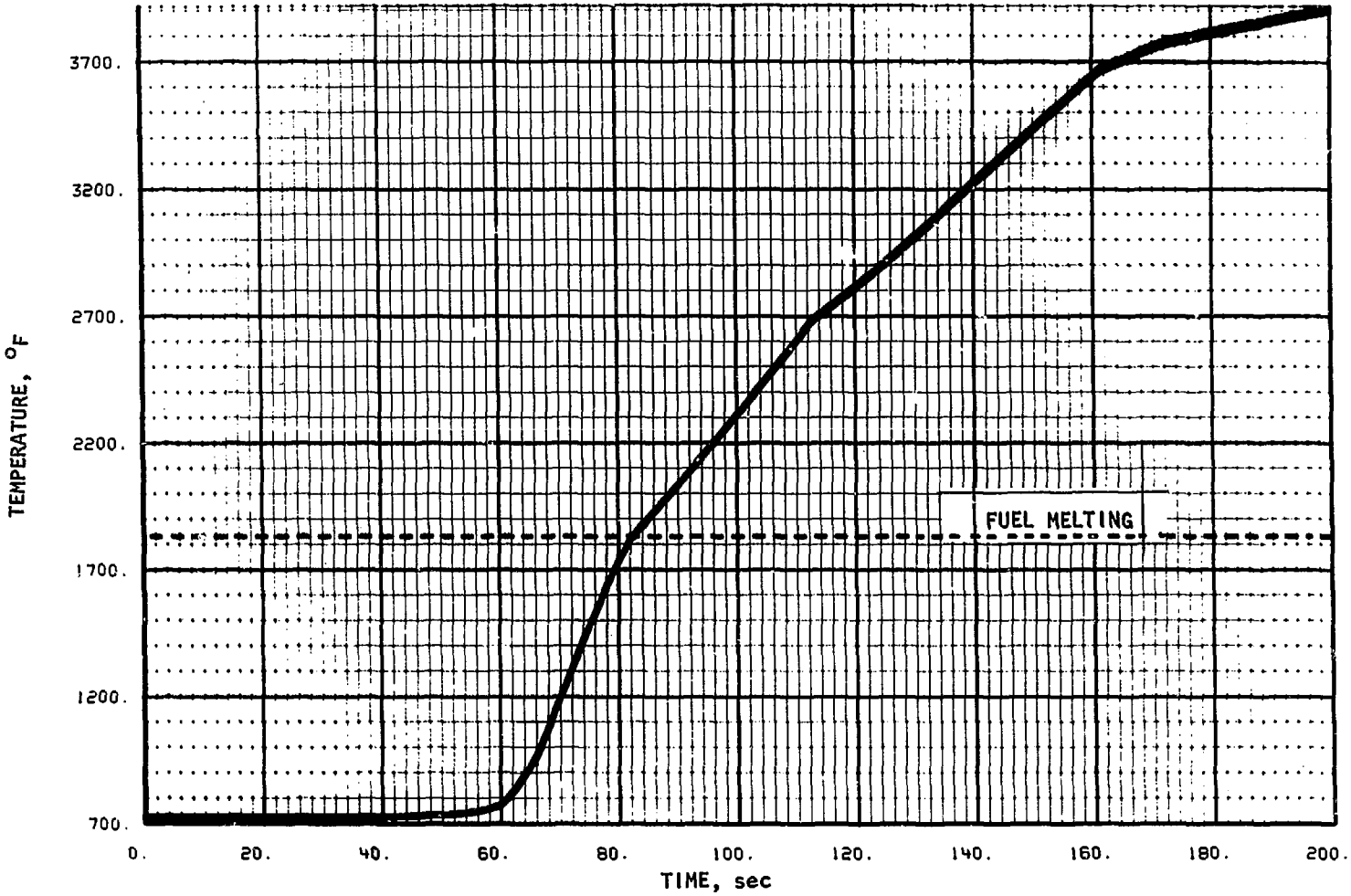

Fig. 19. Peak Driver-fuel-element Temperatures After One Control Rod Worth 1.227$ is Driven into a Stainless-steel-reflected Core; Initial Power of 50 kW and 1% Flow

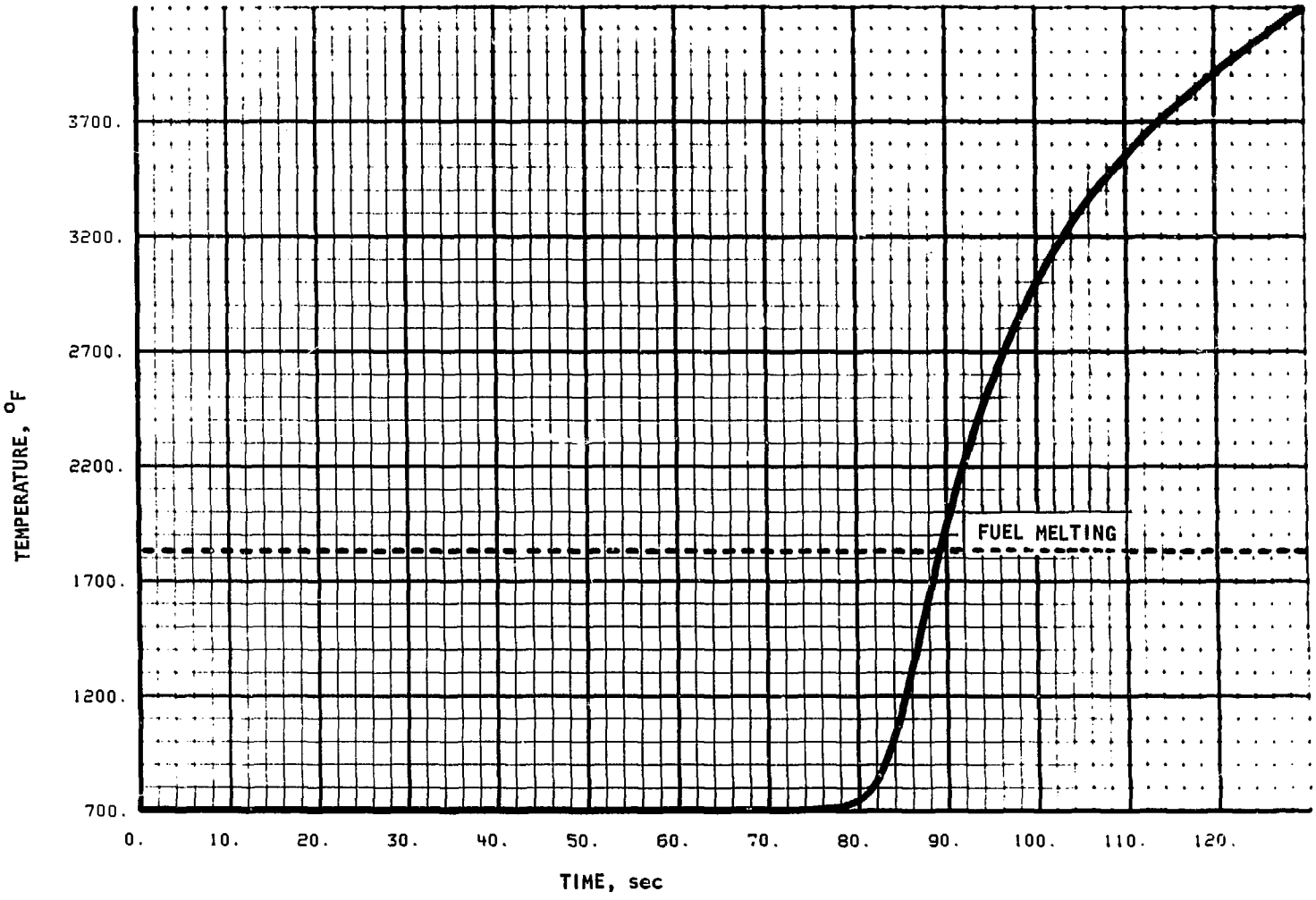

Fig. 20. Peak Driver-fuel-element Temperatures After One Control Rod Worth 1.227$ is Driven into a Stainless-steel-reflected Core; Initial Power of 8 W and Zero Flow

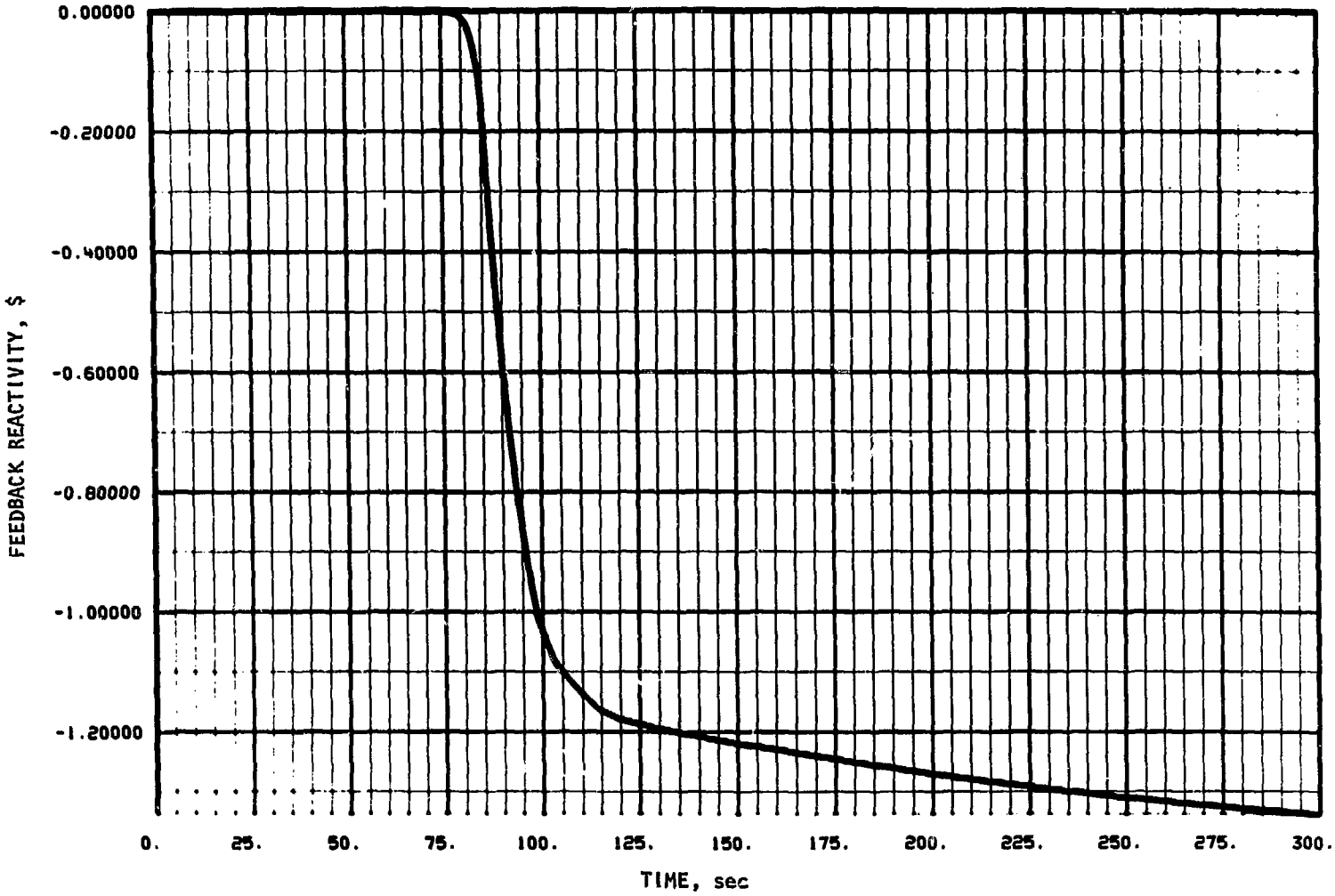

Fig. 21. Feedback Reactivity vs Time After One Control Rod Worth 1.227$ is Driven into a Stainless-steel-reflected Core; Initial Power of 8 W and Zero Flow

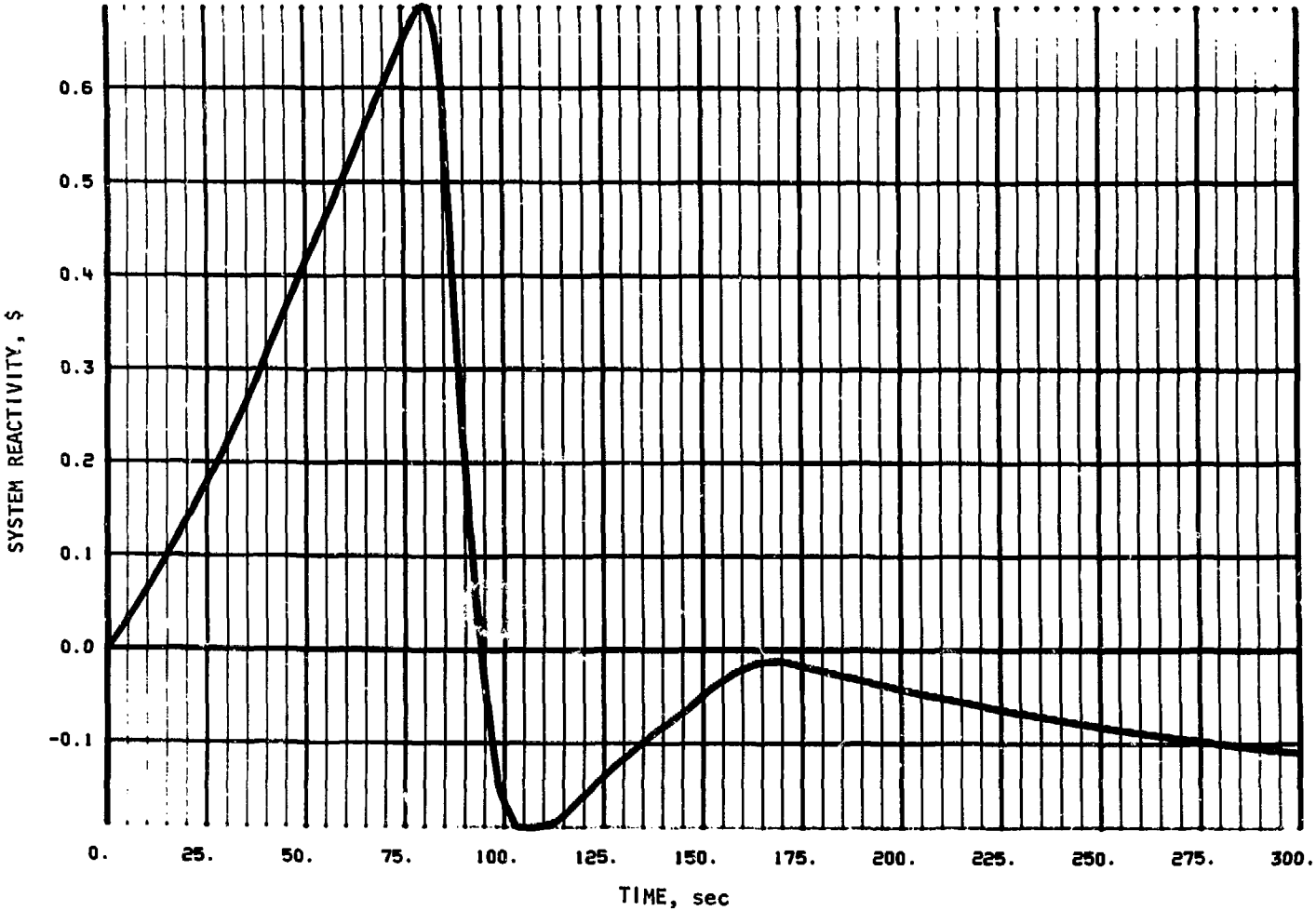

Fig. 22. System Reactivity vs Time After One Control Rod Worth 1.227$ is Driven into a Stainless-steel-reflected Core; Initial Power of 8 W and Zero Flow

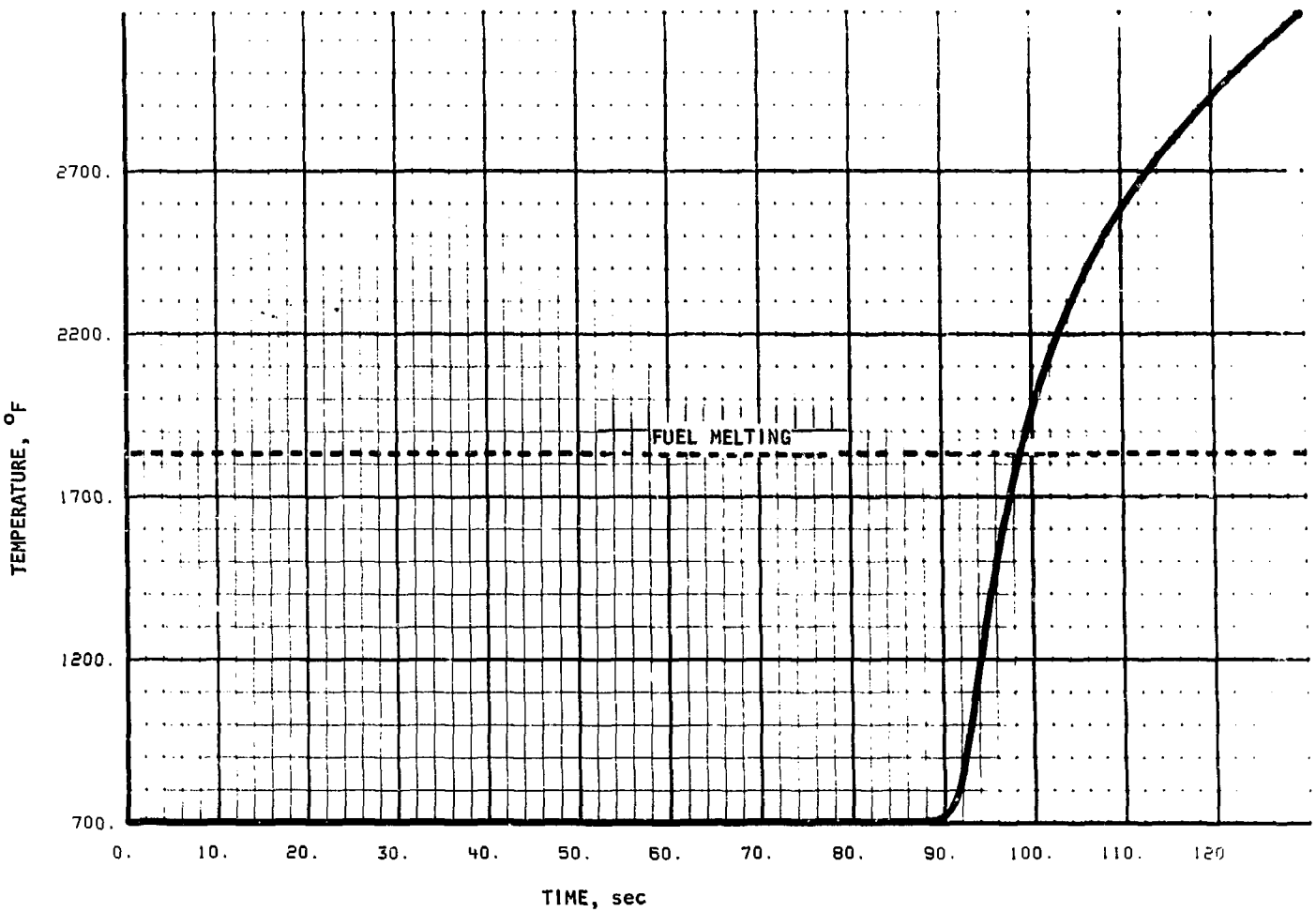

Fig. 23. Peak Driver-fuel-element Temperatures After One Control Rod Worth 1.227$ is Driven into a Depleted-uranium-blanketed Core; Initial Power of 8 W and Zero Flow

to be banked at 11 in., and the highest-worth rod, which has a total worth of 1.227$, is assumed to be driven into the core at 5 in./min from the full-out position. Feedback is assumed from the driver subassemblies and consists of core-driver-fuel axial expansion and core-driver-fuel sodium expansion. Additional feedback comes from the change in position of the control-rod bank because of expansion of the control-rod shafts.

(2) Results: The centerline fuel temperature in the hottest driver exceeds melting at 44 sec into the transient, and the fuel-cladding eutectic temperature is reached at 31 sec. The shortest reactor period is 37 sec and occurs 40 sec after initiation of the transient. The maximum excess reactivity of the system is 16.1¢ and occurs at 50 sec. The reactor is therefore below prompt critical at all times during the transient.

Figure 24 is the plot of the temperature history of the hottest driver element during this transient. Figures 25, 26, and 27 are plots of the inserted reactivity, feedback reactivity, and system reactivity.

b. Second Subcase at Power

(1) Assumptions: Conditions are the same as for the first subcase at power except that the rod being driven in has a total worth of 0.5% $\Delta k/k$ (0.7576$) instead of 0.81% $\Delta k/k$ (1.227$).

(2) Results: The centerline temperature in the hottest metallic pin exceeds melting at 62 sec. The fuel-cladding eutectic temperature is exceeded at 43 sec. The shortest reactor period is 52 sec and occurs 43 sec into the transient. The maximum excess reactivity is 12.7¢ and occurs at 59.6 sec.

Figure 28 is the temperature history in the hottest driver. Figures 29 and 30 are plots of the feedback and system reactivity.

c. Third Subcase at Power

(1) Assumptions: The core is blanketed with depleted uranium instead of having a stainless steel reflector. All rods are banked at 11 in. except one, which is assumed to have the same worth as that of the highest-worth control rod in the stainless-steel-reflected core (1.227$). The feedback includes core-driver-fuel sodium expansion and core-driver-fuel axial expansion plus the uranium and sodium expansion in the blanket and control-rod expansion effects.

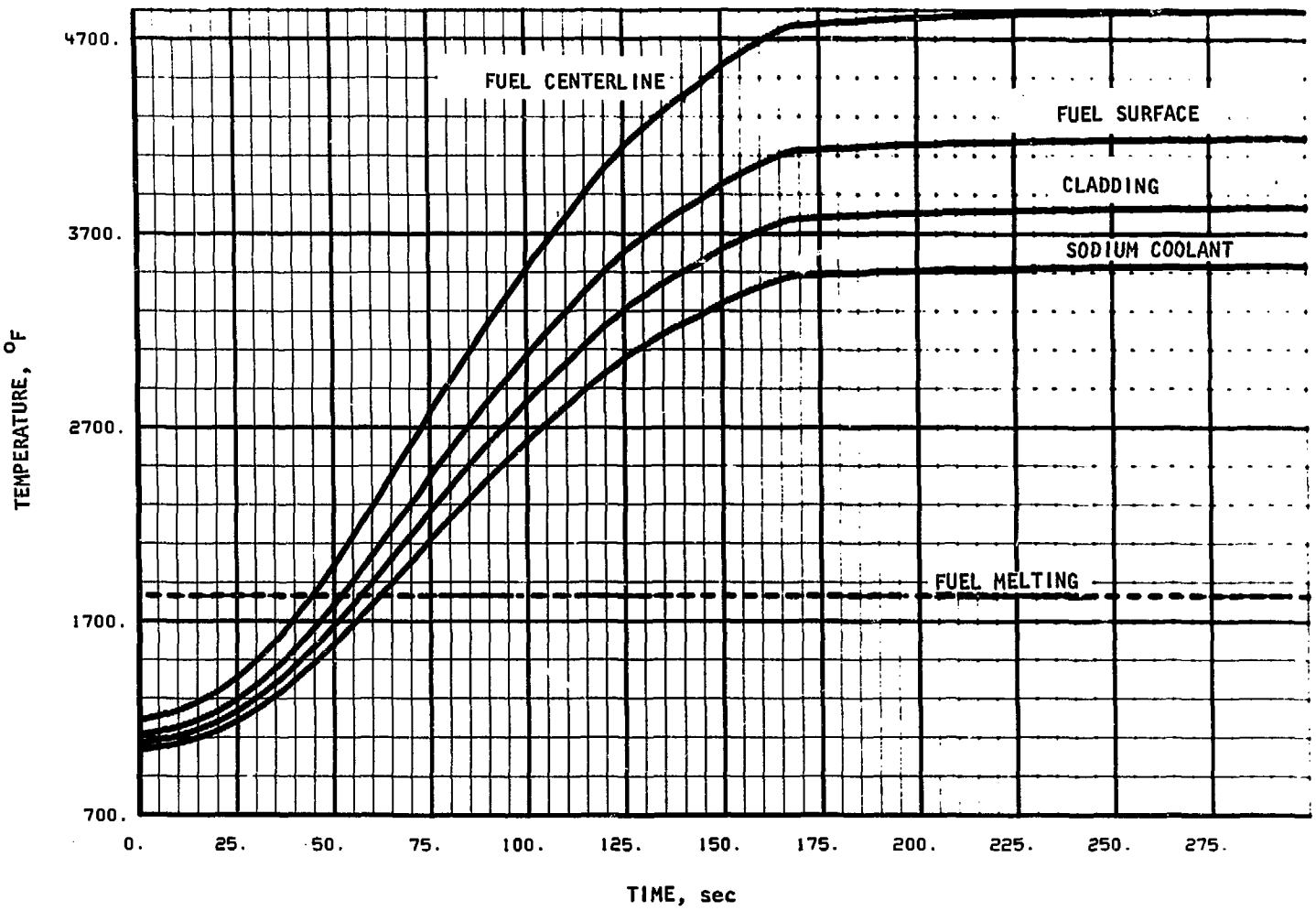

Fig. 24. Peak Driver-fuel-element Temperatures After One Control Rod Worth 1.227$ is Driven into a Stainless-steel-reflected Core at 62.5 MW

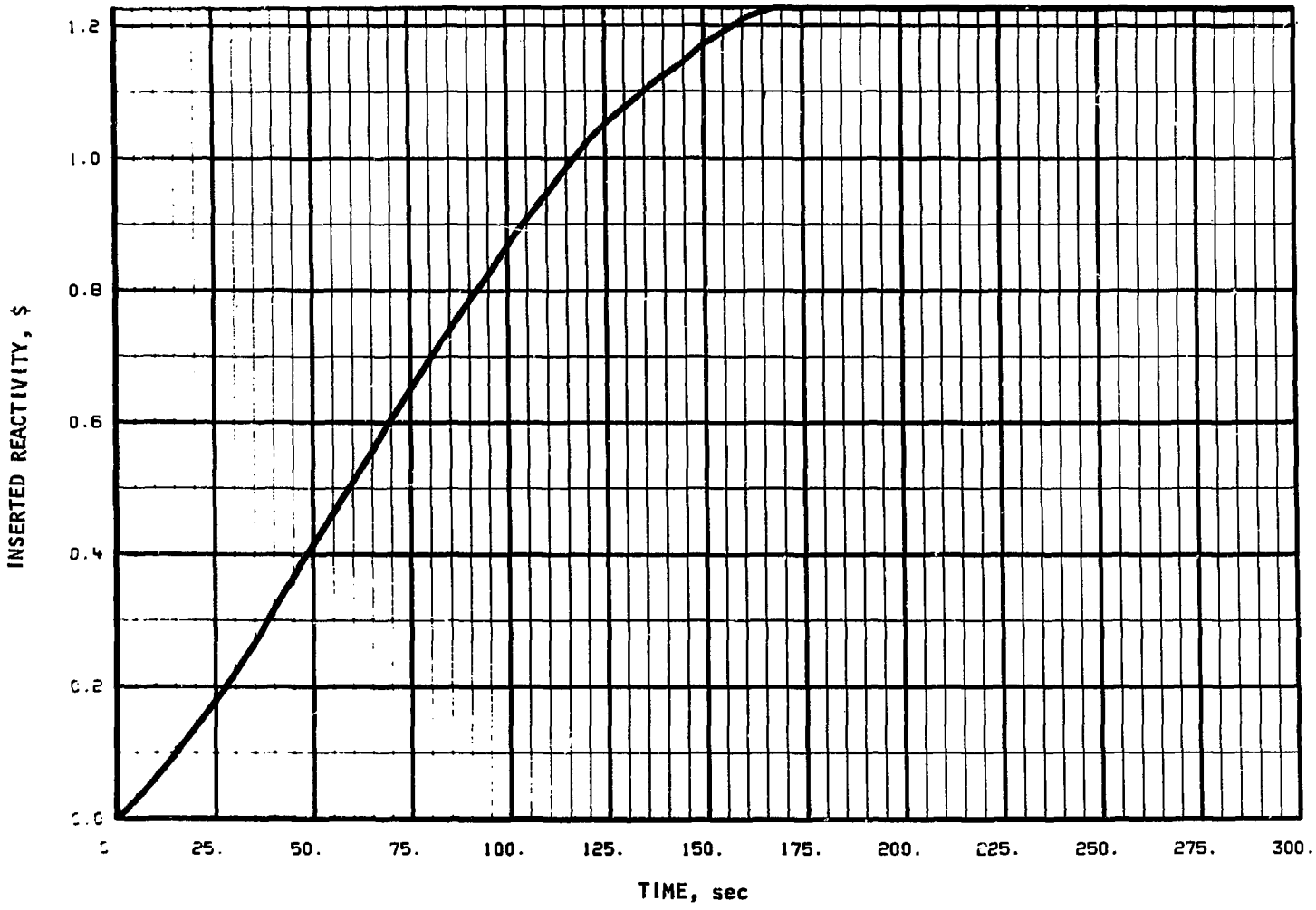

Fig. 25. Inserted Reactivity vs Time After One Control Rod Worth 1.227$ is Driven into a Stainless-steel-reflected Core at 62.5 MW

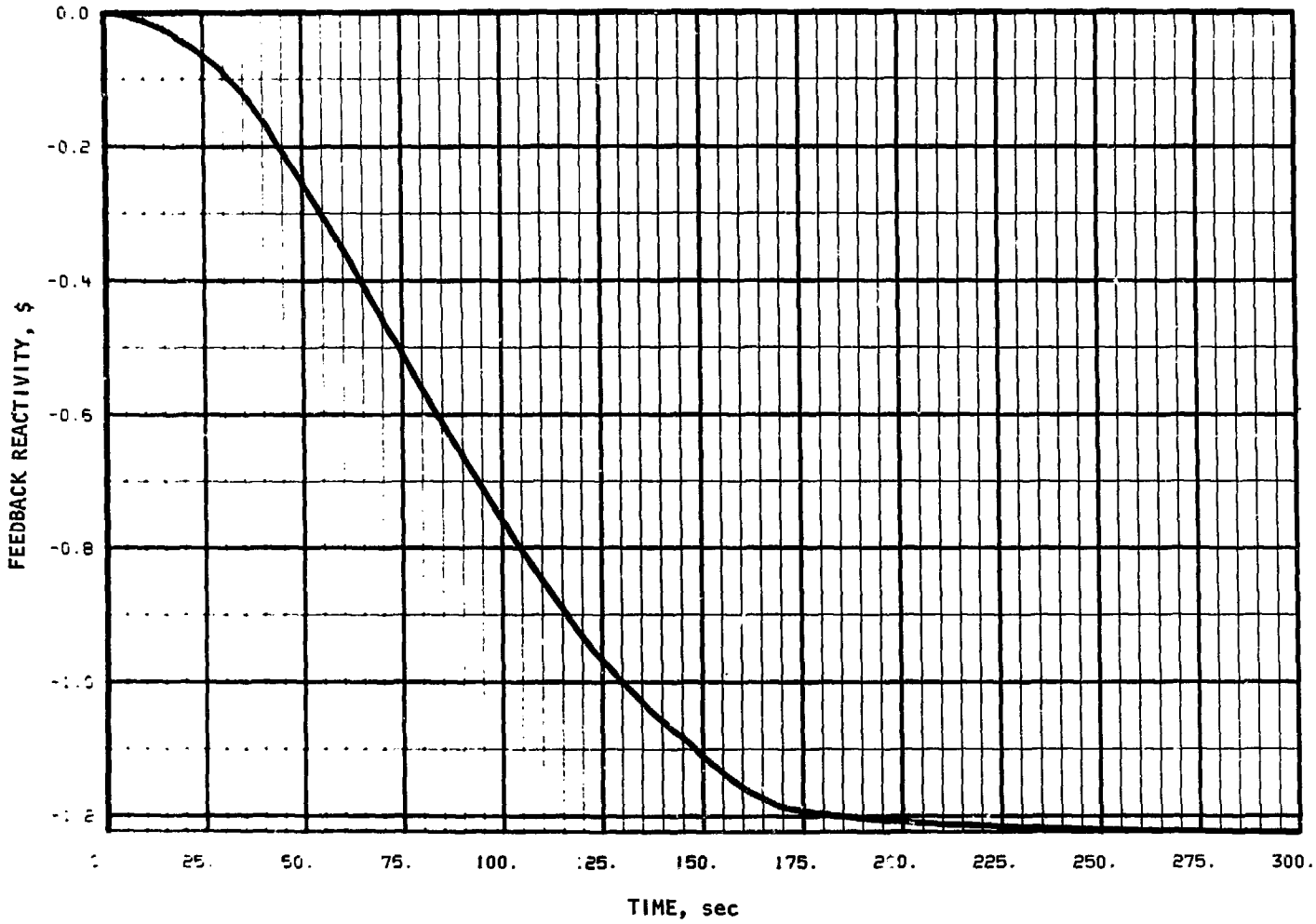

Fig. 26. Feedback Reactivity vs Time After One Control Rod Worth 1.227 is Driven into a Stainless-steel-reflected Core at 62.5 MW

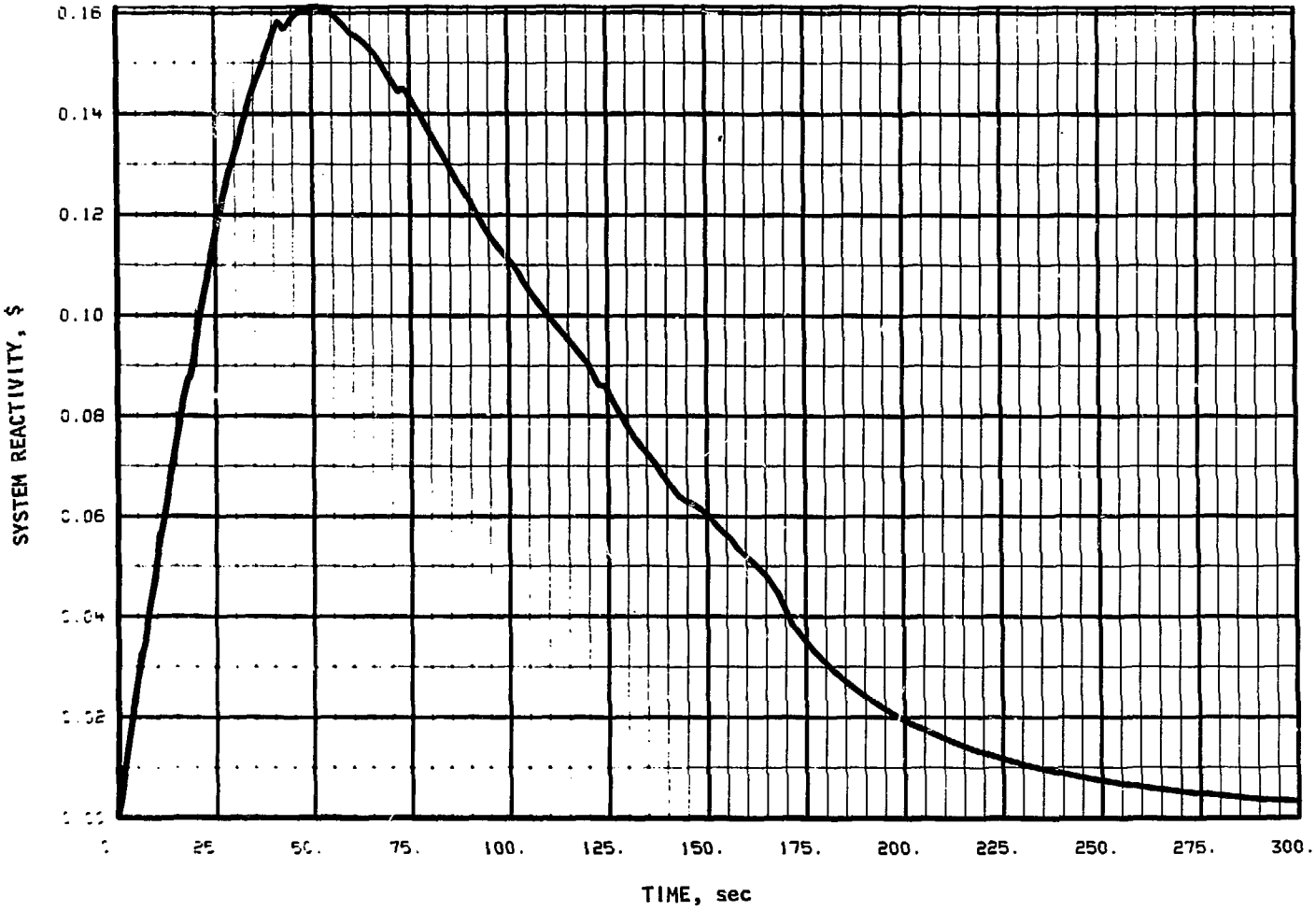

Fig. 27. System Reactivity vs Time After One Control Rod Worth 1.227$ is Driven into a Stainless-steel-reflected Core at 62.5 MW

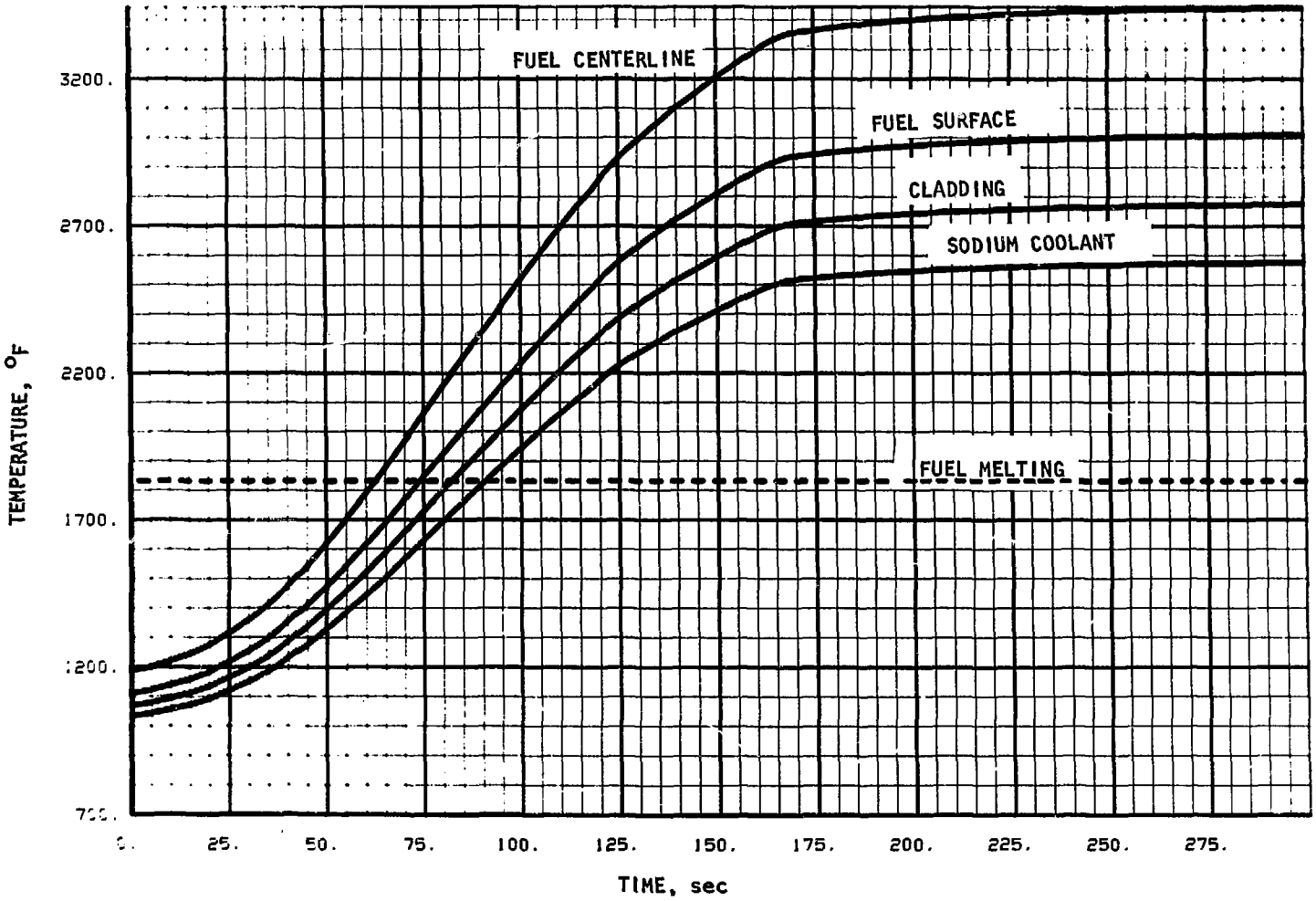

Fig. 28. Peak Driver-fuel-element Temperatures After One Control Rod Worth 0.757$ is Driven into a Stainless-steel-reflected Core at 62.5 MW

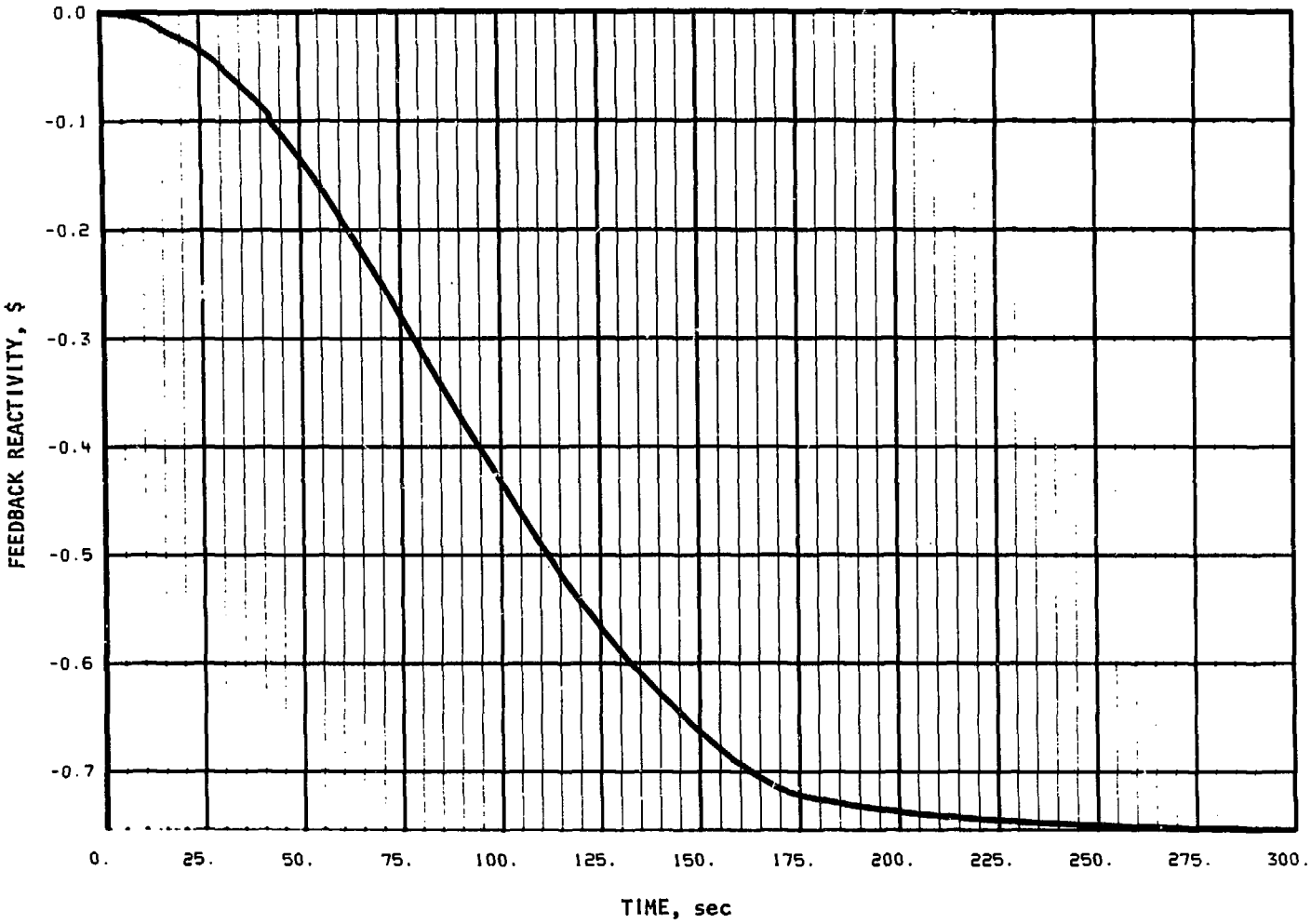

Fig. 29. Feedback Reactivity vs Time After one Control Rod Worth 0.7576$ is Driven into a Stainless-steel-reflected Core at 62.5 MW

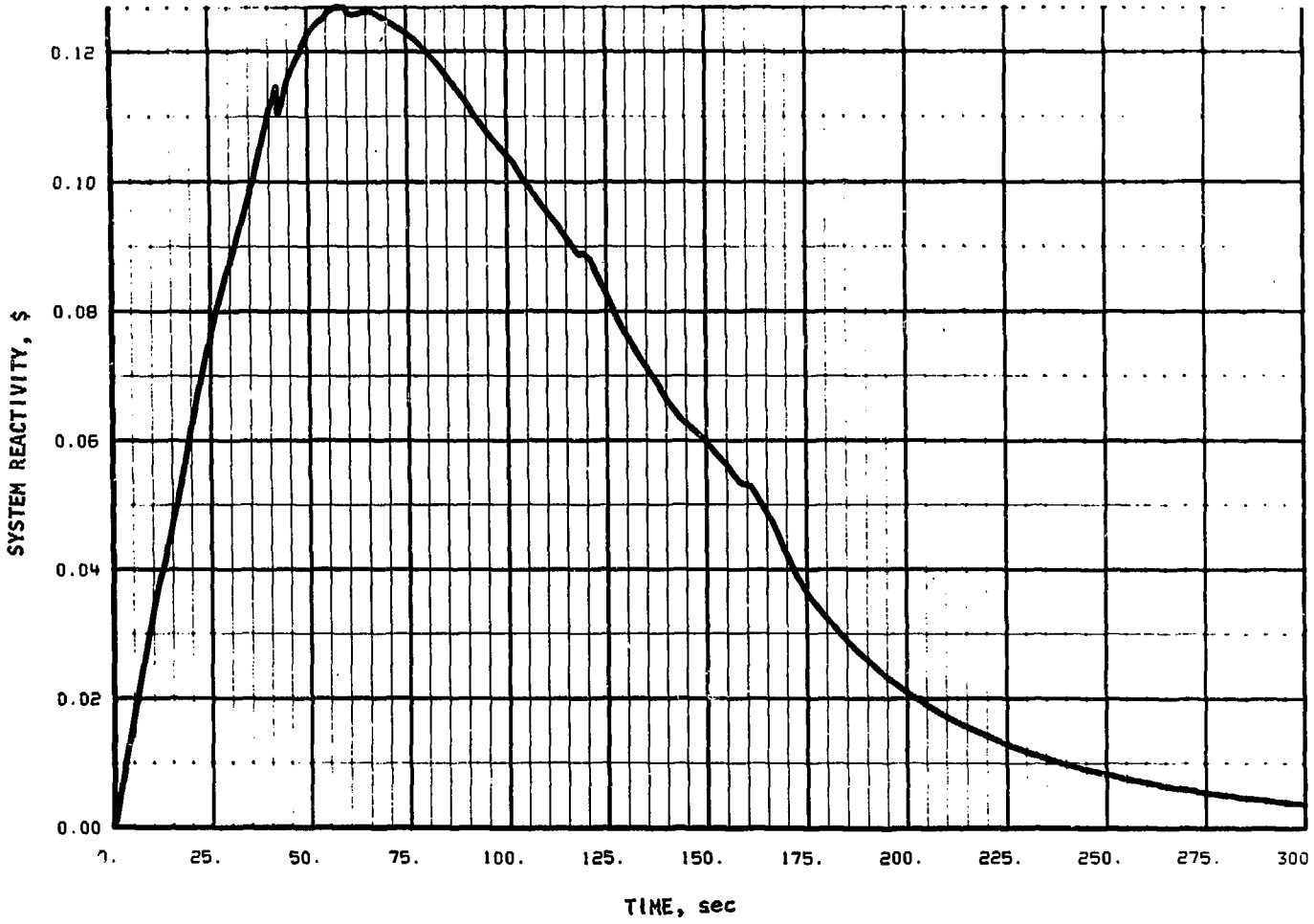

Fig. 30. System Reactivity vs Time After One Control Rod Worth 0.7576$ is Driven into a Stainless-steel-reflected Core at 62.5 MW.

(2) Results: The melting temperature in the peak driver is exceeded at 48 sec into the transient, and the eutectic temperature is exceeded at 35 sec. The shortest reactor period is 44.8 sec and occurs at 36 sec. The maximum excess reactivity occurs at 50 sec and is 14.1¢. Figure 31 is the temperature history in the hottest driver element.

4. Cases 3 and 4 with Protection

To assess the effects of HWCR's under more realistic conditions, the two types of control-rod-insertion accidents were analyzed with the plant protective system operative.

a. First Subcase with Protection

(1) Assumptions: The HWCR is inserted with all conditions identical to those in the first subcase at startup (Section 2.a above), except that the plant protective system is operative. The reactor trip is set for a 20-sec period with a 0.4-sec delay. Worth of the inserted rod is 1.227$.

(2) Results: Reactor trip occurs 28 sec after initiation of the accident. Peak temperature never exceeds 702°F.

b. Second Subcase with Protection

(1) Assumptions: The HWCR is inserted with the same conditions as in the first subcase at power (Section 3.a above), except that the plant protective system is operative. The system is set to trip at 10% overpower with a delay of 0.063 sec. The 0.063 sec is the sum of the longest measured time to operate the control-power relays in nuclear channels 9, 10, and 11 and the longest measured time to release the scram clutch.

(2) Results: The trip occurs 9.5 sec after initiation of the accident. The peak temperature in hottest driver element occurs at 9.5 sec and is 1237°F. The shortest reactor period occurs at 9.51 sec and is 69 sec; and the maximum excess reactivity occurs at 9.51 sec and is 4.8¢. Figure 32 is a plot of temperatures in the hottest driver-fuel element.

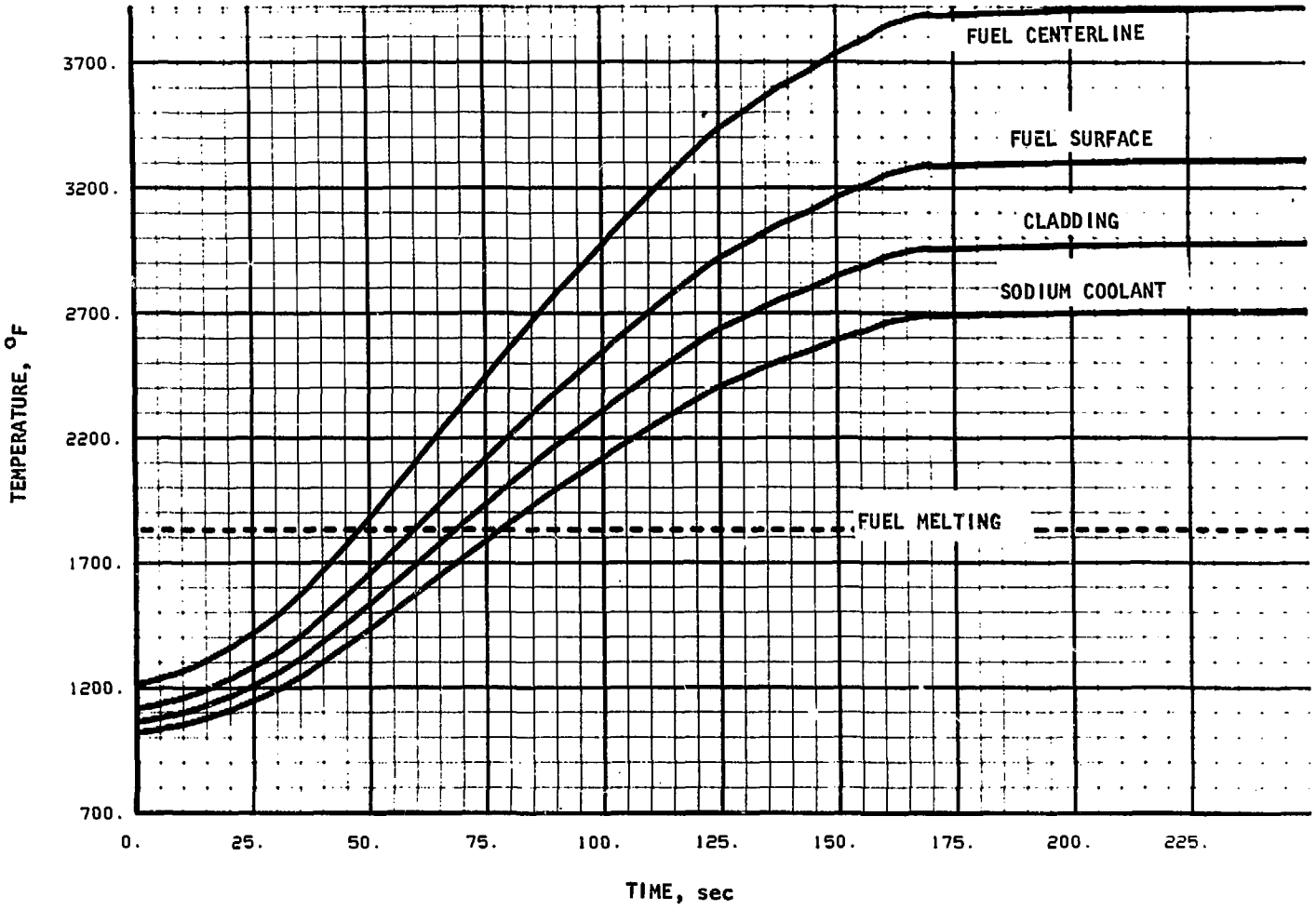

Fig. 31. Peak Driver-fuel-element Temperatures After One Control Rod Worth 1.227$ is Driven into a Depleted-uranium-blanketed Core at 62.5 MW

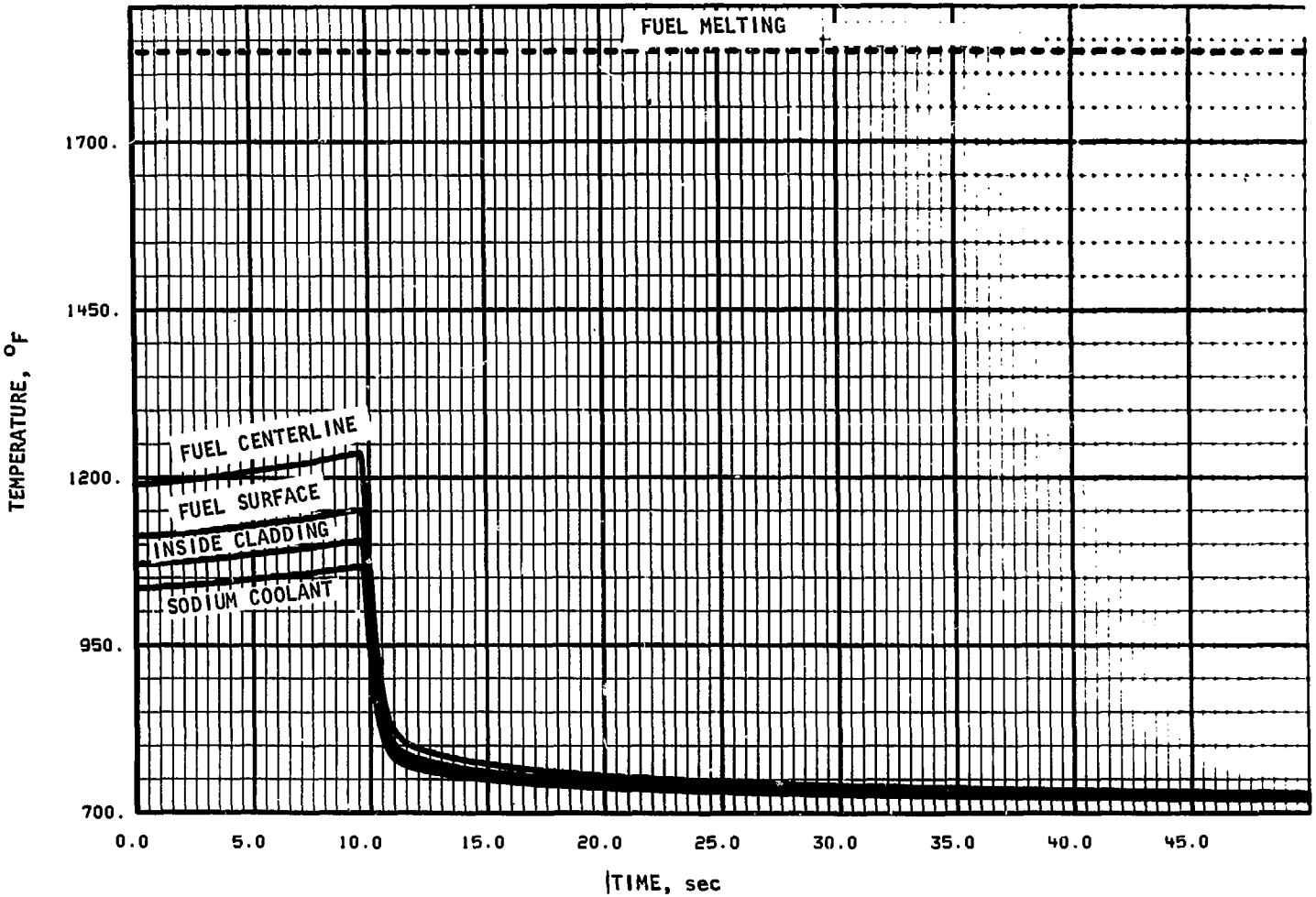

Fig. 32. Peak Driver-fuel-element Temperatures After One Control Rod Worth 1.227$ is Driven into a Stainless-steel-reflected Core at 62.5 MW; Power Trip at 10% Overpower

5. Tabulation of Calculational Results

Table XVII summarizes the eight EROS analyses that were performed to investigate the transient behavior of unprotected cores with HWCR's. The table includes the results of EROS calculations for Cases 3 and 4 performed on the original EBR-II core and reported in Ref. 11. Table XVIII is a reproduction of the summary table in Ref. 2 for Cases 3 and 4.

6. Experimental Subassemblies

The preceding discussion has not explicitly considered experimental subassemblies. Each experiment that is placed in EBR-II is subjected to a set of required analyses by the experimenter. These analyses are reviewed by the EBR-II Project before the experiment can be inserted in the reactor. Such a review must conclude that the experiment is within the envelope defined by the Guide for Irradiation Experiments in EBR-II. Individual irradiation experiments are similarly reviewed when significant changes are made to the reactor configuration. Among the safety analyses that are required by the Guide, the only one affected by a change in the control-rod system is in Section VII.3.a: the case to determine the effect of the insertion of a control rod at power. To analyze this condition, the experimenter is provided with a power-vs-time curve for the accident. Figure 33 shows the relation between the power-vs-time curve presently in the Guide and those that have been calculated for an HWCR. As the figure indicates, the curves for the HWCR rise somewhat faster than the curve presently in the Guide. However, with the plant protective system operative, an experimental subassembly will experience essentially the same overpower condition as it would in a core with standard control rods. This is primarily due to the short time (0.063 sec), relative to the speed of the accident, taken to detect the overpower and scram the reactor.

In postulated startup accidents with the plant protective system operative, no measurable temperature above 700°F occurs in any experimental subassembly.

B. Nonreactivity Aspects

The nonreactivity safety aspects of operating EBR-II with HWCR's consist of ensuring that the rod will function as it was designed to. The

TABLE XVII. Summary of Results of EROS Calculations for Control-rod Insertion at Startup and at 62.5 MWt with the Plant Protective System Inoperative

	Calculation[a]									
	1	2	3	4	5	Startup, Ref. 11[b]	6	7	8	Power, Ref. 11[c]
Time to fuel-cladding eutectic (1319°F), sec	76	108	72	84	95	165	31	43	35	84
Time to driver-fuel melting (1834°F), sec	79	112	82	86	98	--	44	62	48	94.5
Maximum rate of temperature rise, °F/sec	81	49.9	43.0	75.2	126	15	29	18	22	13
Shortest positive period, sec	4.16	6.39	5.6	1.73	0.952	10.0	37.5	52.4	44.8	97
Maximum reactivity, ¢	53.07	45.14	47.3	68.67	77.59	48	16.13	12.69	14.10	8.5
Initial temperature rise, sec	53	72	--	75	88	110	--	--	--	

a
Assumed conditions:

1. HWCR insertion at startup, SS reflector, 50 kW power, full flow, rod worth = 1.227$.
2. HWCR insertion at startup, SS reflector, 50 kW power, full flow, rod worth = 0.7576$.
3. HWCR insertion at startup, SS reflector, 50 kW power, 1% flow, rod worth = 1.227$.
4. HWCR insertion at startup, SS reflector, 8 W power, zero flow, rod worth = 1.227$.
5. HWCR insertion at startup, dep. U blanket, 8 W power, zero flow, rod worth = 1.227$.
6. HWCR insertion at power, SS reflector, rod worth = 1.227$.
7. HWCR insertion at power, SS reflector, rod worth = 0.7576$.
8. HWCR insertion at power, dep. U blanket, rod worth = 1.227$.

b
EROS calculation for standard control rod in Case 3 of Ref. 1, reported in Ref. 11

c
EROS calculation for standard control rod in Case 4 of Ref. 1, reported in Ref. 11

TABLE XVIII. Summary of Two Hypothetical Accidents

(Taken from Table F-3 in Ref. 2)

Case No.[a]	Initial Power, watts	Loss of Administrative Control?[b]	How Terminated	Time, sec[c]	Power Level, watts	Time for Melting,[d] sec
3	8	No	Period	?[e]	--	230[f]
			Level	~100	10^3	
4	6×10^7	No	Period	--[g]	--	20-50[h]
			Level	~5	6.9×10^7	

[a] Case Descriptions:

3 Control rod drive, 5 in./min
4 Control rod drive, 5 in./min

[b] Is loss of administrative control required to initiate the accident?

[c] After reactivity insertion is initiated.

[d] Time required for melting to occur after reactivity insertion is initiated if both period and level trips are inoperative or not effective.

[e] A 20-sec period trip setting may cause a period scram at ~100 sec.

[f] Melting may not occur but fuel alloy-clad eutectic formation temperatures will be exceeded in the fuel alloy.

[g] Period will not be short enough to cause period scram.

[h] To achieve fuel alloy-clad eutectic formation temperature on surface of hottest fuel pin. The clad temperature will be lower. The range is large because the required time depends on (1) control-rod position, and (2) the influence of uncertainty factors.

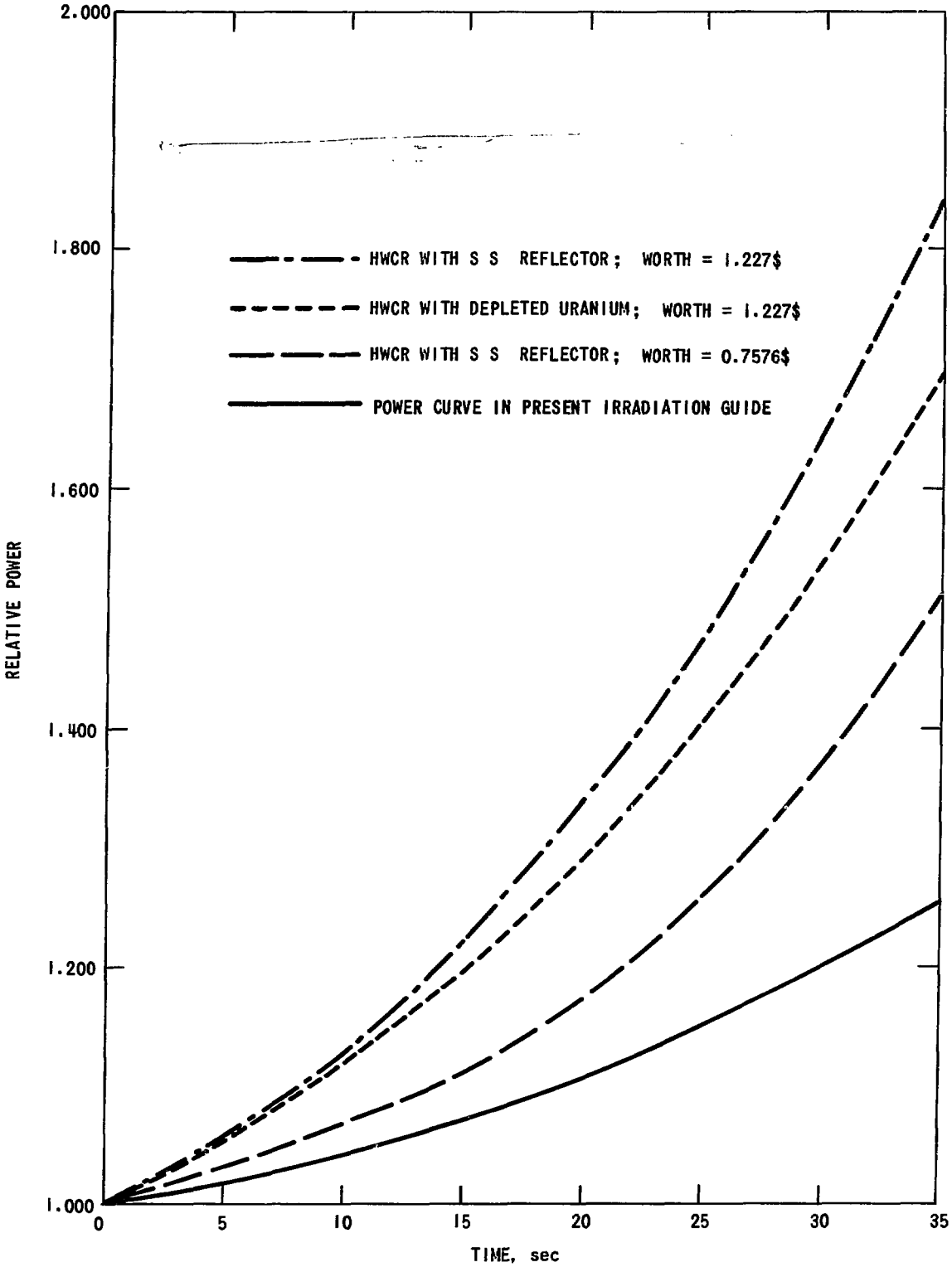

Fig. 33. Power-vs-Time Curves for Insertion of One Control Rod, Comparing HWCR Curves with Power Curve in Present Irradiation Guide

HWCR is identical to the standard control rod in the fuel portion, so only the differences in the HWCR resulting from the inclusion of the B_4C portion are of concern. The successful operation of the prototype HWCR's makes this safety analysis more simple than it would be otherwise and gives added assurance of the validity of the results.

As discussed in Section II, the B_4C portion of the control rod replaces the sodium deflector, sodium, and upper shield of the standard control rod. According to Ref. 2, the purpose of the sodium deflector (flow twister) "is to reduce the temperature differentials in the control rod hexagonal can and, therefore, to minimize bowing of the control rod within its thimble." On the basis of operation of the prototype HWCR's this deflector is not necessary. The radial flux, and thus temperature, gradient is flatter in row 5 with a stainless steel reflector than with the present depleted-uranium blanket (see Fig. 8), so that there will be less of a radial temperature differential across the HWCR subassembly than in the present standard control-rod subassembly.

The B_4C capsules cause the major pressure drop across the control rod to occur in the capsule region. Under design conditions, with 61 gpm of sodium flowing through the subassembly, the calculated pressure drop through the fuel-element region is 5.5 psi, and through the B_4C capsule region, 22.2 psi. This increased pressure drop above the fuel causes no change in flow distribution in the fuel region; and the time required for the prototype HWCR's to drop during the reactor-operation interlock checks has been indistinguishable from that for standard control rods. The coolant velocity in the capsule region is calculated, using HECTIC, to be a maximum of 29.7 ft/sec, less than 10% higher than the velocity past the fuel in a row-1 or -2 driver subassembly with a stainless-steel-reflected core. No problem of erosion of the capsule cladding is expected.

If a problem with the safety of the B_4C portion of an HWCR were to arise, it would be based on a failure of the cladding of the B_4C capsule. Assuming that the capsule is properly manufactured, such a cladding failure would be caused by overpressurization of the capsule due to a buildup of helium released in the (n,α) reaction with ^{10}B. Results of design calculations to determine the tube stress are given in Ref. 4. The maximum allowable stress was set at 9400 psi; for this stress, the gas pressure inside the capsule must reach 1100 psi. Two B_4C capsules from the first prototype HWCR have been examined

to determine the pressure at the end of their operating life (1.44 at.% burnup of the fuel). One capsule contained a volume of gas, at STP, of 38.7 ml, and the other, 40.8 ml.[14] The volume within the capsules available for the gas was 54.2 ml and 54.6 ml, respectively. For both capsules, the pressure within the capsule at room temperature was thus close to atmospheric (16.0 and 15.3 psia, respectively, at 24°C). The capsules were sealed in a glovebox with about a 1-psia overpressure, so the amount of helium released from the B_4C appears to be insignificant.

A calculation has been made to determine the expected release of helium in the capsules from the first prototype HWCR. A correlation developed at HEDL by Russcher and Pitner[15] was used for this calculation. Based on a capture density in the B_4C of 1×10^{20} captures/g and an assumed B_4C temperature of 1100°F, this correlation predicted a release of 72 ml (STP) of helium during the 5472 MWd that the first control rod was in service. This corresponds to an increase in pressure in the capsule due to helium release of about 20 psi, or a total pressure of about 35 psi at room temperature. At 1100°F, this would increase to about 110 psia, only 10% of the allowable. As pointed out in Ref. 15, the helium-release rate using this correlation is higher, at capture densities less than 4×10^{20} captures/sec, than the helium rate predicted from the correlation given in "Design Criteria for Nuclear Control Components."[16] That correlation,

$$R = 0.3c \exp(-5050/T),$$

where

R = fraction of helium generated that is released,

c = 10^{-20} times capture density in captures/cm^3,

and

T = temperature in °F,

predicts that 3% of the helium produced is released, or 15 ml STP. A newer correlation[17] is dependent only on temperature. This correlation,

$$R = \frac{\exp\{0.004(T - 1900)\}}{1 + \exp\{0.004(T - 1900)\}}$$

where the nomenclature is the same as for the previous equation, predicts a 20% gas release, or 103 ml STP. This last estimate corresponds to an increase

in pressure within the capsule at room temperature of 28 psi, or a total pressure of about 43 psi, which would increase, at 1100°F, to about 146 psia, well below the 1100-psia limit.

It is thus apparent that helium production in the B_4C during the service life of an HWCR will not cause a cladding failure. Swelling of the B_4C pellets will also not cause a cladding failure. The pellets from capsules in the first prototype HWCR slid easily from the capsules when they were dismantled. In addition, there is a nominal 0.006-in. diametral gap (greater than 1% of the diameter) between the pellets and the inside of the capsule when fabricated. The latest correlation[18] for swelling of B_4C in a fast flux,

$$\%\Delta D/D = 0.0234c,$$

where c is 10^{-20} times capture density in captures/cm^3, predicts about 0.12% diametral change, or less than 1 mil increase. The pellets from two capsules of the first prototype HWCR had a consistent increase in their 1-in. length of about 1 mil.

Although a cladding failure cannot be reasonably expected to occur, a discussion of the consequences of such a failure is now presented.

If a B_4C capsule were to release gas to the primary-tank cover-gas system, the event could be observed during one of the routine cover-gas analyses. All of the B_4C capsules in an HWCR subassembly will be tagged with a unique mixture of xenon isotopes. At present, an analysis of the cover gas for xenon isotopes is made on a biweekly basis. It may be necessary to increase the frequency of analyzing the cover gas to a weekly basis, since the residence half-life of the cover gas is 3-5 days, depending on the leakage, frequency of fuel handling, and purge rate. There is also a possibility that no gas would be released from the capsule during reactor operation even if it had a cladding failure. If the leak occurred in the lower end, there could well be sufficient external pressure to force sodium into the capsule, rather than a low enough external pressure to allow gas to escape, at least until the primary pumps were turned off after reactor shutdown.

The purpose of xenon-tagging the capsules is primarily to indicate that any boron or carbon that might be released to the system as a result of a leak came from the B_4C, and to preclude concern that the carbon might be a result of a failure of an irradiation experiment or the stainless steel cladding for the neutron shield.

Data on the compatibility of irradiated B_4C, sodium, and stainless steel are few. HEDL is carrying out tests with irradiated and unirradiated B_4C sealed in Type 316 stainless steel capsules filled with sodium and heated to various temperatures. The results appear to be quite temperature-sensitive, and the presence of sodium increases the reaction rate of B_4F with steel by a factor of 2.4 to 5. Tests with unirradiated 90%-theoretical-densit pellets heated for 2500 hr at 1100°F and 1300°F showed interaction rates in th stainless steel of 0.0017 and 0.013 in./yr and no measurable change in the B_4C pellet dimensions (less than 0.05%).[19] Similar tests, but with pellets previously irradiated in EBR-II at 1400°F to 7 x 10^{20} captures/cm^3, have been carried out at 1350°F and 1500°F for 234 hr with penetration rates of 0.065 and 0.19 in./hr, respectively. In these latter tests, the surfaces of the B_4F pellets were very friable after exposure to sodium, and the average weight losses of pellets at 1350°F and 1500°F were 6% and 10%, respectively.[20] The cladding temperature of the B_4C capsules in the HWCR's will be about 1050°F, so reaction rates and pellet attack should be low.

Temperature distributions were calculated for the HWCR based on power distributions provided by the neutronics calculations in Section III. The quantity of power produced in the fuel was determined from calculation 3 of Table IV, and the axial distribution in the fuel and B_4C portions from calculations 6 through 9. The results of the latter calculations are shown in Figs. 34-37. These Figs. show the volumetric gamma-power generation in W/cm^3 for all the axial regions of the HWCR. Also shown are the volumetric fission-power generation for the fuel and the (n,α) power generation for the B_4C in the insertion positions corresponding to calculations 6 through 9. (Reference to Fig. 11, which diagrams the HWCR regions and insertion positions, may help in understanding Figs. 34 and 37.)

The fission power generated in the fuel is insensitive to position between 10.85 and 14 in. of insertion, while the (n,α) power decreases as the HWCR insertion is increased, so that the power-generation profile from the 10.85-in. insertion position (Fig. 35) was used in subsequent HECTIC calculations for both the fuel and B_4C portions. (Note that if one uses Fig. 35 to obtain a subassembly linear heat rating in kW/ft, the value of the ordinate must be multiplied by the conversion factor 0.916. This factor follows from the fact that the ordinate as given is based on a smeared composition over the 30.04-cm^2 cross section of the subassembly.)

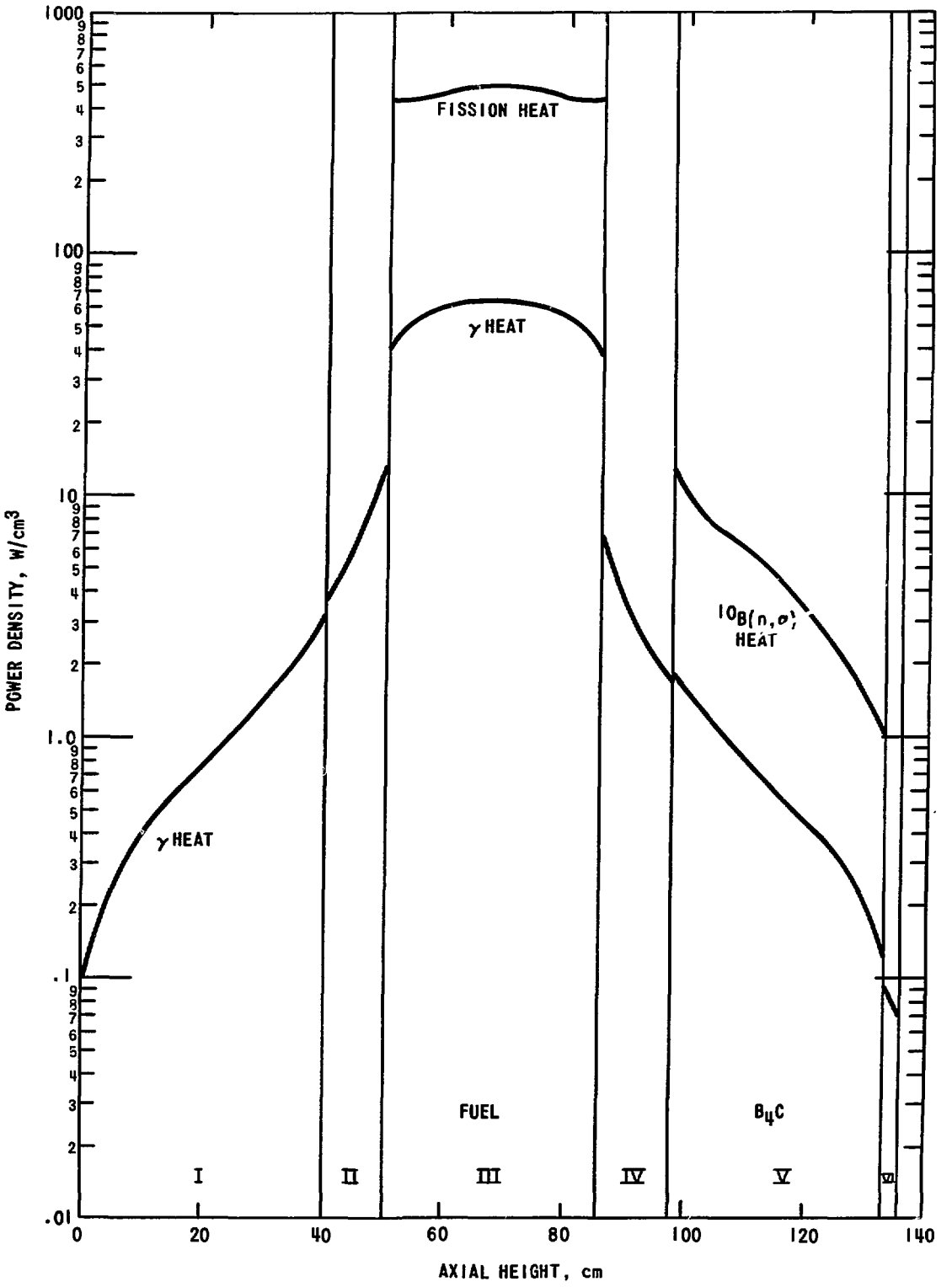

Fig. 34. Volumetric Power Generation in HWCR with 14-in. Insertion (Fully Up)

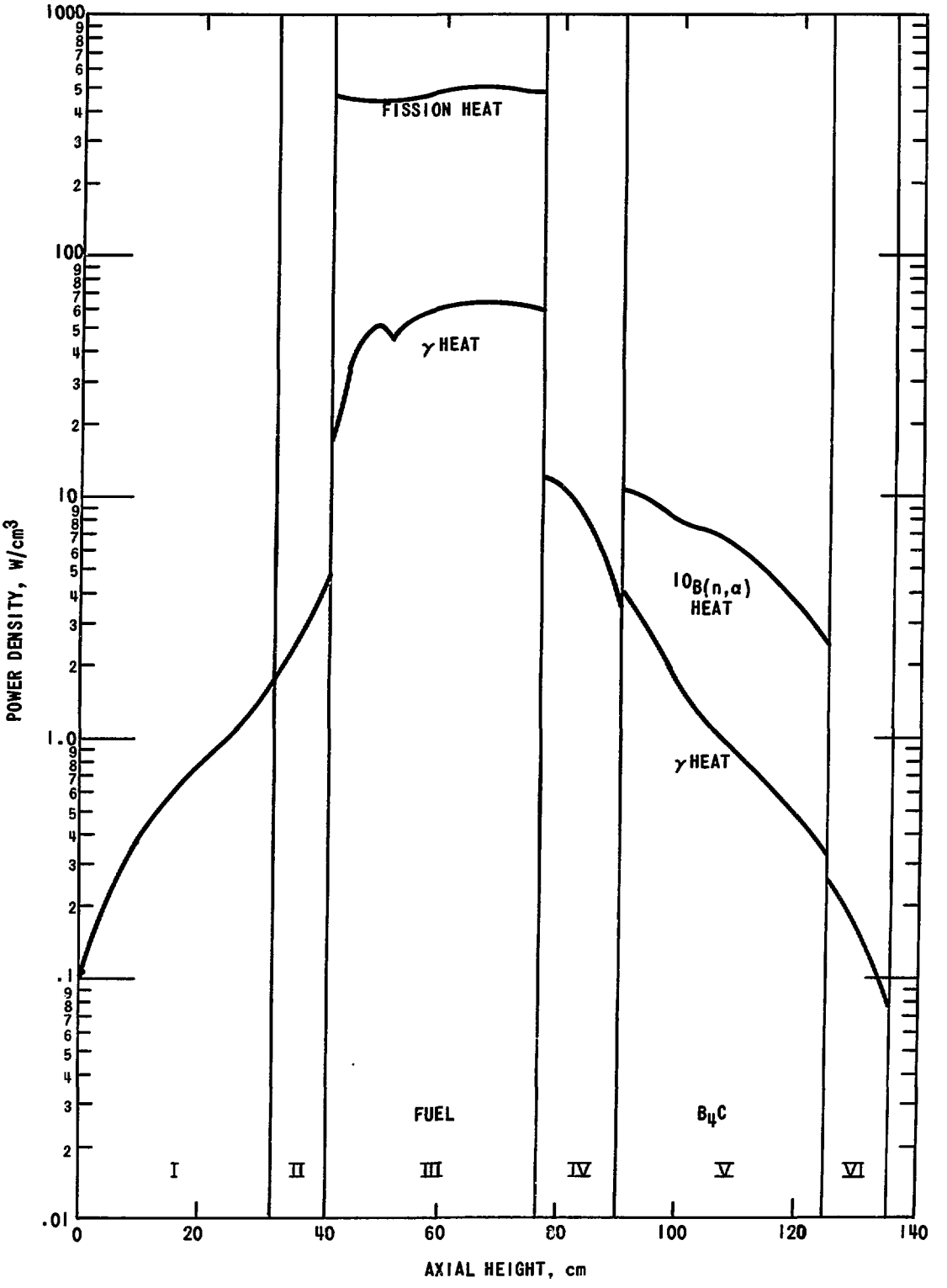

Fig. 35. Volumetric Power Generation in HWCR with 10.85-in. Insertion (8 cm Below Up)

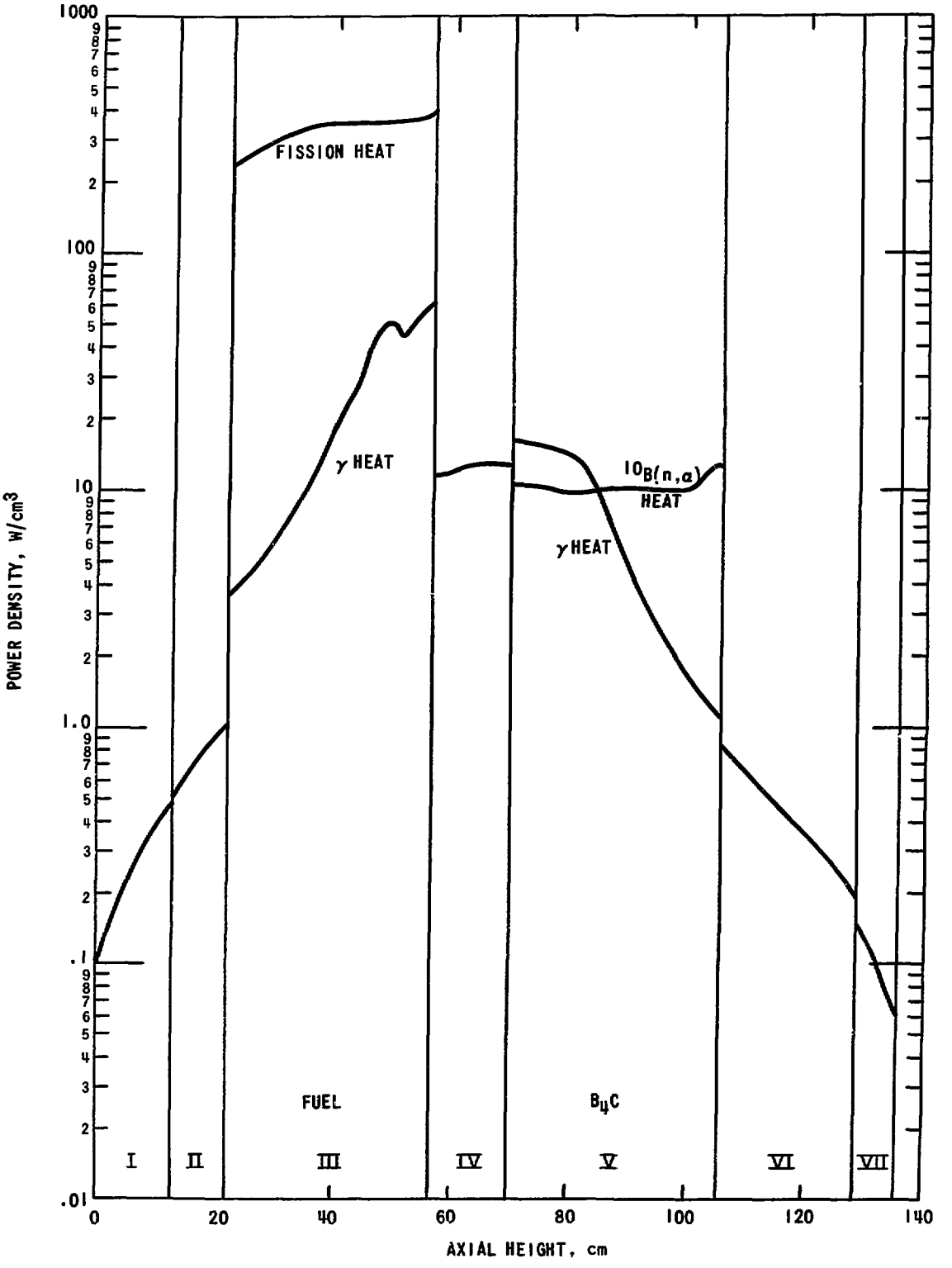

Fig. 36. Volumetric Power Generation in HWCR with 3.15-in. Insertion (8 cm Above Down)

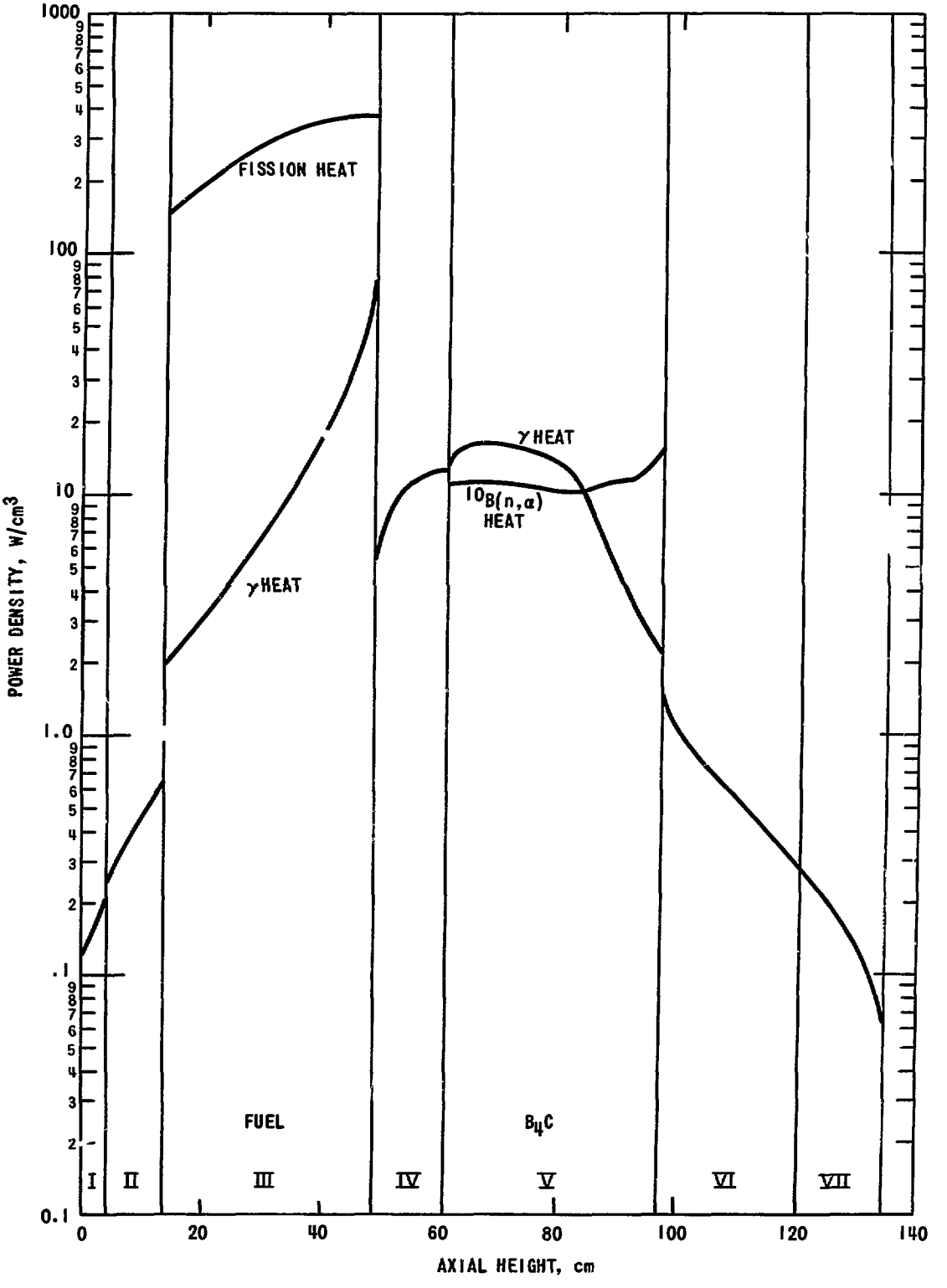

Fig. 37. Volumetric Power Generation in HWCR with Zero Insertion (Fully Down)

The axial distribution for the fission power was used in the HECTIC calculations for the fuel section. For the B_4C section, however, the sum of the (n,α) and gamma powers was obtained, and the axial distribution was obtained from this sum. In calculating the temperature distribution within the B_4C capsule, it was conservatively assumed that all of the power was generated in the B_4C itself, although about half of the gamma power is actually generated in the stainless steel cladding. The total power in the fuel section was 575 kW, and in the B_4C section, 8.2 kW. The sodium flow-rate through the HWCR was 61 gpm.

The results of the HECTIC calculations for the HWCR with 10.85-in. insertion are plotted in Figure 38, which gives the temperatures along the 13.5-in. length of the fuel section, and Figure 39, which gives the temperatures along the 14-in. length of B_4C section. The hottest channel in a 5N3 position was used for the fuel, and for the sake of conservatism, the coolant-outlet temperature from this channel (1000°F) was used as the inlet temperature for the entire B_4C region. The mixed-mean coolant-outlet temperature of the fuel region was calculated to be 940°F.

The behavior of the B_4C center temperature in Figure 39 is noteworthy. Because of the steep axial gradient in power generation in the B_4C, the centerline temperature monotonically decreases with distance along the element. The coolant temperature rise is but 4°F, owing the low heat input from the B_4C section.

An investigation was carried out to determine the effect of blocking a flow channel in the B_4C section of the HWCR. There are three types of flow channels in this section: central, corner, and edge.

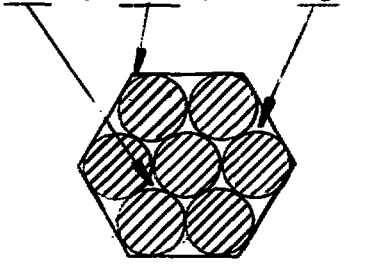

Blockage of an edge channel would be the most severe case, as each of these six channels normally carries about 11% of the total flow, so this case was analyzed. The effect of blocking this channel would be to decrease the flow

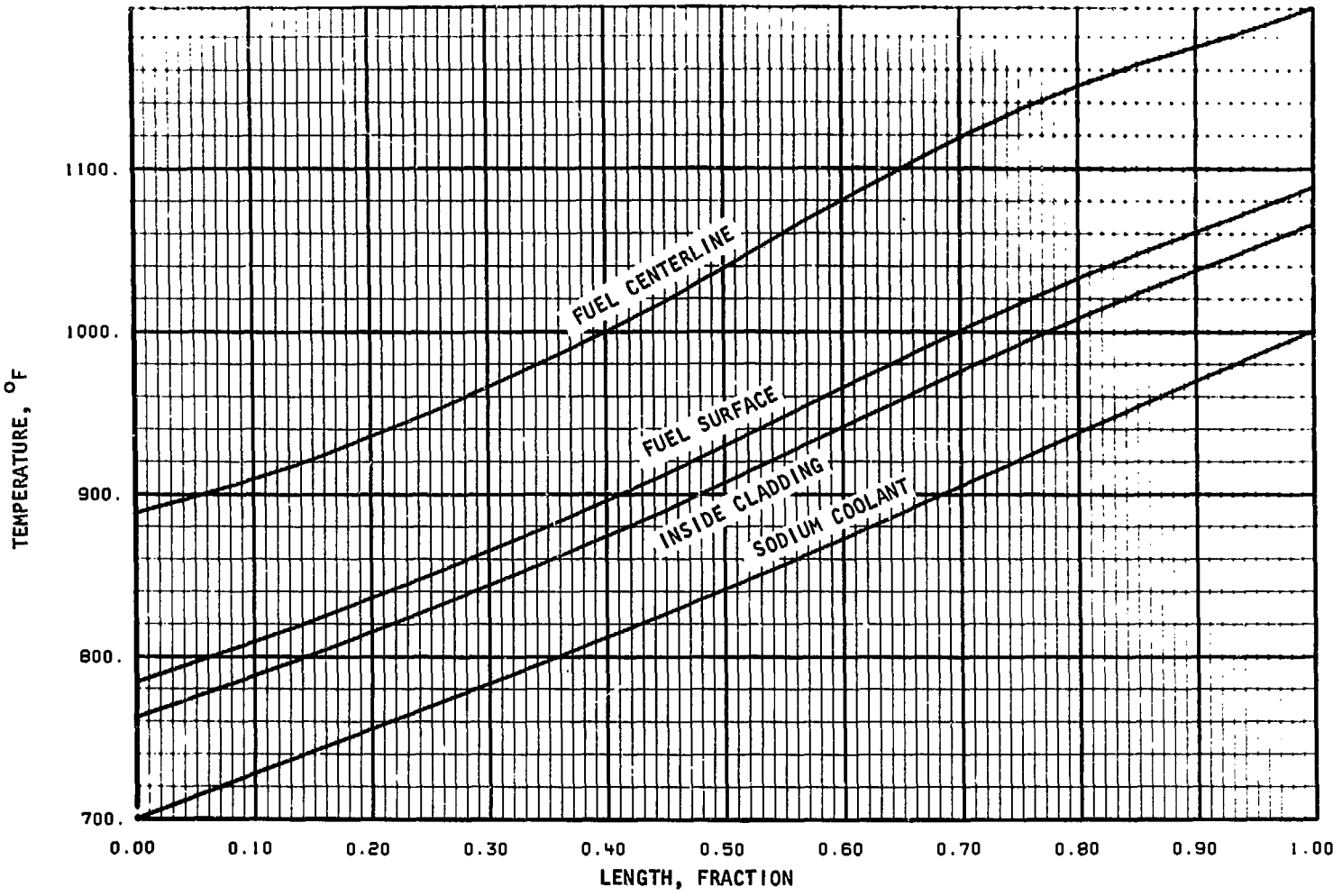

Fig. 38. Temperature Distribution in Fuel Section of HWCR with 10.85-in. Insertion

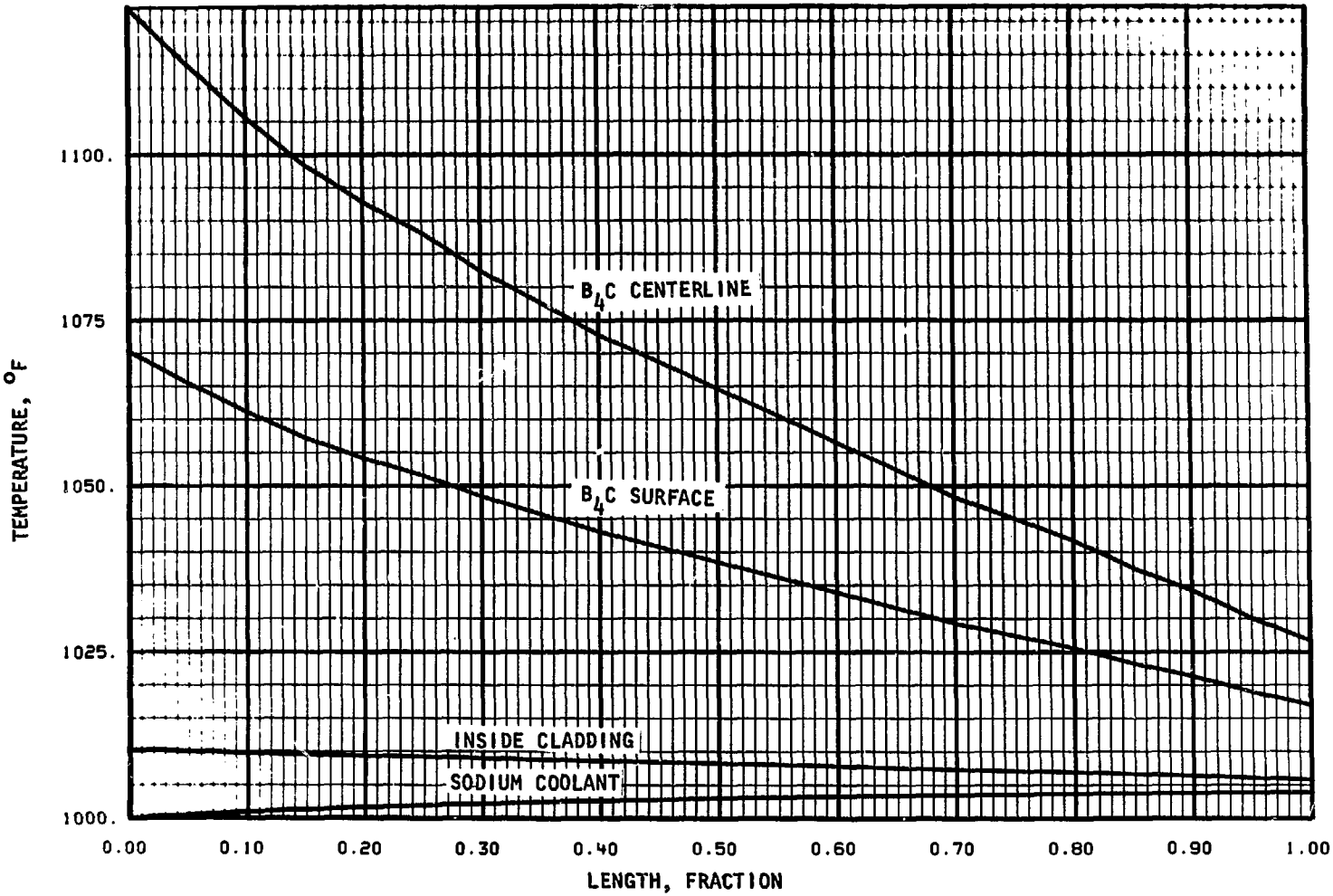

Fig. 39. Temperature Distribution in B_4C Section of HWCR with 10.85-in. Insertion

through the entire subassembly by 9% and still produce the same pressure drop across the fuel element and B_4C capsule portions of the subassembly. A further effect of the blockage would be to produce a 9% increase in the coolant temperature rise along the fuel portion, although the temperature differences between the coolant and the fuel or cladding would not change. The result would be a hot-channel outlet temperature of 1028°F, still below that for a row-6 hot channel (Fig. 10). In the B_4C portion, the blocked channel would cause an increase in temperature in the B_4C of less than 250°F at the peak heat-production point.

A further analysis was carried out to determine the effect of gas blanketing of a B_4C capsule, an event that could be caused by the release of fission gas from a fuel element. The low power production in the B_4C makes the effect inconsequential. If there were no heat transfer whatever to the coolant, the maximum rate of temperature increase, based on the maximum element linear heat rate of 2.2 kW/ft, would be less than 20°F/sec.

The use of HWCR's will increase the amount of tritium produced and released during EBR-II operation. An estimate has been made for the tritium activity generated in the stainless-steel-reflected core. Tritium is produced in the fissioning of the fissile isotopes in the driver and experimental fueled subassemblies, in the $^{10}B(n,t)2\alpha$ reaction in the B_4C portion of the HWCR's and in the same reaction in the B_4C experimental subassemblies in rows 4, 6, and 7 (see Table III). During a 2000-MWd run, the tritium production in the fuel amounts to 23.5 Ci; in eight HWCR's assumed to be at the 10-in. bank position, 14.4 Ci; and in B_4C experimental subassemblies, 16.4, 21,7, and 11.4 Ci for rows 4, 6, and 7 respectively. Thus, there are 61% as many curies of tritium produced in HWCR's as in the fuel in the core, but the production due to HWCR's is only 16% of the total, based on the projected core containing 10 B_4C experimental subassemblies.

VI. SUMMARY AND CONCLUSIONS

The preceding sections have shown that replacing the present standard control rods with high-worth control rods will allow the number of control rods in use to be reduced while providing more variation in system reactivity than is possible at present. The high-worth control rods are completely compatible with the overall EBR-II system. The suitability of HWCR's from a safety viewpoint has been established.

The use of a system of HWCR's will release at least four of the 12 control-rod positions for use by experimental equipment of various types (e.g., instrumented subassemblies, oscillator rods); the system will also provide a greater reactivity margin for the reactor and can permit run lengths up to 3000 MWd. No significant effect on the core environment is caused by the HWCR's, because the natural-B_4C follower is above the core height during reactor operation.

Cores with a depleted-uranium blanket and with a stainless steel reflector in rows 7-10 have been analyzed. The major emphasis has been placed on cores with a stainless steel reflector, since such a reflector was scheduled for installation and was in fact installed in May 1972.

The maximum worth of an HWCR has been calculated to be 0.81% $\Delta k/k$, compared to a value of 0.6% $\Delta k/k$ for the control rods specified in the original safety documents.[1,2] The maximum rate of reactivity insertion with a single HWCR has been calculated to be 0.0067% $\Delta k/k$ per second, compared to the original 0.006% $\Delta k/k$ per second.

The safety aspects of an uncontrolled insertion of an HWCR (with a worth of 0.81% $\Delta k/k$) have been analyzed for the low-power (startup) and full-power (62.5 MWt) conditions. If the plant protective system is operative, the reactor trips before any damage results; if the protective system is not operative, results similar to those with the present control-rod system occur, but in 31 rather than 43 sec.

The mechanical design of the HWCR poses no safety problem. A plenum has been provided for the retention of the helium given off by the (n,α) reaction in ^{10}B, and expected gas pressures within the B_4C capsule are less than 15% of the design value. Evidence indicates that B_4C, sodium, and stainless steel are compatible under the service conditions expected for the HWCR.

Operation of EBR-II with a prototype HWCR has been satisfactory and has given important information relative to the use of a system of HWCR's. Although the reactivity worth of a bank of HWCR's is slightly uncertain, analytical and experimental results now agree within 10%. Verification of the total worth of a system of HWCR's will come only after installation of the system.

The recommendation is made that a system of HWCR's be installed in EBR-II. However, one or two standard control rods should be retained for use as the regulating rod, because they would operate over a flatter portion of their

incremental worth curve than would an HWCR. The total worth of a system of eight HWCR's is more than adequate for most projected applications. For these reasons, it is recommended that the HWCR system used be composed of seven (or six) HWCR's and one (or two) standard control rods. The standard control rod would be used as the regulating rod. The standard-rod location would be moved from one corner position to another as the 1.8-at.% burnup limit was reached, to equalize long-term wear on the control-rod drives.

REFERENCES

1. L. J. Koch et al., Hazard Summary Report, Experimental Breeder Reactor II (EBR-II), ANL-5719 (May 1957).

2. L. J. Koch, W. B. Loewenstein, and H. O. Monson, Addendum to Hazard Summary Report, Experimental Breeder Reactor II (EBR-II), ANL-5719 (Addendum) (June 1962).

3. J. C. Case, Core-Loading Diagrams for EBR-II Runs 39 through 50 (December 1969 through mid-August 1971), ANL/EBR-043 (Sept 1971).

4. Argonne National Laboratory, Reactor Development Program Progress Report: July 1968, ANL-7478, pp. 57-59 (Aug 28, 1968).

5. Argonne National Laboratory, EBR-II System Design Descriptions, Volume II. Primary System, Chapter 2: "Reactor" (June 15, 1971).

6. O. S. Seim, Argonne National Laboratory, private communication (Oct 21, 1971).

7. B. R. Sehgal, R. K. Lo, and R. H. Rempert, Neutronic and Thermal-Hydraulic Characteristics of a HWCR for EBR-II, (unpublished ANL report).

8. Argonne National Laboratory, Reactor Development Program Progress Report: August 1970, ANL-7737, pp. 61-62 (Sept 29, 1970).

9. F. S. Kirn, Argonne National Laboratory, private communication (Dec 9, 1971).

10. R. A. Blaine and R. F. Berland, Simulation of Reactor Dynamics Vol. 1 A Description of AIROS-IIA, NAA-SR-12452 (Sept 5, 1967).

11. A. V. Campise, A Study of the Dynamic Response of Various Malfunctions in the Reactor System, ANL-7613 (Nov 1969).

12. M. Levenson, Argonne National Laboratory, Design of Radial Steel Reflector for EBR-II, letter to M. Shaw, U. S. Atomic Energy Commission (Aug 20, 1971).

13. Argonne National Laboratory, Reactor Development Program Progress Report: October 1968, ANL-7513, pp. 46-48 (Nov 29, 1968).

14. M. T. Laug, Argonne National Laboratory, private communication (Nov 15, 1971).

15. G. E. Russcher and A. L. Pitner, A Function to Predict Helium Release Based on Boron Carbide Irradiation Data from Thermal Reactors, HEDL-TME 71-127 (Sept 30, 1971).

16. Westinghouse Electric Corporation, Advanced Reactors Division, Design Criteria for Nuclear Control Components, FRP-294, (Sept 1, 1970).

17. J. A. Basmajian, WADCO Corporation, private communication (Dec 27, 1971).

18. D. E. Mahagin, WADCO Corporation, private communication (Dec 28, 1971).

19. WADCO Corporation, Monthly Technical Progress Report, HEDL-TME 71-8 (Aug 1971).

20. WADCO Corporation, Monthly Technical Progress Report, HEDL-TME 71-10 (Oct 1971).